

## STATUS OF THESIS

Title of thesis

**Synthesis and Characterisation of Carbon Nanotubes Grown  
by Catalytic Method**

I TAN YEE CHECH hereby allow my thesis to be placed at the Information Resource Centre (IRC) of Universiti Teknologi PETRONAS (UTP) with the following conditions:

1. The thesis becomes the property of UTP
2. The IRC of UTP may make copies of the thesis for academic purposes only.
3. This thesis is classified as

Confidential

Non-confidential

If this thesis is confidential, please state the reason:

---

---

The contents of the thesis will remain confidential for \_\_\_\_\_ years.

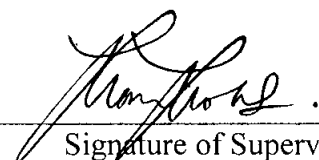
Remarks on disclosure:

---

---

Endorsed by

  
\_\_\_\_\_  
Signature of Author

  
\_\_\_\_\_  
Signature of Supervisor

Permanent: 24, Jalan Tempua 14,  
address Bandar Puchong Jaya,  
47100 Puchong,  
Selangor Darul Ehsan.

Assoc. Prof. Dr. Norani Muti Mohamed

Date: 19 JULY 2005

Date: 19 JULY 2005

APPROVAL PAGE

UNIVERSITI TEKNOLOGI PETRONAS

Approval by Supervisor (s)

The undersigned certify that they have read, and recommend to The Postgraduate Studies Programme for acceptance, a thesis entitled "**Synthesis and Characterisation of Carbon Nanotubes Grown by Catalytic Method**" submitted by **Tan Yee Chech** for the fulfilment of the requirements for the degree of Master of Science in Electrical and Electronics Engineering.

19 JULY 2005

Signature

:



Main Supervisor

:

Assoc. Prof. Dr. Norani Muti Mohamed

Date

:

19 JULY 2005

Co-Supervisor 1

:

\_\_\_\_\_

Co-Supervisor 2

:

\_\_\_\_\_

**TITLE PAGE**

UNIVERSITI TEKNOLOGI PETRONAS

**Synthesis and Characterisation of Carbon Nanotubes**

**Grown by Catalytic Method**

By

© **Tan Yee Cheh**

A THESIS

SUBMITTED TO THE POSTGRADUATE STUDIES PROGRAMME

AS A REQUIREMENT FOR THE

DEGREE OF MASTER OF SCIENCE IN

ELECTRICAL AND ELECTRONICS ENGINEERING

ELECTRICAL AND ELECTRONICS ENGINEERING PROGRAMME

BANDAR SERI ISKANDAR,

PERAK

JULY, 2005

## DECLARATION

I hereby declare that the thesis is based on my original work except for quotations and citations, which have been duly acknowledged. I also declare that it has not been previously or concurrently submitted for any other degree at UTP or other institutions.

Signature :  \_\_\_\_\_

Name : Tan Yee Chech

Date : 19 JULY 2005

## ACKNOWLEDGEMENT

In this disproportionately small section, I would like to thank those people, together with those that I unintentionally might forget to mention. First and foremost, I would like to thank my supervisor, Associate Professor Dr. Norani Muti Mohamed. Her insight, guidance and encouragement were invaluable. Her faith in my abilities often exceeded my own. I would like to thank Dr. Abdul Kadir Masrom (Advance Materials Research Centre (AMREC), Kulim Hi-tech) for his interest in my work and for being source of ideas and inspiration. We have many insightful discussions regarding my research.

Thanks to Mr. Abdul Hakim Hashim and Mr. Suffian Saad from AMREC. Without their knowledge, skill and help, I would not have succeeded with this project. Dr. Abdul Kadir and them had taught me a lot on materials characterisation. I would like to thank Associate Professor Dr. Francis Tay Eng Hong and Dr. Zhang Wei De from Institute of Materials Research and Engineering (IMRE), Singapore for teaching and sharing their expertise in growing carbon nanotubes (and the daily evening coffee talks).

Specially thanks Dr. Tim Smith from Renishaw plc, United Kingdom for his help and explaining the theoretical aspects in Raman spectroscopy characterisation. I would like to thank Dr. Chang Wei from Seiko Instruments, Japan for his explanation on atomic force microscope characterisation. Thanks also go to The University of Queensland chief librarian, Mrs. Karen Borchardt for helping me to get some important research papers.

I would like to thank our wonderful Nanotechnology Laboratory technician, Mr. Rosli Mohd for his unlimited support to succeed this project. I should also thank Universiti Sains Malaysia for its exceptional facilities and its technicians for giving me opportunity to learn how to use some of the characterisation tools.

I am grateful to all my fellow postgraduate students in Universiti Teknologi PETRONAS (UTP) for many useful discussions and the pleasant time. They taught me well on how to “work hard and play harder” especially my housemates. I wish them the best of luck in their future undertaking.

Finally, I would like to thank my parents, for giving me this opportunity in the first place and thanks all my family for many yawns and blank stares at the mention of word nanotube. Their love and support were essential. Last but not least, I thank Miss Chow Mee Ling for her support and keeping me motivated.

This project was funded by UTP Short-term Grant Programme.



## **ABSTRACT**

Carbon nanotube (CNT), the hottest nanostructured material has a very wide application because of its remarkable mechanical and electrical properties. At present, one serious weakness of all the techniques to produce CNTs is the wide range of tube sizes and structures obtained which could be a drawback for this kind of application, as it requires specific tube structures. The objective of this work is to produce good quality CNTs with defined structure specifically narrow diameter range through investigation of the growth parameter in the catalytic synthesis.

The catalytic method adopted to synthesise CNTs involved using three different catalysts namely iron (Fe), cobalt (Co) and nickel (Ni). Various wet etching time duration was adopted in the process of preparing nanosized catalyst. These prepared catalysts were used to grow CNTs by using thermal chemical vapour deposition method. The final raw product were oxidised and subjected to acid treatment to eliminate impurities. The purified products in the form of fine black powder CNTs were then characterized structurally by scanning electron microscope (SEM) and X-ray diffractometry (XRD). The crystalline perfection of CNTs grown on different catalysts was determined by transmission electron microscope (TEM) and was further verified by thermal gravimetry analysis (TGA) and Raman spectroscopy.

The CNT diameter range of Fe, Ni and Co obtained is 31-38 nm, 19-24 nm and 23-26 nm respectively. These indicate that the diameter range follows the sequence of Fe>Ni>Co catalysts. The sequence agrees well with the degree of crystalline perfection results. This implies that the structure and diameter range of CNTs can be defined and their degree of crystallinity perfection can be manipulated by selection of catalyst. As evidence from the results, the newly developed catalyst preparation has proven to be the promising method to prepare nanosized catalyst leading to the production of CNTs with defined structures. The technique developed is believed to have benefited the research area by paving the way for more research such as nanocomposite and nanoelectronics, which require defined structured CNTs to be conducted.

## **ABSTRAK**

Tiub nano karbon (CNT) merupakan bahan berstruktur nano yang mempunyai pelbagai aplikasi kerana sifat mekanikal dan elektrik yang istimewa. Sehingga kini, terdapat satu kelemahan yang mana CNT yang dihasilkan mempunyai saiz taburan yang besar dan struktur yang tidak tentu. Ini merupakan suatu halangan untuk sesetengah aplikasi kerana struktur tertentu diperlukan. Oleh itu, objektif penyelidikan ini adalah untuk menghasilkan CNT yang berkualiti dengan struktur tertentu yakni, julat diameter yang kecil melalui kajian kesan parameter pertumbuhan dalam sintesis pemangkinan.

Sintesis pemangkinan merupakan cara penghasilan CNT yang digunakan. Mangkin yang digunakan adalah besi (Fe), kobalt (Co) dan nikel (Ni). Masa punaran basah yang berlainan dikaji dalam proses penyediaan mangkin bersaiz nano. Mangkin tersebut digunakan untuk pertumbuhan CNT dengan menggunakan cara penguapan wap kimia termal (CVD). Serbuk halus hitam CNT yang dituliskan, dianalisa secara struktur dengan menggunakan mikroskopi electron imbasan (SEM) dan pembelauan sinar-X (XRD). Manakala kesempurnaan habluran CNT yang dihasilkan ditentukan dengan menggunakan mikroskopi electron pancaran (TEM) dan dikaji lebih lanjut dengan analisis termal gravimetri (TGA) dan spektroskopi Raman.

Taburan diameter CNT untuk mangkin Fe, Ni dan Co yang diperolehi adalah 31-38 nm, 19-24 nm dan 23-26 nm masing-masing. Ini menunjukkan taburan diameter mengikut susunan Fe>Ni>Co. Susunan ini juga sama dengan keputusan darjah kesempurnaan habluran. Ini menunjukkan struktur dan taburan diameter CNT dan darjah kesempurnaan habluran boleh ditentukan dengan memanipulasikan mangkin tertentu. Daripada keputusan yang didapati, penghasilan CNT dengan struktur tertentu telah terbukti dapat dihasilkan melalui cara penyediaan mangkin bersaiz nano yang terbaru ini. Teknik yang dibangunkan ini dipercayai dapat memanfaatkan bidang penyelidikan seperti nanokomposit dan nanoelektronik yang memerlukan CNT berstruktur tertentu.

## **TABLE OF CONTENTS**

|  |             |
|--|-------------|
| <b>DECLARATION .....</b>                                 | <b>i</b>    |
| <b>ACKNOWLEDGEMENT .....</b>                             | <b>ii</b>   |
| <b>ABSTRACT .....</b>                                    | <b>iv</b>   |
| <b>ABSTRAK.....</b>                                      | <b>v</b>    |
| <b>TABLE OF CONTENTS.....</b>                            | <b>vi</b>   |
| <b>LIST OF TABLES.....</b>                               | <b>ix</b>   |
| <b>LIST OF FIGURES.....</b>                              | <b>x</b>    |
| <b>LIST OF ABBREVIATIONS.....</b>                        | <b>xvii</b> |
| <b>Chapter 1: INTRODUCTION.....</b>                      | <b>1</b>    |
| 1.1    A Paradigm Shift Towards Nanotechnology .....     | 1           |
| 1.2    Objective and Scope of Research.....              | 4           |
| 1.3    Thesis outline .....                              | 5           |
| <b>Chapter 2: THEORY AND LITERATURE REVIEW .....</b>     | <b>7</b>    |
| 2.1    Carbon Nanotubes.....                             | 7           |
| 2.1.1    Single-Walled Carbon Nanotubes .....            | 9           |
| 2.1.2    Multiwalled Carbon Nanotubes .....              | 11          |
| 2.1.3    Structure of Carbon Nanotubes .....             | 13          |
| 2.1.4    Growth Mechanisms of Carbon Nanotubes.....      | 15          |
| 2.1.5    Mechanical Properties of Carbon Nanotubes ..... | 17          |
| 2.1.6    Electronic Properties of Carbon Nanotubes ..... | 19          |

|                                    |  |           |
|------------------------------------|--|-----------|
| 2.2                                | Advances of Carbon Nanotubes in Cutting Edge Application .....   | 22        |
| 2.3                                | Growth Method for Carbon Nanotubes .....                         | 26        |
| 2.3.1                              | Arc-Discharge.....   | 26        |
| 2.3.2                              | Laser Ablation .....   | 28        |
| 2.3.3                              | Chemical Vapour Deposition .....                                 | 29        |
| 2.4                                | Use of Catalyst in the Synthesis of CNTs.....                    | 32        |
| 2.5                                | Purification of Carbon Nanotubes.....                            | 36        |
| 2.5.1                              | Thermal Treatment .....  | 37        |
| 2.5.2                              | Acid Treatment .....   | 37        |
| <b>Chapter 3: METHODOLOGY.....</b> |  | <b>38</b> |
| 3.1                                | Introduction .....   | 38        |
| 3.2                                | Substrates Preparation.....                                      | 40        |
| 3.2.1                              | Cutting of Silicon Wafers .....                                  | 40        |
| 3.2.2                              | Cleaning of Silicon Wafer .....                                  | 40        |
| 3.3                                | Nanocatalysts Preparation.....                                   | 43        |
| 3.3.1                              | Wet Etching Process of Catalytic Particles .....                 | 43        |
| 3.3.2                              | Dropping Wet Etched Product on Substrate.....                    | 44        |
| 3.3.3                              | Dry Etching Process of Catalytic Particles.....                  | 47        |
| 3.4                                | Growth of Carbon Nanotubes using Chemical Vapour Deposition..... | 48        |
| 3.5                                | Purification Procedure.....                                      | 51        |
| 3.5.1                              | Thermal treatment.....   | 51        |
| 3.5.2                              | Acid treatment .....   | 51        |
| 3.6                                | Characterization Tests.....                                      | 53        |
| 3.6.1                              | Scanning Electron Microscopy (SEM).....                          | 53        |
| 3.6.2                              | X-Ray Diffractometry (XRD).....                                  | 56        |
| 3.6.3                              | Transmission Electron Microscopy (TEM) .....                     | 59        |
| 3.6.4                              | Thermal Gravimetry Analysis (TGA) .....                          | 62        |
| 3.6.5                              | Raman Spectroscopy .....   | 65        |

|  |            |
|--|------------|
| <b>Chapter 4: RESULTS AND DISCUSSION .....</b>                                   | <b>68</b>  |
| 4.1 Introduction .....   | 68         |
| 4.2 Scanning Electron Microscopy (SEM) .....                                     | 71         |
| 4.2.1 Wet Etched Catalyst Samples .....  | 71         |
| 4.2.2 Non-purified Samples .....   | 77         |
| 4.2.3 Purified Samples .....   | 83         |
| 4.3 X-Ray Diffractometry (XRD) .....   | 91         |
| 4.3.1 Non-purified Samples .....   | 93         |
| 4.3.2 Purified Samples .....   | 98         |
| 4.4 Further Investigation of Selected Samples .....                              | 102        |
| 4.4.1 Introduction .....   | 102        |
| 4.4.2 Transmission Electron Microscopy (TEM) .....                               | 102        |
| 4.4.3 Thermal Gravimetry Analysis (TGA) .....                                    | 110        |
| 4.4.4 Raman Spectroscopy .....   | 115        |
| 4.5 Summary .....  | 121        |
| <br>   |            |
| <b>Chapter 5: CONCLUSIONS AND FUTURE WORKS .....</b>                             | <b>124</b> |
| 5.1 Conclusions .....  | 124        |
| 5.2 International Collaboration .....  | 126        |
| 5.3 Recommendations of the Research .....  | 127        |
| <br>   |            |
| <b>APPENDIX A: List of Chemicals .....</b>                                       | <b>138</b> |
| <br>   |            |
| <b>APPENDIX B: Size Determination from Micrograph .....</b>                      | <b>139</b> |
| <br>   |            |
| <b>APPENDIX C: Interlayer Spacing Determination from X-Ray Diffraction .....</b> | <b>141</b> |
| <br>   |            |
| <b>LIST OF PUBLICATION .....</b>   | <b>142</b> |

## LIST OF TABLES

|  |     |
|--|-----|
| <b>Table 2.1:</b> Applications of carbon nanotubes. ....   | 23  |
| <b>Table 2.2:</b> A summary of the major production methods and their efficiency. ....                     | 31  |
| <b>Table 3.1:</b> RCA solution composition. (Reproduced from Van Zant, 1997).....                          | 41  |
| <b>Table 4.1:</b> Description and coding for each individual synthesised samples. ....                     | 69  |
| <b>Table 4.2:</b> Summary of wet etched samples under different etching time. ....                         | 75  |
| <b>Table 4.3:</b> The effect of dry etching process to the catalysts size. ....                            | 79  |
| <b>Table 4.4:</b> Diameter measurement of CNTs. ....   | 86  |
| <b>Table 4.5:</b> Main diffraction peaks related to graphite and pure metal Fe, Co and Ni. .               | 91  |
| <b>Table 4.6:</b> XRD summary of non-purified samples.....   | 95  |
| <b>Table 4.7:</b> XRD summary of purified samples. ....  | 101 |
| <b>Table 4.8:</b> Description of purified samples for the investigation of TEM and TGA techniques. ....    | 102 |
| <b>Table 4.9:</b> Summary of TGA results of FeD <sub>3</sub> , CoB <sub>3</sub> and NiC <sub>3</sub> ..... | 112 |
| <b>Table 4.10:</b> Raman intensity value for carbon nanotubes at 514.5 nm excitation. ....                 | 117 |
| <b>Table 4.11:</b> Raman intensity value for carbon nanotubes at 623.8 nm excitation. ....                 | 119 |

## LIST OF FIGURES

|   |    |
|---|----|
| <b>Figure 2.1:</b> Typical high resolution TEM image of a nanotube cap. (Reproduced from Harris, 1999).   | 9  |
| <b>Figure 2.2:</b> A single walled carbon nanotube. (Reproduced from Dresselhaus <i>et al.</i> , 2002).   | 10 |
| <b>Figure 2.3:</b> A multiwalled carbon nanotube. (Reproduced from Dresselhaus <i>et al.</i> , 2002).   | 13 |
| <b>Figure 2.4:</b> Classical construction of nanotube structure. (Reproduced from Saito <i>et al.</i> , 1998).  | 14 |
| <b>Figure 2.5:</b> Variety of SWNT structures corresponding to the many ways a sheet of graphite can be wrapped into a seamless tube. (Reproduced from Saito <i>et al.</i> , 1998).             | 14 |
| <b>Figure 2.6:</b> Visualization of a possible carbon nanotube growth mechanism. (Reproduced from Kónya, 2001).   | 16 |
| <b>Figure 2.7:</b> CNT will rather buckle than break when force applies on it. (Reproduced from Smalley, n.d.)  | 18 |
| <b>Figure 2.8:</b> (a) An atomically resolved STM image of a chiral carbon nanotube compared to (b) a theoretical model of a nanotube with a similar chirality. (Reproduced from Ajayan, 2000). | 20 |
| <b>Figure 2.9:</b> Two classes of STM spectra can be observed on nanotubes. (Reproduced from Dekker, 1999).   | 21 |

|   |    |
|---|----|
| <b>Figure 2.10:</b> Nanotube kinks. <b>(a)</b> A theoretical model and <b>(b)</b> a nanotube that contains a kink lying across electrodes. The scale bar is 200 nm. (Reproduced from Yao <i>et al.</i> , 1999). | 21 |
| <b>Figure 2.11:</b> Schematic illustration of arc-evaporation apparatus. (Reproduced from Harris, 1999).  | 27 |
| <b>Figure 2.12:</b> Schematic drawings of a laser ablation apparatus. (Reproduced from Iljin, 2001).  | 28 |
| <b>Figure 2.13:</b> Schematic diagram of thermal CVD apparatus. (Reproduced from Iljin, 2003).  | 30 |
| <b>Figure 2.14:</b> Catalyst provides an alternate path of lower activation energy by which the reactants can proceed to form the products. (Reproduced from Rearece <i>et al.</i> , 1981).                     | 33 |
| <b>Figure 3.1:</b> Schematic diagram of carbon nanotubes synthesis process.   | 39 |
| <b>Figure 3.2:</b> Desiccator that contain substrates.  | 41 |
| <b>Figure 3.3:</b> Flow chart that summarised substrate preparation procedures.   | 42 |
| <b>Figure 3.4:</b> Dropper dropping sonicating mixture of ethanol and catalyst particles on a silicon wafer.  | 44 |
| <b>Figure 3.5:</b> Spreading process of catalytic particles on a silicon wafer.   | 45 |
| <b>Figure 3.6:</b> Flow chart that summarised nanocatalysts preparation procedures.   | 46 |
| <b>Figure 3.7:</b> Dry etching process to reduce catalyst particles size.   | 47 |

|  |    |
|--|----|
| <b>Figure 3.8:</b> Thermal CVD system for carbon nanotubes growth. <b>(a)</b> Alumina tube electrical tubular furnace. <b>(b)</b> Quartz tube electrical tubular split furnace. .... | 48 |
| <b>Figure 3.9:</b> Schematic diagram of thermal chemical vapour deposition (CVD) system. ....  | 49 |
| <b>Figure 3.10:</b> Thermal profile for the CVD process. ....  | 49 |
| <b>Figure 3.11:</b> Carbon nanotubes were grown on Si wafer. ....  | 50 |
| <b>Figure 3.12:</b> Non-purified carbon nanotubes held by tweezers. ....   | 50 |
| <b>Figure 3.13:</b> Flow chart that summarised purification process procedures. ....   | 52 |
| <b>Figure 3.14:</b> LEO 1525 Field Emission Scanning Electron Microscope. ....   | 53 |
| <b>Figure 3.15:</b> X-rays reflected by a series of atoms in a lattice plane interfere constructively in directions given by Bragg's Law. ....                                       | 56 |
| <b>Figure 3.16:</b> Schematic layout of X-ray diffractometer. (Reproduced from Bacon, 1975). ....  | 57 |
| <b>Figure 3.17:</b> Bruker D8 Advance Powder X-ray diffractometer. ....  | 58 |
| <b>Figure 3.18:</b> The principle of a transmission electron microscope. (Reproduced from Wat, 1997). ....   | 59 |
| <b>Figure 3.19:</b> The principle of the electron gun. (Reproduced from Wat, 1997). ....   | 60 |
| <b>Figure 3.20:</b> Phillips Tecnai 20 Transmission Electron Microscope (TEM). ....  | 61 |
| <b>Figure 3.21:</b> Typical TGA chemical reactions. (Reproduced from Spiewak <i>et al.</i> , 1997). ....   | 63 |

|  |    |
|--|----|
| <b>Figure 3.22:</b> METTLER TOLEDO TGA/SDTA851 <sup>e</sup> thermal gravimetry analyser. ...   | 64 |
| <b>Figure 3.23:</b> A CNTs Raman spectrum. Reproduced from (Saito <i>et al.</i> , 2001). .....   | 66 |
| <b>Figure 3.24:</b> Renishaw inVia Raman Reflex microscope. (Reproduced from Renishaw, 2001.). .....   | 66 |
| <b>Figure 4.1:</b> SEM images of FeA1, FeB1, FeC1 and FeD1 under different etching time varying from 30 to 120 minutes at magnification of 10 000x. Scale bar 1 $\mu\text{m}$ . .... | 72 |
| <b>Figure 4.2:</b> SEM images of CoA1, CoB1, CoC1 and CoD1 under different etching time varying from 30 to 120 minutes at magnification of 10 000x. Scale bar 1 $\mu\text{m}$ . .... | 73 |
| <b>Figure 4.3:</b> SEM images of NiA1, NiB1, NiC1 and NiD1 under different etching time varying from 30 to 120 minutes at magnification of 10 000x. Scale bar 1 $\mu\text{m}$ . .... | 74 |
| <b>Figure 4.4:</b> Flakes like structure exhibit by Fe catalysts. ....   | 75 |
| <b>Figure 4.5:</b> Graph of particles size ( $\mu\text{m}$ ) versus etching time (minute). .....   | 76 |
| <b>Figure 4.6:</b> SEM images of FeD2 under magnification of <b>(a)</b> 30 000x and <b>(b)</b> 50 000x. Scale bar 100 nm. ....   | 77 |
| <b>Figure 4.7:</b> SEM images of CoB2 under magnification of (a) 30 000x and (b) 50 000x. Scale bar 100 nm. ....   | 78 |
| <b>Figure 4.8:</b> SEM image of CoC2 under magnification of 20 000x. Scale bar 100 nm.   | 78 |
| <b>Figure 4.9:</b> SEM images of CoD2 under magnification of (a) 30 000x and (b) 50 000x. Scale bar 100 nm. ....   | 79 |
| <b>Figure 4.10:</b> SEM images of NiC2 under magnification of <b>(a)</b> 80 000x, <b>(b)</b> 100 000x and <b>(c)</b> 200 000x. Scale bar 100 nm. ....                                | 80 |

**Figure 4.11:** SEM images of NiD2 under magnification of **(a)** 150 000x, **(b)** 250 000x and **(c)** 400 000x. Scale bar 100 nm for **(a)** and **(b)** while scale bar 20 nm for **(c)**.  
..... 81

**Figure 4.12:** **(a)** Irregular shaped catalysts particles surrounded by CNTs and **(b)** polyhedral nano particles (disordered carbon)..... 82

**Figure 4.13:** Micrograph of **(a)** purified CNTs grown on Fe catalyst (FeD3) and **(b)** non-purified CNTs grown on Fe catalyst (FeD2) under magnification of 50 000x. Scale bar 100 nm..... 84

**Figure 4.14:** Micrograph of purified CNTs grown on Co catalyst (CoB3) under magnification of **(a)** 10 000x, **(b)** 20 000x, **(c)** 50 000x and **(d)** 50 000x. Scale bar 100 nm. .... 85

**Figure 4.15:** Micrograph of purified CNTs grown on Co catalyst (CoC3) under magnification of **(a)** 100 000x and **(b)** 200 000x. Scale bar 100 nm..... 86

**Figure 4.16:** Micrograph of purified CNTs grown on Co catalyst (CoD3) under magnification of **(a)** 50 000x, **(b)** 100 000x and **(c)** 200 000x. Scale bar 100 nm. 87

**Figure 4.17:** Micrograph of purified CNTs grown on Ni catalyst (NiC3) under magnification of **(a)** 5 000x, **(b)** 10 000x, **(c)** 30 000x and **(d)** 50 000x. Scale bar 100 nm. .... 88

**Figure 4.18:** Micrograph of purified CNTs grown on Ni catalyst (NiD3) under magnification of 100 000x. Scale bar 100 nm. .... 88

**Figure 4.19:** Images of helical structure of CNT grown on Co catalyst..... 89

|  |     |
|--|-----|
| <b>Figure 4.20:</b> (a) Schematic drawing of multiwalled nanotube illustrating graphite c-planes. (b) Reciprocal space construction for a tube. (Reproduced from Zhang <i>et al.</i> , 1994).....                      | 92  |
| <b>Figure 4.21:</b> XRD diffractogram of FeD2.....   | 93  |
| <b>Figure 4.22:</b> XRD diffractogram of CoB2, CoC2 and CoD2.....  | 94  |
| <b>Figure 4.23:</b> XRD diffractogram of NiC2 and NiD2.....  | 94  |
| <b>Figure 4.24:</b> XRD diffractogram of FeD3.....   | 99  |
| <b>Figure 4.25:</b> XRD diffractogram of CoB3, CoC3 and CoD3.....  | 99  |
| <b>Figure 4.26:</b> XRD diffractogram of NiC3 and NiD3.....  | 100 |
| <b>Figure 4.27:</b> (a) to (c) TEM images of FeD3 under different magnification. (d) Higher resolution image of FeD3. Scale bar 100 nm for (a) and (b) while (c) scale bar is 20 nm and scale bar for (d) is 5 nm..... | 103 |
| <b>Figure 4.28:</b> (a) and (b) TEM images of CoB3 under different magnification. (c) Higher resolution image of CoB3. Scale bar 100 nm for (a) and (b) while scale bar for (c) is 5 nm.....                           | 104 |
| <b>Figure 4.29:</b> (a) to (b) TEM images of NiC3 under different magnification. (c) Higher resolution image of NiC3. Scale bar 100 nm for (a) and (b) while scale bar for (c) is 5 nm.....                            | 105 |
| <b>Figure 4.30:</b> Open-ended CNT.....  | 106 |
| <b>Figure 4.31:</b> TEM images that illustrate the presence of metal catalyst in purified samples.....   | 107 |

|   |     |
|---|-----|
| <b>Figure 4.32:</b> Schematic illustration of (a) ‘Russian doll’ and (b) ‘Swiss roll’ models for multiwalled nanotubes. (Reproduced from Harris, 1999). ..... | 108 |
| <b>Figure 4.33:</b> TGA plot of percentage weight against oxidation temperature for FeD3, CoB3 and NiC3.....  | 111 |
| <b>Figure 4.34:</b> DTA plot of FeD3, CoB3 and NiC3. ....   | 111 |
| <b>Figure 4.35:</b> Comparison of CNTs spectra collected using different laser powers....   | 116 |
| <b>Figure 4.36:</b> 514.5 nm excitation Raman spectra of CNT.....   | 117 |
| <b>Figure 4.37:</b> Lorentzian curve fit example of CNT spectrum. ....  | 118 |
| <b>Figure 4.38:</b> 632.8 nm excitation Raman spectra of CNT.....   | 119 |
| <b>Figure 5.1:</b> Images sequence of a growing CNT. (Reproduced from Helveg <i>et al.</i> , 2004). .....   | 128 |
| <b>Figure 5.2:</b> Raman spectra at different temperature. (Reproduced from Gogotsi <i>et al.</i> , 2003). .....  | 129 |

## LIST OF ABBREVIATIONS

|                |  |
|----------------|--|
| $\mu\text{m}$  | micrometer                                       |
| a.u.           | Arbitrary units                                  |
| AFM            | Atomic Force Microscope                          |
| AMREC          | Advance Materials Research Centre                |
| Ar             | Argon  |
| $\text{Ar}^+$  | Argon ion  |
| $\text{CH}_4$  | Methane  |
| CNT            | Carbon Nanotube                                  |
| CO             | carbon monoxide                                  |
| Co             | Cobalt   |
| Cps            | Count per second                                 |
| CRT            | Cathode Ray Tube                                 |
| CVD            | Chemical Vapour Deposition                       |
| DOS            | Density of States                                |
| DTA            | Differential Thermal Analysis                    |
| e.g.           | exempli gratia                                   |
| etc            | et cetera  |
| Fe             | Iron   |
| FESEM          | Field Emission Scanning Electron Microscope      |
| HCl            | Hydrochloride Acid                               |
| He             | Helium   |
| HF             | Hydrofluoric Acid                                |
| $\text{HNO}_3$ | Nitric Acid                                      |
| HRTEM          | High Resolution Transmission Electron Microscopy |
| IMRE           | Institute of Materials Research and Engineering  |
| JCPDS          | Joint Committee on Powder Diffraction            |
| MWNT           | Multi-walled Carbon Nanotube                     |
| n.d.           | no date  |

|                 |                                      |
|-----------------|--------------------------------------|
| N <sub>2</sub>  | Nitrogen                             |
| Ne              | Neon                                 |
| NH <sub>3</sub> | Ammonia                              |
| Ni              | Nickel                               |
| nm              | nanometer                            |
| O <sub>2</sub>  | Oxygen                               |
| plc             | Public Limited Company               |
| RBM             | Radial Breathing Mode                |
| sccm            | standard centimetre cubic per minute |
| SEM             | Scanning Electron Microscopy         |
| Si              | Silicon                              |
| STM             | Scanning Tunnelling Microscopy       |
| SWNT            | Single-walled Carbon Nanotube        |
| TEM             | Transmission Electron Microscopy     |
| TGA             | Thermal Gravimetry Analysis          |
| UK              | United Kingdom                       |
| US              | United States of America             |
| UTP             | Universiti Teknologi PETRONAS        |
| wt              | weight                               |
| WTEC            | World Technology Evaluation Centre   |
| XRD             | X-Ray Diffractometry                 |

## **Chapter 1: INTRODUCTION**

### **1.1 A Paradigm Shift Towards Nanotechnology**

Nanotechnology is the art and science of building complex, practical devices with atomic precision. In an effort to construct useful machines, nanotechnologists apply the techniques of engineering to the knowledge generated by the sciences that study molecular structures (Crandall, 1996). In 1960, Nobel laureate Richard Feynman presented a visionary and prophetic lecture at a meeting of the American Physical Society, entitled “There is Plenty of Room at the Bottom,” where he speculated on the possibility and potential of nanosized materials (Poole *et al.*, 2003, Hughes, 2003). He envisioned etching lines a few atoms wide with electrons beam and proposed manipulating individual atoms to make new small structures having very different properties. Many of Feynman’s speculations have become reality.

In recent years nanotechnology has become one of the most important and exciting forefront fields in physics, chemistry, engineering and biology. It shows great promise for providing us in the near future with many breakthroughs that will change the direction of technological advances in a wide range of applications.

The current widespread interest in nanotechnology dates back to the years 1996 to 1998 when a panel under the auspices of the World Technology Evaluation Centre (WTEC), funded by the United States of America National Science Foundation and other federal agencies, undertook a world-wide study of research and development in the area of nanotechnology, with the purpose of assessing its potential for technology innovation.

The WTEC study concluded that this technology has enormous potential to contribute to significant advances over a wide range of technological areas ranging from producing stronger and lighter materials, to shortening the delivery time of nanostructured pharmaceuticals to the body's circulatory system, increasing the storage capacity of magnetic tapes and providing faster switches for computers.

Numerous reports on new physical phenomena and advanced properties of materials in the extremely infinitesimal areas of nanoscale size in recent years have appeared, creating a new area called nanotechnology. This nanotechnology has emerged as a future leader in areas, such as electronic information communications, medicine, material, production process, environment, and energy. As new material properties of carbon nanotubes, in particular, can be realized among other nanotechnologies, both the importance in basic research and industrial applicability are being put in the great limelight.

The research area of nanotechnology is interdisciplinary, covering a wide variety of subjects ranging from the chemistry of the catalysis of nanoparticles to the physics of the quantum dot laser. The present trend towards miniaturisation - the competitive quest for ever smaller machines and components that use less resources (e.g. energy, materials) - while offering the potential for the cheap mass-production of increasingly complex goods is rapidly pushing industry into the nanometer realms.

The coming era of nanotechnology is being made possible by the remarkable convergence of many technological advances in this decade that include:

- Hugely powerful computers that allow the design of new materials and the simulation of their properties.
- A new generation of microscopes that can provide images at the nanometer scale, as well as measure and manipulate atoms and molecules.
- The advent of virtual reality that enables us to visit and experience the wonders of this new and hitherto unimaginable nanoworld.

As the work of scientists tends increasingly towards the size domains of molecules and atoms, the very nature of matter is increasingly close to being controlled and manipulated. The possibilities this opens up are endless: from the production of new, lighter and stronger materials which have applications in areas as diverse as space travel to bone implants, to the creation of therapeutic drugs with individual specific properties.

The role of nanotechnology as a major driver of technological change and its consequent importance in the shaping of world economies in the next millennium is undisputed, as evidenced by the commitment to nanoscale research by the United States (US) and Japan. It is crucial that the United Kingdom (UK) also identifies those technologies that may offer the most economic benefits.

A recent survey has demonstrated that the market for microengineered products is greatest in electronics and biomedicine. These conclusions can in very general terms be extrapolated to nanotechnology. The UK is not an owner of electronics or semiconductor technology in the main, but tremendous opportunities exist in integrating these technologies into systems or components in high added value niche market products for biomedical and related applications. These applications include medical and environmental sensors, diagnostic and analytical devices, and range of equipment for minimally invasive surgery. There may be also being some potential for low cost, high volume applications in these areas.

## 1.2 Objective and Scope of Research

Nanotechnology research in Malaysia is still at infancy stage specifically carbon nanotube, a newly introduced nanostructured material in this country. Not much work has been done especially on the application of CNTs. This is due to lack of understanding of the behaviour and the synthesis fundamental of the material.

CNT has exhibited remarkable mechanical properties whereby its Young's modulus for example is about 1.25 TPa (Krishnan *et al.*, 1998), which is six times higher than steel ( $\sim 0.2$  TPa) (Smith, 1996) while they are one-sixth its weight. This has caught the attention to use CNTs as reinforcement for lightweight composite applications. In order to produce a good composite, narrow diameter range of CNTs are required (Qian *et al.*, 2000 and Cadek *et al.*, 2004).

The objective of this work is to produce good quality CNTs with narrow diameter range, high purity and uniformity to be used as a component for composite reinforcement. Previous works (Ivanov *et al.*, 1995, Yudasaka *et al.*, 1995) reported that highly uniform CNTs can be obtained by using catalytic method. Thus, investigation on the effect of growth parameter specifically the catalysts preparation is needed in order to understand the effect on the structure of CNTs produced.

However, because of the infancy of this field in Malaysia especially on preparing nanosized catalysts, many unanswered questions remained. Thus, the focus of this work is to develop a new method of catalysts preparation, which may lead to producing narrower diameter range of CNTs. One of the growth parameter identified to be the main factor affecting the structure of CNTs is the etching time in preparing the catalysts. The catalyst effect on the quality of CNT will also be studied by using three different catalysts. Iron, cobalt and nickel are selected because previous works have shown promising results by using these catalysts on catalytic method.

The successfully grown CNTs would then be examined structurally by scanning electron microscope and X-ray diffractometer in order to verify the diameter range obtained and analyse the morphology of CNTs grown on different catalyst. Crystallinity properties of the products can be investigated by using high-resolution transmission microscope, thermo gravimetric analyser and Raman spectroscopy. The purification of CNTs will also be studied by structural characterisation in order to produce a highly purified CNTs.

The ultimate aim of the work would be to propose a tested and proven methodology to produce CNTs with defined structure specifically narrow diameter range, high uniformity and crystallinity. All the work would lead to produce CNTs that may be used as the component for mechanical reinforcement of the polymer composite.

### 1.3 Thesis outline

The thesis we will discuss the research on synthesis process of carbon nanotube that cater our own research purpose. Beside that, several characterisation tests have been carried out in order to understanding characteristic of the materials.

Chapter 1 gives a general introduction of nanotechnology and carbon nanotubes, both from a fundamental point of view and for future applications. The objective given here will be able to show how the research work fit in the current research activities genuinely in Malaysia and specifically in nanotechnology research.

Chapter 2 gives an overview of carbon nanotubes properties. The most eye-catching features of carbon nanotubes are their structure, growth mechanism, mechanical and electronic properties, which open a way to future applications. Its growth method or fabrication issues that are needed to make carbon nanotube were also discussed in detail. The most common techniques used nowadays are: arc discharge, laser ablation

and chemical vapour deposition. A short overview on the theory of XRD, SEM, TEM, TGA and Raman spectroscopy, which is the main characterization technique in this thesis to study each synthesized individual carbon nanotubes characteristic also is briefly discuss.

Chapter 3 describes the experimental methods employed for this study. Comment and observations of characterisation results obtained were presented and discussed in chapter 4. Finally, in chapter 5, the conclusions and future works are discussed in a broader perspective.

## **Chapter 2: THEORY AND LITERATURE REVIEW**

### **2.1 Carbon Nanotubes**

One of the nanostructured materials that have spurred a tremendous interest worldwide for various applications is carbon nanotube. CNTs provide a unique structure that has stimulated research in both science and engineering. What makes them so intriguing is that they consist of a nanotube lattice of carbon-carbon covalent bonding that is one of the strongest in nature, and they have many unique properties such as high conductivity, chemical specificity, inertness, and an unusual electronic structure. The nano-dimensions of the hollow carbon nanotubes result in a high surface area as well as a low density, which lead to many potential mechanical and chemical applications.

In ideal case, a carbon nanotube consists of a hexagonal network of carbon atoms rolled up into a hollow cylinder and is capped off by two fullerene (buckyball) halves. These tubes can reach tens of micrometers long and still have diameters as low as 0.7 nm (Dresselhaus *et al.*, 1996). The first reported discovery of carbon nanotubes was in 1991 by Sumio Iijima of the NEC Laboratory in Tsukuba, Japan (Iijima, 1991). Multiwalled carbon nanotubes were first discovered using transmission electron microscope, and two years later single-walled carbon nanotubes were discovered experimentally by Iijima in Japan and Bethune at the IBM Almaden Laboratory in California (Iijima *et al.*, 1993; Bethune *et al.*, 1993). In 1992, it was predicted that carbon nanotubes could either be semiconducting or metallic depending on their geometrical characteristics like the diameter and the chiral winding of the carbon

network along the tube shell. Later in 1998, these predictions were experimentally proven. With their wide range of properties, research continues at a rapid pace. New synthesis techniques continue to undergo research and development to provide a larger quantity of pure carbon nanotubes as well as a lower price which would allow for research to extend out and pave the way for more manufactured applications.

Nanotubes are composed entirely of  $sp^2$  bonds, similar to graphite. Stronger than the  $sp^3$  bonds found in diamond, this bonding structure provides them with their unique strength. Nanotubes naturally align themselves into "ropes" held together by Van der Waals force. Under high pressure, nanotubes can merge together, trading some  $sp^2$  bonds for  $sp^3$  bonds, giving great possibility for producing strong, unlimited-length wires through high-pressure nanotube linking. Carbon nanotubes are fullerene-related structures, which consist of graphene cylinders closed at either end with caps (see Figure 2.1) containing pentagonal rings. The first discovery in 1991 by the Japanese electron microscopist Sumio Iijima was made when he studied the material deposited on the cathode during the arc-evaporation synthesis of fullerenes. He found that the central core of the cathodic deposit contained a variety of closed graphitic structures including nanoparticles and nanotubes, of a type, which had never previously been observed. A short time later, Thomas Ebbesen and Pulickel Ajayan, from Iijima's lab, showed how nanotubes could be produced in bulk quantities by varying the arc-evaporation conditions. This paved the way to an explosion of research into the physical and chemical properties of carbon nanotubes in laboratories all over the world.

A major event in the development of carbon nanotubes was the synthesis in 1993 of single-layer nanotubes. The standard arc-evaporation method produces only multilayered tubes. It was found that addition of metals such as cobalt to the graphite electrodes resulted in extremely fine tube with single-layer walls. The availability of these structures should enable experimentalists to test some of the theoretical predictions, which have been made about nanotube properties.

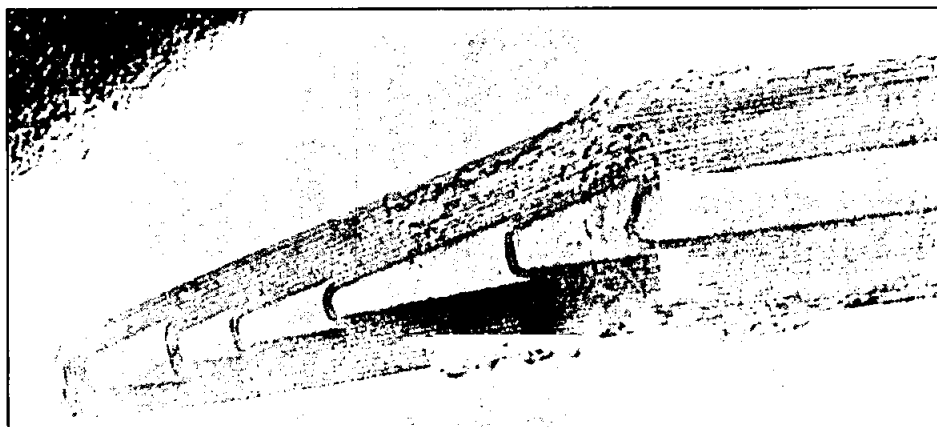


**Figure 2.1:** Typical high resolution TEM image of a nanotube cap. (Reproduced from Harris, 1999).

An alternative method of preparing single-walled nanotubes was described by Smalley's group in 1996. Like the original method of preparing  $C_{60}$ , this involved the laser-vaporisation of graphite, and resulted in a high yield of single-walled tubes with unusually uniform diameters. These highly uniform tubes had a greater tendency to form aligned bundles than those prepared using arc-evaporation, and led Smalley to christen the bundles nanotube "ropes". Initial experiments indicated that the rope samples contained a very high proportion of nanotubes with a specific armchair structure. Subsequent work has suggested that the rope samples may be less homogeneous than originally thought. Nevertheless, the synthesis of nanotube ropes gave an important boost to nanotube research, and some of the most impressive work has been carried out on these samples.

### 2.1.1 Single-Walled Carbon Nanotubes

Since their discovery, multiwalled carbon nanotubes (MWNTs) and single-walled carbon nanotubes (SWNTs) have attracted great interest because of their unique mechanical and electronic properties. SWNTs comprise single (capped) graphene cylinder, with typical diameters of 1 to 2 nm although larger diameters up to nearly 6 nm may be accessed depending on production method and catalyst. SWNT bulk

samples are often made up of intertwined crystalline bundles, which in turn consist of hexagonally close-packed individual tubes. Bundles will be forming during SWNT synthesis.

SWNTs give every indication that they will make a major impact on science and technology. Their unusual physical and chemical properties, which depend on nanotube diameter and helicity, make them particularly attractive for future molecular nanotechnology applications. Production of a variety of nanotubes will be necessary to explore novel properties arising from a variety of detailed atomic structures. Adding catalyst promoter alters the diameter range to a much smaller range, with a variety of helicities, and dramatically increases the nanotube yields. The results indicate the need for a general growth mechanism that accounts for the effect of catalyst promoters.

Single walled nanotubes (see Figure 2.2) are long tubes made entirely out of carbon. They can be thought of as being made from a planer sheet of graphite (a hexagonal planar carbon network) that is wrapped into a seamless tube, nanometers in diameter and microns in length. The tubes can be either open at their ends or capped at one or both ends with half a spheroidal fullerene. A nanotube is completely specified by what is referred to as a roll up vector, which identifies its helicity and diameter. Depending on its roll-up vector, a nanotube can be either semiconducting or metallic in its electronic transport characteristics.

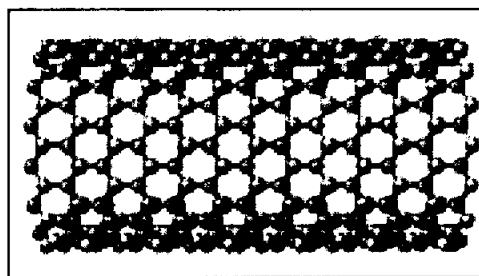


**Figure 2.2:** A single walled carbon nanotube. (Reproduced from Dresselhaus *et al.*, 2002).

Since the discovery of single-walled carbon nanotubes (SWNTs) in 1993, numerous studies have shown that they are stable and possess many useful chemical, electrical, and mechanical properties. Many applications, ranging from hydrogen storage in fuel cells to molecular electronic devices, would benefit from the availability of SWNTs of varying diameters and helicities. SWNTs with a variety of diameters in significant quantities is advantageous for testing many theoretical predictions and for practical applications such as hydrogen storage, molecular electronics, nanoelectrical machines, and gas separations. For example, a 3-nm diameter nanotube may achieve the goal as hydrogen storage medium for practical vehicular fuel-cell applications. Since several purification and separation techniques have been developed, one may soon be able to separate SWNTs according to their sizes. Many of the electrical, mechanical, and chemical properties that depend on the diameters may now be tested.

The effect of different chemical elements on the growth of SWNTs should provide opportunities for both optimizing the synthetic process and understanding the growth mechanism. Different promoters having similar catalytic effect suggests that growth of SWNTs is dominated by factors that are intrinsic to the mechanism. Thus only modifying the reaction pathway can significantly alter the range, whereas changing reaction environment may only fine-tune the range.

Large-scale production of exclusively SWNT in high yields is a crucial step toward future advances in carbon nanotubes research. A credible growth model should be able to explain the effect of catalyst promoters and allow the formation of a wide range of SWNT structures.

### **2.1.2 Multiwalled Carbon Nanotubes**

Carbon nanotubes and nanorods have attracted attention in recent years not only for their small dimension and unique morphologies, but also for their potential of

applications in various technologies. Nanotubes can be thought of as single graphite sheets wrapped into seamless cylinder. They can be semiconducting, semi metallic, or metallic, depending on the wrapping angle and tube diameter. Their high mechanical strength, capillary properties, and remarkable electronic structure allow envisagement of potential uses. Another important use of CNTs is that some other important one-dimensional nanomaterials can be produced, such as tubular oxides, wire- or rod like carbides, and rod like Galium Nitride, by using the CNTs as the pre-existing templates. Most nanotubes consist of several concentric layers as show in Figure 2.3 and is called multiwalled nanotubes. However single-walled nanotubes as described earlier have also been found.

Multiwalled nanotubes are synthesized through different methods depending on their application. The growth of multiwalled carbon nanotubes in the absence of metal catalyst is observed for the first time in hydrothermal conditions. Formation of quality multiwalled carbon nanotubes has never been observed previously in the C-H-O system at this range of relatively mild temperatures (below 800°C) (Yoshimura *et al.*, 2001). Multiwall formation does not take place from the gas phase in these liquids like experimental conditions. It involves rearranging atomic bonds of amorphous carbon induced by the reactivity of the hot hydrothermal fluid and the enhanced mobility of carbon clusters.

Molecular level components, like multiwalled carbon nanotubes (MWNT), show great potential for future nanoelectronics. At low frequencies, only the outermost carbon layer determines the transport properties of the MWNT. Due to the multiwalled structure and large capacitive interlayer coupling, also the inner layers contribute to the conduction at high frequencies. Consequently, the conduction properties of MWNTs are not very far from those of regular conductors with well-defined electrical characteristics.

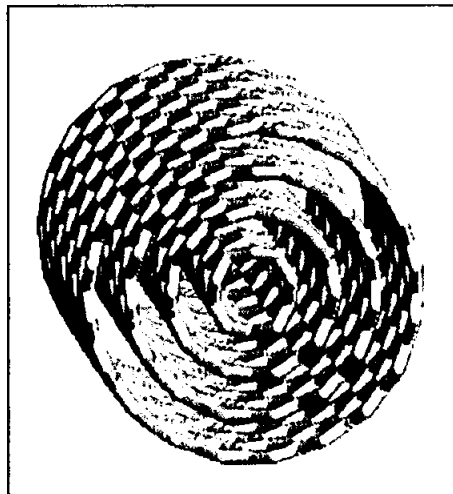


**Figure 2.3:** A multiwalled carbon nanotube. (Reproduced from Dresselhaus *et al.*, 2002).

### 2.1.3 Structure of Carbon Nanotubes

Even though it is not the way in which nanotubes are formed, the most intuitive way to illustrate the structure of nanotubes involves the rolling up of a single sheet of graphite. Figure 2.4 illustrates classical construction of nanotube structure. The vector  $OA$  connects two equivalent points on a graphene sheet. This sheet can then be "cut" along arbitrary, parallel vectors  $OB$  and  $AB'$  and the resulting strip of graphene rolled into a tube. The unit cell of the tube is then specified by  $OA$  called the chiral vector  $C_h$ , and  $T$ , the lattice vector, defined by the first inter-section along  $OB$  with a point of the graphene lattice. (Saito *et al.*, 1998).

The chiral vector itself can be expressed in terms of the unit vectors  $a_1$  and  $a_2$  of the graphene lattice, as seen in the lower part of Figure 2.4. In this way a particular nanotube is most often specified by a pair of integers  $(n, m)$  such that  $C_h = na_1 + ma_2$ , or it can be specified in terms of the angle  $\theta$  between  $a_1$  and the chiral vector, and its diameter  $d$ . Due to symmetry, all tubes can be described by  $0 \leq m \leq n$  and  $0 \leq \mu \leq 30^\circ$ .

Additionally, relations between the different parameters exist, such that for instance the diameter can be computed from the indices (n, m).

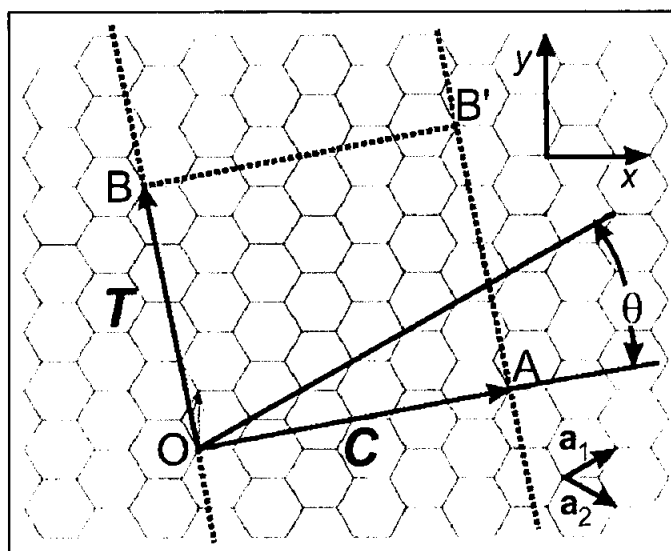


Figure 2.4: Classical construction of nanotube structure. (Reproduced from Saito *et al.*, 1998).

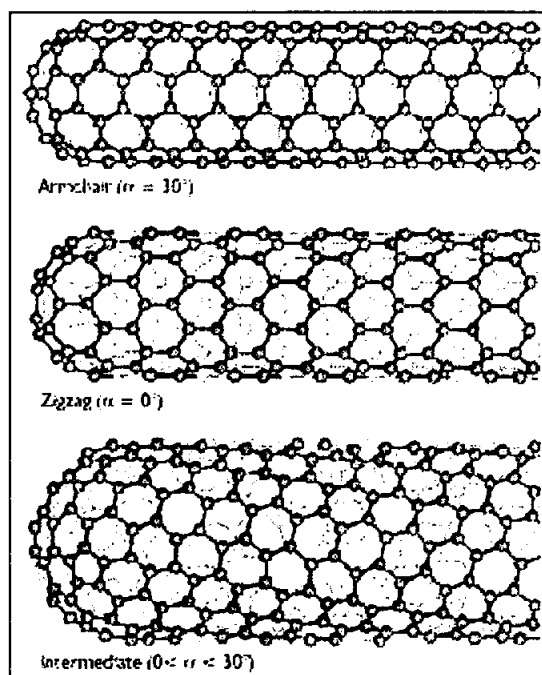


Figure 2.5: Variety of SWNT structures corresponding to the many ways a sheet of graphite can be wrapped into a seamless tube. (Reproduced from Saito *et al.*, 1998).

As will be further justified, a natural classification of nanotubes divides them into three groups based on the visual appearance of their physical structure: Armchair nanotubes where  $C_h = (n, n)$ , zigzag nanotubes where  $C_h = (n, 0)$  and chiral nanotubes where  $C_h = (n, m)$  as illustrated in Figure 2.5. Each structure has a specific diameter and chirality, or wrapping angle ( $\alpha$ ). The “armchair” structures, with  $\alpha = 30^\circ$ , have metallic character. The “zigzag” tubes, for which  $\alpha = 0^\circ$ , can be either semi metallic or semiconducting, depending on the specific diameter (see Figure 2.5). Nanotubes with chiral angles intermediate between 0 and  $30^\circ$  include both semimetals and semiconductors. “Armchair” and “zigzag” refer to the pattern of carbon–carbon bonds along a tube’s circumference. (Saito *et al.*, 1998).

The structure described above was confirmed through the use of two techniques, electron diffraction in the early days of nanotube research, i.e. the first papers published by Iijima *et al.*, (1993) and later by Scanning Tunnelling Microscopy (Wildöer *et al.*, 1998).

#### 2.1.4 Growth Mechanisms of Carbon Nanotubes

The way in which nanotubes are formed is not exactly known. The growth mechanism is still a subject of controversy, and more than one mechanism might be operative during the formation of CNTs. One of the mechanisms consists out of three steps. First a precursor to the formation of nanotubes and fullerenes,  $C_2$ , is formed on the surface of the metal catalyst particle. From this metastable carbide particle, a rod like carbon is formed rapidly. Secondly there is a slow graphitisation of its wall. This mechanism is based on in-situ TEM observations (Yasuda *et al.*, 2002).

The exact atmospheric conditions depend on the technique used, later on, these will be explained for each technique as they are specific for a technique. The actual growth of the nanotube seems to be the same for all techniques mentioned.

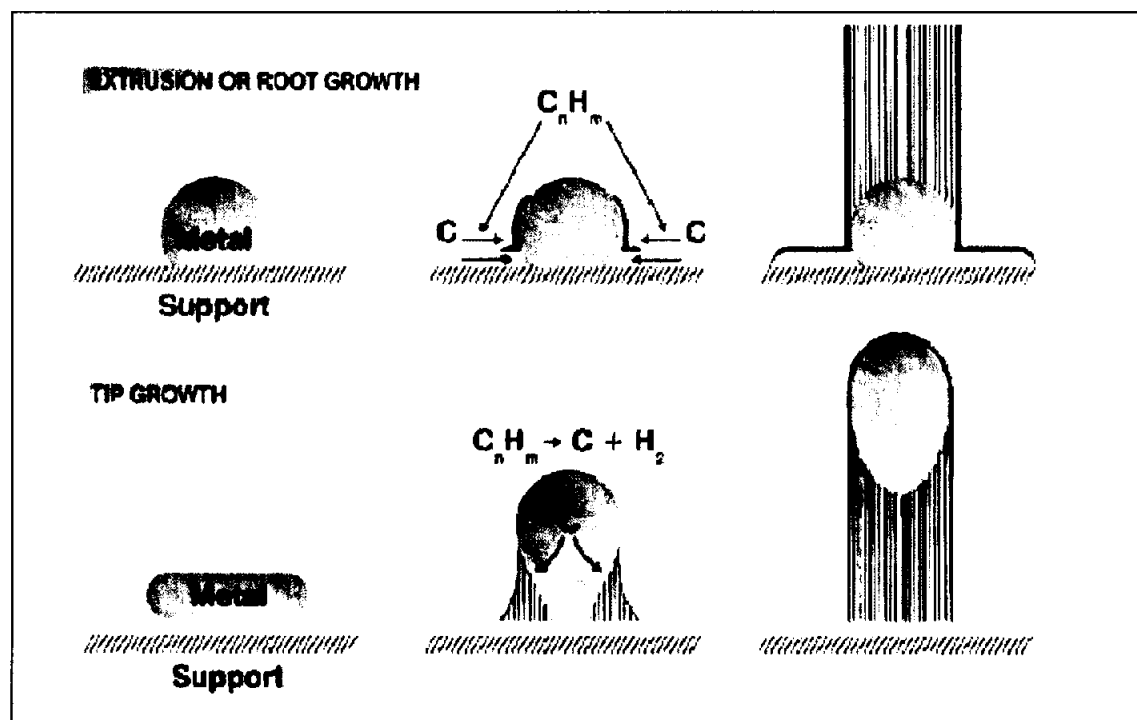


**Figure 2.6:** Visualization of a possible carbon nanotube growth mechanism. (Reproduced from Kónya, 2001).

There are several theories on the exact growth mechanism for nanotubes (see Figure 2.6). One theory postulates that metal catalyst particles are floating or are supported on graphite or another substrate (Sinnot *et al.*, 1999). It presumes that the catalyst particles are spherical or pear-shaped, in which case the deposition will take place on only one half of the surface (this is the lower curvature side for the pear shaped particles). The carbon diffuses along the concentration gradient and precipitates on the opposite half, around and below the bisecting diameter. However, it does not precipitate from the apex of the hemisphere, which accounts for the hollow core that is characteristic of these filaments. For supported metals, filaments can form either by ‘extrusion (also known as base growth)’ in which the nanotube grows upwards from the metal particles that remain attached to the substrate, or the particles detach and move at the head of the growing nanotube, labelled ‘tip-growth’. Depending on the size of the catalyst particles,

SWNT or MWNT are grown. In arc discharge, if no catalyst is present in the graphite, MWNT will be grown on the C<sub>2</sub>-particles that are formed in the plasma.

### 2.1.5 Mechanical Properties of Carbon Nanotubes

The mechanical properties of carbon nanotubes are also of large interest to scientists. Nanotubes may be called the ultimate fibres because of their lightweight and the predicted record-high strength. Carbon nanotubes can be hundred times stronger than steel while they are one-sixth its weight. There are no experiments done yet to confirm such a high tensile strength. However, experiments have already demonstrated that nanotubes have an extremely high Young's modulus, on the order of TPa, and that they resist deformation remarkably well. When they are strongly bent, nanotubes do not break but 'buckle', which means that the cylindrical structure locally stretched, just as what happens to a drinking straw. When the bending strain is released, the nanotube resumes its original straight shape. Nanotubes therefore appear to be ideal tips for scanning probe microscopes since they are not only very small but also survive crashes with the sample surface (Ajayan, 2000).

High-resolution transmission electron microscopy (HRTEM) observations reveal that nanotubes are remarkably flexible (Ajayan *et al.*, 1994 and Iijima *et al.*, 1996). For instance, they can be bent mechanically by sonication, grinding or by being embedded in a polymer resin (Ajayan *et al.*, 1994). Theoretical calculations predicted these properties, noting that the tubes would soften with decreasing radius. It was also predicted that the tube stiffness would be dependent upon chirality (e.g. zigzag tubes would be less stiff than that of armchair tubes).

The first attempt to determine Young's modulus for individual MWNTs was made by Treacy *et al.* (1996) who measured by TEM, the amplitudes of thermal vibrations in single nanotubes. The results showed that the nanotubes possess an average Young's

modulus of  $Y = 1.8 \text{ TPa}$ , which is much higher than that of commercially available carbon fibres ( $Y \sim 800 \text{ GPa}$ ).

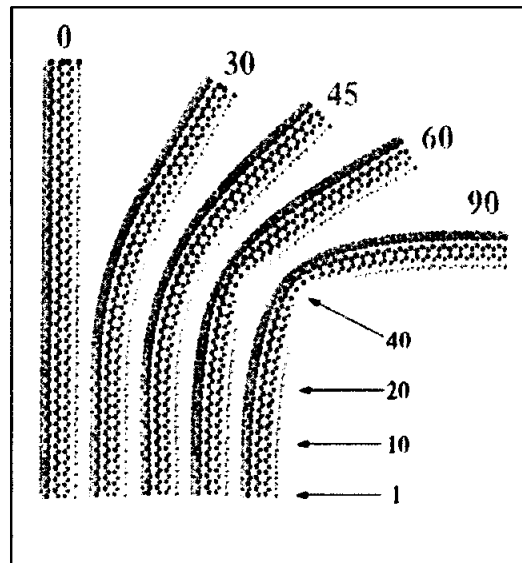


**Figure 2.7:** CNT will rather buckle than break when force applies on it. (Reproduced from Smalley, n.d.)

Recently, direct measurements of the bending force as a function of displacement, inside an atomic force microscope (AFM), on individual CNTs revealed an average Young's modulus of  $1.28 \text{ TPa}$ . In this context, Falvo *et al.* (1997) reported that CNTs could be repeatedly bent through large angles using the tip of an AFM, without undergoing catastrophic failure. Local strains as large as 16% have been sustained without separating a nanotube. In fact, separation of a nanotube by the repeated application of bending stresses has yet to be observed. The compressive strength of thin- and thick-walled nanotubes was reported to be more than two orders of magnitude higher than the compressive strength of any known fibre (which lies in the  $0.5 \text{ GPa}$  range). Furthermore, TEM micrographs of MWNTs under compression show that they behave as elastic rods and form bends and loops, although under high bending, they collapse to form kinks on the internal (compression) side of the bend (Lourie *et al.*, 1998).

Remarkably, the addition of only 1 wt.% MWNTs to polystyrene increases the polymer mechanical properties significantly. Tensile tests performed on composite films show that 1 wt.% MWNT additions result in 36 to 42 % and approximately 25 % increase in elastic modulus and break stress, respectively, indicating significant load transfer across the nanotube-matrix interface. Tensile tests and in situ TEM observations have shown that an external load can be effectively transferred to the nanotubes (Qian *et al.*, 2000).

In MWNTs there is a weak coupling between the outer and inner layers of the tube (Van der Waals forces). This is especially true under tensile loading when the load transfer occurs from the matrix to only the outer nanotube layer bonded to the polymer. The situation in SWNT composites is different; the polymer infiltrates the interstices of the nanotube ropes and creates a certain degree of interlocking, therefore further enhancing mechanical strength. This section demonstrates that carbon nanotubes are a material with extraordinary strength, which makes them good candidates for super strong carbon fibre reinforced materials.

### 2.1.6 Electronic Properties of Carbon Nanotubes

Carbon nanotubes can be semiconducting or metallic which depends on two parameters, the diameter and the chiral winding of the carbon network along the tube shell. Although this prediction was already made in 1992, it was confirmed experimentally only six years later by scanning tunnelling microscopy (STM) measurements (Wildöer *et al.*, 1998). STM proved to be a useful technique to study nanotubes since it has the power to reveal both the atomic and electronic structure. It is possible to obtain beautiful images of atomically resolved nanotubes from which their chiralities can be obtained. An example is shown for example in Figure 2.8 together with a theoretical model of a nanotube with a comparable chirality (Ajayan, 2000).

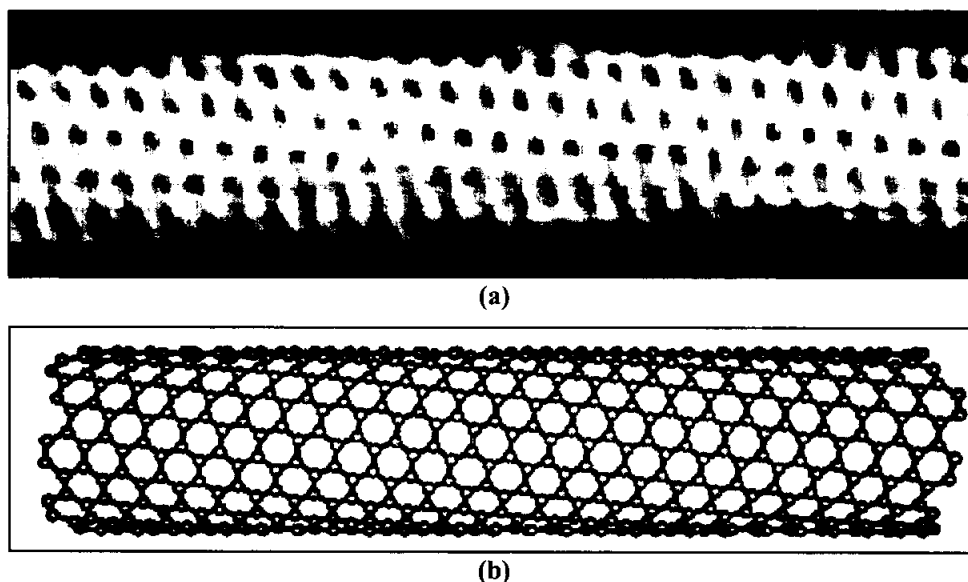


**Figure 2.8:** (a) An atomically resolved STM image of a chiral carbon nanotube compared to (b) a theoretical model of a nanotube with a similar chirality. (Reproduced from Ajayan, 2000).

The tip of an STM can also be used as a spectroscopic probe by keeping the tip fixed above the sample and measure the tunnel current as a function of the bias voltage. By taking current-voltage spectra on a large number of nanotubes with various chiralities, two classes of nanotubes could be identified (see Figure 2.9). The STM spectra for these two classes corresponded remarkably well to the predicted electronic density of states (DOS) for the metallic and the semiconducting type, respectively. Due to the quantization of available energy modes in the circumferential direction the DOS for nanotubes does not consist of one smooth band but it splits up into several sub-bands with sharp singularities at the onsets. These sub-bands represent separate one-dimensional channels for conduction along the nanotube. The sub-bands and their sharp onsets were indeed observed in the tunnelling DOS that was obtained from the STM spectroscopy measurements.

Both the semiconducting and metallic type of nanotubes may be of use for nanoscale electronic devices. Junctions between two different nanotubes that have a different electronic character are interesting as well. Theoretical calculations have shown that two nanotubes with different chirality and similar diameter can connect to each other

when defect pairs of five- and seven-rings of carbon are present in the hexagonal carbon lattice (Lambin *et al.*, 1995). The connections appear as sharp kinks (see Figure 2.10(a)), which have been also observed in real nanotube material. Figure 2.10(b) shows for example a sharply kinked nanotube lying across electrodes. Recent electronic transport measurements on this type of sample indicate that these kinks can indeed be semiconductor-metal junctions (Yao *et al.*, 1999).

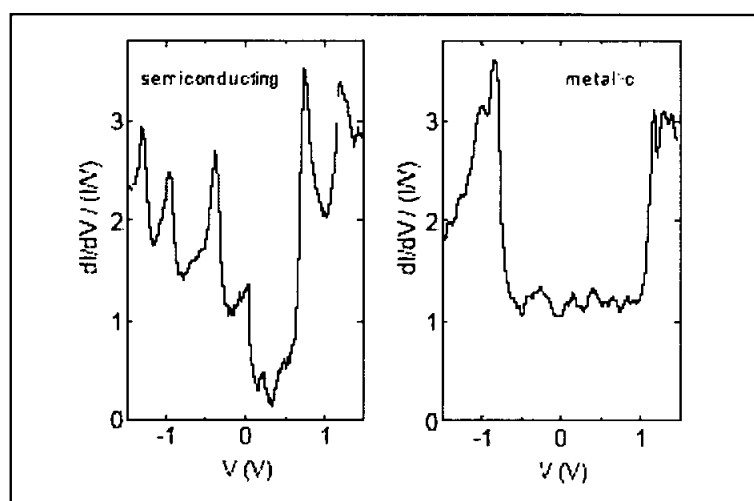


**Figure 2.9:** Two classes of STM spectra can be observed on nanotubes. (Reproduced from Dekker, 1999).

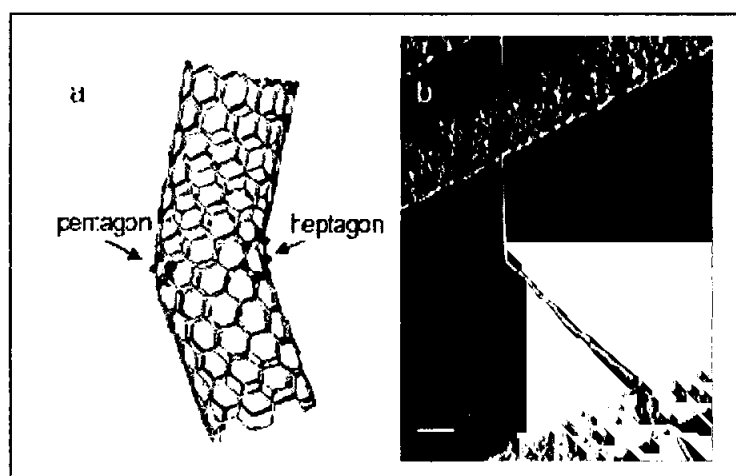


**Figure 2.10:** Nanotube kinks. (a) A theoretical model and (b) a nanotube that contains a kink lying across electrodes. The scale bar is 200 nm. (Reproduced from Yao *et al.*, 1999).

## 2.2 Advances of Carbon Nanotubes in Cutting Edge Application

The overwhelming message to convey is the unique structure, topology and dimensions of carbon nanotubes have created a superb all carbon material, which can be considered as the most perfect fibre that has ever been fabricated. The remarkable physical properties of nanotubes creates a host of application possibilities, some derived as an extension of traditional carbon fibre application, but many are new possibilities, based on the novel electronic and mechanical behaviour of nanotubes as shown in Table 2.1. It needs to be said that the excitement in this field arises due to the versatility of this material and the possibility to predict properties based on its well-defined crystal lattice. Nanotubes truly bridge the gap between the molecular realm and the macro-world, and are destined to be a star in future technology. The last few years, however, have seen important breakthroughs in the potential of materials science related applications of nanotubes and the challenges that need to be overcome to reach these hefty goals.

Carbon nanotubes possess many unique and remarkable properties (chemical, physical, and mechanical), which make them desirable for many applications. The slender proportions of carbon nanotubes hide a staggering strength: it is estimated that they are six times stronger than steel at only one sixth of the weight, almost certainly the strongest fibres that will ever be made out of anything, strong enough even to build an elevator to space. In addition they conduct electricity better than copper and transmit heat better than diamond.

Researchers anticipate nanotube applications in several important areas. One use is as field emitters in flat-panel display technologies - an application that will probably become available as products sooner than any other. Samsung demonstrated a working nanotube display prototype in 1999, and the company may introduce a product during 2004. In Samsung's display, the small, rod-shaped nanotubes provide sharp conductive points that allow a field-emission display to work more efficiently than today's

television screens and computer monitors. SWNT displays could eventually displace liquid crystal and plasma displays in large flat panels because the carbon nanotube panels should be less complex and less expensive to manufacture.

**Table 2.1:** Applications of carbon nanotubes.

| <b>Applications of Carbon Nanotubes</b>     |  |
|---|--|
| Micro-electronics / semiconductors          | Conducting composites                                    |
| Controlled drug delivery/release            | Artificial muscles                                       |
| Super capacitors                            | Batteries  |
| Field emission flat panel displays          | Reinforcement of polymer                                 |
| Nanolithography                             | Nanoelectronics  |
| Doping                                      | Nanobalance  |
| Nanotweezers                                | Data storage   |
| Magnetic nanotube                           | Nanogear   |
| Nanotube actuator                           | Molecular quantum wires                                  |
| Hydrogen storage                            | Noble radioactive gas storage                            |
| Solar storage                               | Waste recycling  |
| Electromagnetic shielding                   | Dialysis filters   |
| Thermal protection                          | Nanotube reinforced composites                           |
| Reinforcement of armour and other materials | Field Effect transistors and single electron transistors |
| Avionics                                    | Collision-protection materials                           |

Because carbon nanotubes are very strong, there is also interest in them for their mechanical properties. Thus, SWNTs may provide reinforcing elements for composite materials that would have exceptional mechanical and, possibly, superior thermal characteristics. Another potential application lies in ultra miniaturized electronics. Companies such as IBM have active research programs investigating how they could

use carbon nanotubes for future generations of non-silicon microchip circuitry, which could be 0.01% the size of today's most advanced versions, or even smaller.

Enhancements in miniaturisation, speed and power consumption, and size reduction of information processing devices, memory storage devices and flat displays for visualisation are currently being developed.

The most immediate application for nanotubes is in making strong, lightweight materials. It will be possible to build a car that is lighter than its human driver, yet strong enough to survive a collision with a tank.

Aircraft built with stronger and lighter materials will have longer life spans and will fly at higher temperatures, faster and more efficiently.

Nanotubes are being explored as receptacles - storage tanks - for hydrogen molecules to be used in the fuel cell that could power automobiles of the future. Hydrogen does not produce pollution or greenhouse emissions when burned and is considered to be the clean energy of the future.

Global Warming is of great concern to all nations. It is believed that carbon nanotubes will contribute to the development of an advanced method for collecting and storing the solar energy that falls upon the earth in large quantities to meet energy needs in 2050.

Carbon nanotubes are sought after for their multiple uses in cutting-edge research projects. They are the most suitable material to nanotechnology research.

Carbon nanotubes additionally can also be used to produce nanowires of other chemicals, such as gold or zinc oxide. These nanowires in turn can be used to cast nanotubes of other chemicals, such as gallium nitride. These can have very different properties from CNTs - for example, gallium nitride nanotubes are hydrophilic, while

CNTs are hydrophobic, giving them possible uses in organic chemistry that CNTs could not be used for.

One use for nanotubes that has already been developed is as extremely fine electron guns, which could be used as miniature cathode ray tubes (CRT) in thin high-brightness low-energy low-weight displays. This type of display would consist of a group of many tiny CRTs, each providing the electrons to hit the phosphor of one pixel, instead of having one giant CRT whose electrons are aimed using electric and magnetic fields. These displays are known as Field Emission Displays. A nanotube formed by joining nanotubes of two different diameters end to end can act as a diode, suggesting the possibility of constructing electronic computer circuits entirely out of nanotubes. Nanotubes have been shown to be superconducting at low temperatures.

The potential commercial applications of carbon nanotubes technology are under considerable investigation. Scientific emphasis in the technology is broad, ranging from basic research, for example, to improve means of synthesis and explore the properties of carbon nanotubes to application oriented research to fabricate strong and light composite structures, light-emission devices, probes, sensors, energy and storage devices.

Commercial interest in carbon nanotechnology will continue to increase in the coming years because opportunities exist at all levels, from commercialising these basic materials to creating new types of structures and devices. Organizations need to pay attention to this emerging technology because of its potential to disrupt well-established commercial technologies. For example, not only can carbon nanotubes improve the properties of existing electronics device but also they can enable the development of next generation electronics technologies, such as molecular electronics. However, the important commercial opportunities will be a long time coming because of the technology's numerous drawbacks, including tough competition in the materials market today's high production costs and low-volume production techniques.

## 2.3 Growth Method for Carbon Nanotubes

Carbon nanotubes are generally produced by three main techniques namely arc discharge, laser ablation and chemical vapour deposition. Though scientists are researching more economic ways to produce these structures. In arc discharge, a vapour is created by an arc discharge between two carbon electrodes with or without catalyst. Nanotubes self-assemble from the resulting carbon vapour. In the laser ablation technique, a high-power laser beam impinges on a volume of carbon - containing feedstock gas (methane or carbon monoxide). At the moment, laser ablation produces a small amount of clean nanotubes, whereas arc discharge methods generally produce large quantities of impure material. In general, chemical vapour deposition (CVD) results in MWNTs or poor quality SWNTs. The SWNTs produced with CVD have a large diameter range, which can be poorly controlled. But on the other hand, this method is very easy to scale up, which favours commercial production.

### 2.3.1 Arc-Discharge

The carbon arc discharge method, initially used for producing C<sub>60</sub> fullerenes, is the most common and perhaps easiest way to produce carbon nanotubes as it is rather simple to undertake. However, it is a technique that produces a mixture of components and requires separating nanotubes from the soot and the catalytic metals present in the crude product. This method creates nanotubes through arc-vaporisation of two carbon rods placed end to end, separated by approximately one millimeter, in an enclosure that is usually filled with inert gas (helium, argon) at low pressure (between 50 to 700 mbar). Recent investigations have shown that it is also possible to create nanotubes with the arc method in liquid nitrogen (Jung *et al.*, 2003). A direct current of 50 to 100 A driven by approximately 20 V creates a high temperature discharge between the two electrodes. The discharge vaporises one of the carbon rods and forms a small rod shaped deposit on the other rod. Producing nanotubes in high yield depends on the

uniformity of the plasma arc and the temperature of the deposit form on the carbon electrode (Ebbesen *et al.*, 1992).

Insight in the growth mechanism is increasing and measurements have shown that different diameter ranges have been found depending on the mixture of helium and argon. These mixtures have different diffusion coefficients and thermal conductivities. These properties affect the speed with which the carbon and catalyst molecules diffuse and cool, affecting nanotube diameter in the arc process. This implies that single-layer tubules nucleate and grow on metal particles in different sizes depending on the quenching rate in the plasma and it suggests that temperature and carbon and metal catalyst densities affect the diameter range of nanotubes (Ebbesen *et al.*, 1992).

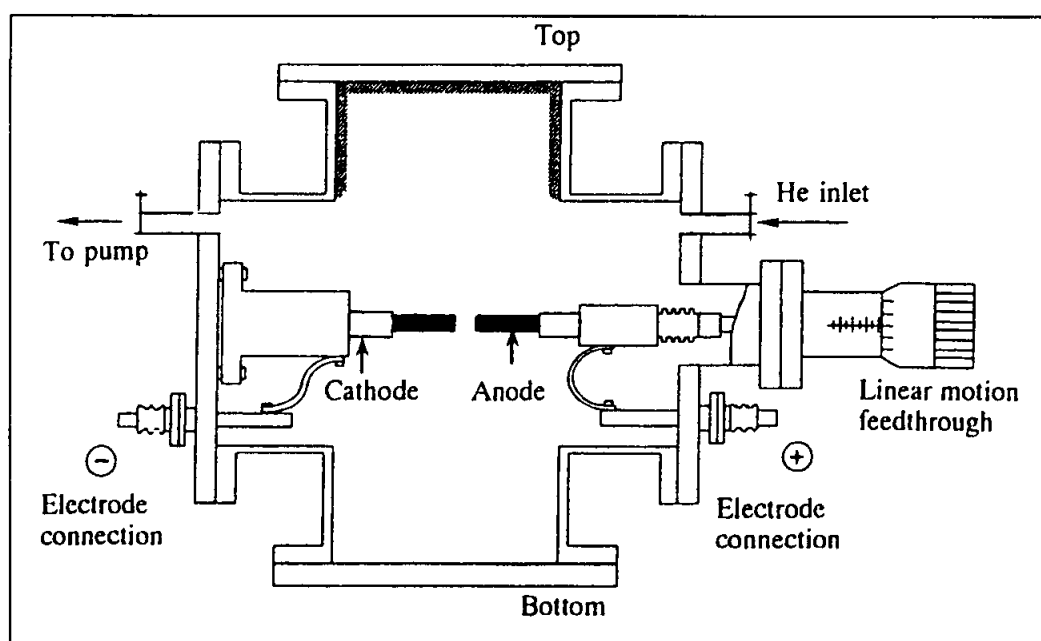


**Figure 2.11:** Schematic illustration of arc-evaporation apparatus. (Reproduced from Harris, 1999).

### 2.3.2 Laser Ablation

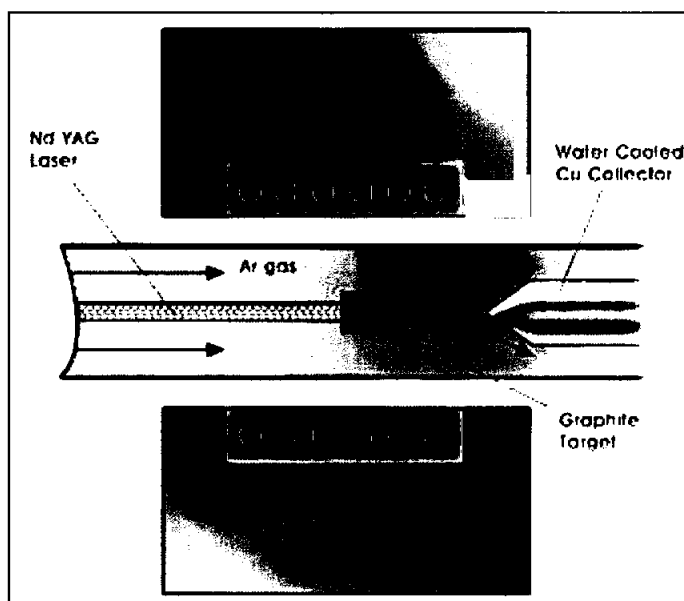


**Figure 2.12:** Schematic drawings of a laser ablation apparatus. (Reproduced from Iljin, 2001).

In 1995, Smalley's group (Guo *et al.*, 1995) at Rice University reported the synthesis of carbon nanotubes by laser vaporisation. The laser vaporisation apparatus used by Smalley's group is shown in Figure 2.12. A pulsed (Yudasaka *et al.*, 1999; Eklund *et al.*, 2002) or continuous laser (Maser *et al.*, 2002) is used to vaporize a graphite target in an oven at 1200°C. The main difference between continuous and pulsed laser, is that the pulsed laser demands a much higher light intensity (100 kW/cm<sup>2</sup> compared with 12 kW/cm<sup>2</sup>). The oven is filled with helium or argon gas in order to keep the pressure at 500 Torr. A very hot vapour plume forms, then expands and cools rapidly. As the vaporized species cool, small carbon molecules and atoms quickly condense to form larger clusters, possibly including fullerenes. The catalysts also begin to condense, but more slowly at first, and attach to carbon clusters and prevent their closing into cage structures (Scott *et al.*, 2001). Catalysts may even open cage structures when they attach to them. From these initial clusters, tubular molecules grow into single-wall carbon nanotubes until the catalyst particles become too large, or until conditions have cooled sufficiently that carbon no longer can diffuse through or over the surface of the

catalyst particles. It is also possible that the particles become that much coated with a carbon layer that they cannot absorb more and the nanotube stops growing. The SWNTs formed in this case are bundled together by Van der Waals forces (Scott *et al.*, 2001).

There are some striking, but not exact similarities, in the comparison of the spectral emission of excited species in laser ablation of a composite graphite target with that of laser-irradiated C<sub>60</sub> vapour. This suggests that fullerenes are also produced by laser ablation of catalyst-filled graphite, as is the case when no catalysts are included in the target. However, subsequent laser pulses excite fullerenes to emit C<sub>2</sub> that adsorbs on catalyst particles and feeds SWNT growth. However, there is insufficient evidence to conclude this with certainty (Scott *et al.*, 2001).

Laser ablation is almost similar to arc discharge, since the optimum background gas and catalyst mix is the same as in the arc discharge process. This might be due to very similar reaction conditions needed, and the reactions probably occur with the same mechanism.

### 2.3.3 Chemical Vapour Deposition

Chemical vapour deposition (CVD) is a material deposition technique whereby gaseous compounds react chemically near or on a heated substrate to form a solid. In thermally activated CVD, which is the subject to be discussed here, the chemical reactions are initiated only with thermal energy.

Carbon nanotubes synthesis is achieved by putting a carbon source in the gas phase and using an energy source, such as plasma or resistively heated coil, to transfer energy to a gaseous carbon molecule. Commonly used gaseous carbon sources include methane, carbon monoxide and acetylene. The energy source is used to “crack” the molecule into

reactive atomic carbon. Then, the carbon diffuses towards the substrate, which is heated and coated with a catalyst (usually a first row transition metal such as Ni, Fe or Co) where it will bind. Carbon nanotubes will be formed if the proper parameters are maintained. Excellent alignment as well as positional control on nanometer scale can be achieved by using CVD. Control over the diameter, as well as the growth rate of the nanotubes can also be maintained. The appropriate metal catalyst can preferentially grow single rather than multi-walled nanotubes.

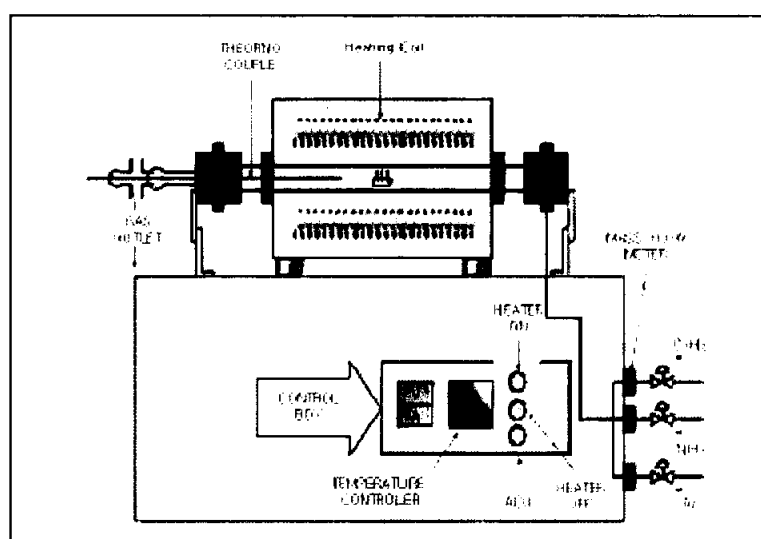


Figure 2.13: Schematic diagram of thermal CVD apparatus. (Reproduced from Iljin, 2003).

CVD carbon nanotube synthesis is essentially a two-step process consisting of a catalyst preparation step followed by the actual synthesis of the nanotube. The catalyst is generally prepared by sputtering a transition metal onto a substrate and then using either chemical etching or thermal annealing to induce catalyst particle nucleation. Thermal annealing results in cluster formation on the substrate, from which the nanotubes will grow. Ammonia may be used as the etchant (Ren *et al.*, 1999). The temperatures for the synthesis of nanotubes by CVD are generally within the 650-1050°C range (Ren *et al.*, 1999). Typical yields for CVD are approximately 30%.

These are the basic principles of the CVD process. In the last decennia, different techniques for the carbon nanotubes synthesis with CVD have been developed, such as

plasma enhanced CVD, thermal chemical CVD, alcohol catalytic CVD, vapour phase growth, aero gel-supported CVD and laser assisted CVD.

In Table 2.2, a short summary of the three most common techniques used nowadays is given.

**Table 2.2:** A summary of the major production methods and their efficiency.

| <b>Method</b>        | <b>Arc discharge method</b>  | <b>Chemical vapour deposition</b>   | <b>Laser ablation (vaporization)</b>   |
|----------------------|--|---|--|
| <b>Who</b>           | Ebbesen and Ajayan, NEC, Japan 1992  | Endo, Shinshu University, Nagano, Japan 1994  | Smalley, Rice University, 1995   |
| <b>How</b>           | Connect two graphite rods to a power supply, place them a few millimeters apart, and throw the switch. At 100 amps, carbon vaporises and forms a hot plasma. | Place substrate in oven, heat to 600°C, and slowly add a carbon-bearing gas such as methane. As gas decomposes it frees up carbon atoms, which recombine in the form of nanotubes | Blast graphite with intense laser pulses; use the laser pulses rather than electricity to generate carbon gas from which the nanotubes form; try various conditions until hit on one that produces prodigious amounts of SWNTs |
| <b>Typical yield</b> | 30 to 90%  | 20 to 100 %   | Up to 70%  |
| <b>SWNT</b>          | Short tubes with diameters of 0.6-1.4 nm   | Long tubes with diameters ranging from 0.6-4 nm   | Long bundles of tubes (5-20 microns), with individual diameter from 1-2 nm.  |
| <b>MWNT</b>          | Short tubes with inner diameter of 1-3 nm and outer diameter of approximately 10 nm  | Long tubes with diameter ranging from 10-240 nm   | Not very much interest in this technique, as it is too expensive, but MWNT synthesis is possible.  |

Table 2.2: Continued.

| Method        | Arc discharge method   | Chemical vapour deposition  | Laser ablation (vaporization)   |
|---------------|--|---|---|
| <b>Pro</b>    | Can easily produce SWNT and MWNTs. SWNTs have few structural defects; MWNTs without catalyst, not too expensive, open air synthesis possible | Easiest to scale up to industrial production; long length, simple process, SWNT diameter controllable, quite pure | Primarily SWNTs, with good diameter control and few defects. The reaction product is quite pure.    |
| <b>Contra</b> | Tubes tend to be short with random sizes and directions; often needs a lot of purification   | Nanotubes are usually MWNTs and often riddled with defects  | Costly technique, because it requires expensive lasers and high power requirement, but is improving |

## 2.4 Use of Catalyst in the Synthesis of CNTs

In this research work, catalyst has been used in chemical vapour deposition system to grow carbon nanotubes. Thus fundamental theory on catalyst will be discussed in this section.

A catalyst was defined by J.J. Berzelius in 1836 as a compound, which increases the rate of a chemical reaction, but which is not consumed by the reaction. This definition allows for the possibility that small amounts of the catalyst are lost in the reaction or that the catalytic activity is slowly lost. However, the catalyst affects only the rate of the reaction; it changes neither the thermodynamics of the reaction nor the equilibrium composition.

An acceleration of the rate of a process or reaction, brought about by a catalyst, usually present in small managed quantities and unaffected at the end of the reaction. A catalyst

permits reactions or processes to take place more effectively under milder condition than would otherwise be possible.

Catalysis occurs when the presence of the catalyst provides an alternate path of lower activation energy by which the reactants can proceed to form the products. In other words, a catalyst lowers the energy of the transition state, or activated complex, significantly while the energies of the reactants and products remain the same. This is shown in the Figure 2.14.

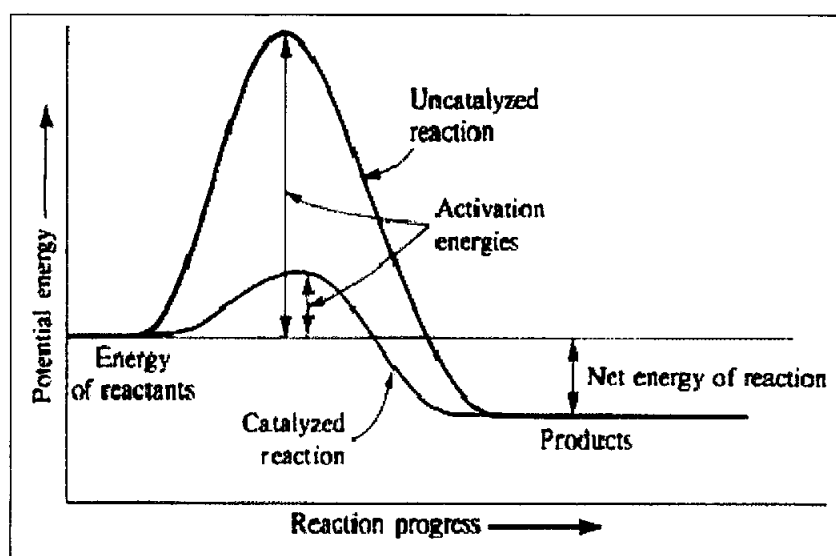


**Figure 2.14:** Catalyst provides an alternate path of lower activation energy by which the reactants can proceed to form the products. (Reproduced from Rearse *et al.*, 1981).

Since a catalyst provides a path that requires a lower energy of activation, a much higher proportion of the total molecules will have sufficient energy to react effectively along the catalysed path than could have reacted along the uncatalysed path and so the rate of the reaction can be greatly increased by the presence of the catalyst. However, there is no change in the free energy of the reaction since the catalyst does not affect the energies of the products and reactants. The decrease in activation energy applies to the reverse reaction as well as to the forward reaction, and the position of equilibrium will remain unchanged on the addition of a catalyst because the rates of the forward and

reverse reactions will both have been increased. These are important properties of catalysts. No catalyst will change the position of a chemical equilibrium and any catalyst will accelerate both the forward and reverse reactions along the same path.

Catalysts fall into two classes – homogeneous and heterogeneous. The former are present in the same phase as the reactants. Normally, this is the liquid phase. Heterogeneous catalysis applies to reaction where the catalyst is in a separate phase, these reactions may be gas/solid, liquid/solid and gas/liquid. In either case the catalytic act may be represented by five essential steps:

- a. Diffusion to the catalytic site (reactant)
- b. Bond formation at the catalytic site (reactant)
- c. Reaction of the catalyst – reactant complex
- d. Bond rupture at the catalytic site (product)
- e. Diffusion away from the catalytic site (product)

In the case of homogeneous catalysis, step (b) to (e) represents the formation and decay of the reactive intermediate; in heterogeneous catalysis they represent surface-adsorption and desorption with reaction of the surface intermediates.

In some cases of homogeneous catalysis, the general mechanisms are now well established – perhaps the simplest case is that of acid-catalysed rearrangements involving carbonium ions. In others, the identity of the reactive, intermediate complex is subject to debate; nevertheless, the fact that such a complex is a molecular entity often reduces the number of possibilities. This not so with heterogeneous catalysts where the true nature of any surface species is still a matter of conjecture. Moreover, the surface of a heterogeneous catalyst is energetically non-uniform: that is to say, surface atoms are exposed with varying degrees of coordinative unsaturation. Therefore, it is possible that adsorbed reactants may be too strongly bonded to undergo further reaction. Equally, adsorption may be too weak to allow a reactive enough intermediate to form. These arguments can be extended to compare the activity of

different catalysts for the same reaction. Therefore, optimum conditions for adsorption or desorption in relation to any particular reaction. These conditions can affect not only the rates of the catalytic reaction, but also the nature of that reaction.

The origin of catalytic selectivity is more complex. In the simplest case, the heat of desorption of product can determine how selective the reaction will be for that product. If the heat of desorption is low, the product can leave the surface easily and escape further reaction, which may be possible if the heat of desorption is high. More important, however, is the nature of the interaction between reactant and the active sites of the catalyst and, for that matter, the nature of the active sites. The type of activated complex, which is formed, will clearly be reflected in the products into which it decomposes.

In synthesis carbon nanotubes by catalytic method, most of the past researchers were using iron, cobalt and nickel as their catalysts to grow CNTs (Ivanov *et al.*, 1995 and Yudasaka *et al.*, 1995). The mechanism of formation of CNT that has generally been accepted includes hydrocarbon adsorption on the surface, conversion of the adsorbed hydrocarbon to adsorbed surface carbon via surface reactions, subsequent segregation of surface carbon into the layer near the surface, diffusion of carbon through metal catalyst, and then precipitation on the rare side of the metal catalyst particle.

One of the proposed possible mechanisms (Chen *et al.*, 2005), as presented in the following equations:

Surface reactions:



Dissolution/ segregation:



Diffusion of carbon through nickel:



Precipitation/ dissolution of carbon:



Encapsulating carbon formation:



where  $S$  is the adsorption site;  $C_{Ni,f}$  is the carbon dissolved in nickel at the front of the particle, just below the selvage;  $C_{Ni,r}$  is the carbon dissolved in nickel at the rear of the particle (support side);  $C_{\text{encapsulating}}$  represents the encapsulating carbon formation on the Ni surface, which deactivates catalysts; and  $n$  is the ensemble size for encapsulating carbon.

## 2.5 Purification of Carbon Nanotubes

A large problem with nanotube application is that next to large-scale synthesis is the purification. In this section the purification of carbon nanotubes will be discussed. The produced carbon nanotubes contains a lot of impurities. The main impurities are graphite (wrapped up) sheets, amorphous carbon, metal catalyst and the smaller fullerenes. These impurities will interfere with most of the desired properties of the carbon nanotubes. Also in the fundamental research, it is preferred to obtain carbon nanotubes, as pure as possible without changing them. In order to understand, the carbon nanotubes samples also have to be as homogeneous as possible. The common

industrial techniques use strong oxidation and acid refluxing techniques, which have an effect on the structure of the tubes.

In this section, thermal and acid treatment purification techniques of the carbon nanotubes will be discussed. Basically, the thermal treatment is to eliminate amorphous carbon and others low oxidation resistance impurities and acid treatment is to remove the metal catalyst.

### 2.5.1 Thermal Treatment

Due to high temperatures (873 – 1873 K) the nanotubes will be rearranged and defects will be consumed (Borowiak *et al.*, 2002; Chiang *et al.*, 2001a, Chiang *et al.*, 2001b). The high temperature also causes the graphitic carbon and the short fullerenes to pyrolyse. When using high temperature vacuum treatment (Kajiura *et al.*, 2002) (1873 K) the metal will be melted and can also be removed.

### 2.5.2 Acid Treatment

In general the acid treatment will remove the metal catalyst. First of all, the surface of the metal must be exposed by oxidation or sonication. The metal catalyst is then exposed to acid and solvated. The carbon nanotubes remain in suspended form. When using a treatment in nitric acid (HNO<sub>3</sub>), the acid only has an effect on the metal catalyst. It has no effect on the carbon nanotubes and other carbon particles (Borowiak *et al.*, 2002, Kajiura, *et al.*, 2002). If a treatment in HCl is used, the acid has also a little effect on the carbon nanotubes and other carbon particles (Chiang *et al.*, 2001a; Moon *et al.*, 2001; Chiang *et al.*, 2001b). The mild acid treatment (4M-HCl reflux) (Bandow *et al.*, 1997) is basically the same as the HNO<sub>3</sub> reflux, but here the metal has to be totally exposed to the acid to solvate it.

## **Chapter 3: METHODOLOGY**

### **3.1 Introduction**

This chapter will report the methodology of carbon nanotubes (CNTs) synthesis and characterisation procedures. Carbon nanotubes are synthesized by combining a source of carbon with a catalyst that has nanosized particles, at high temperatures. These catalysts can be compounds of iron (Fe), cobalt (Co) or nickel (Ni). Carbon sources include bulk graphite, hydrocarbons ( $C_xH_y$ ) and carbon monoxide (CO). At elevated temperatures, the catalyst has a high solubility for carbon; the carbon then links up to become graphene and wraps around the catalyst to form a cylinder. Subsequent growth occurs from the continuous addition of carbon to the tube.

Basically, the entire synthesis process can be divided into 4 major processes. They are substrate preparation, nanocatalysts preparation, growing carbon nanotubes and purification process. The schematic diagram of the carbon nanotubes synthesis process is as shown Figure 3.1. The list of chemicals used for this research has been attached in Appendix A.

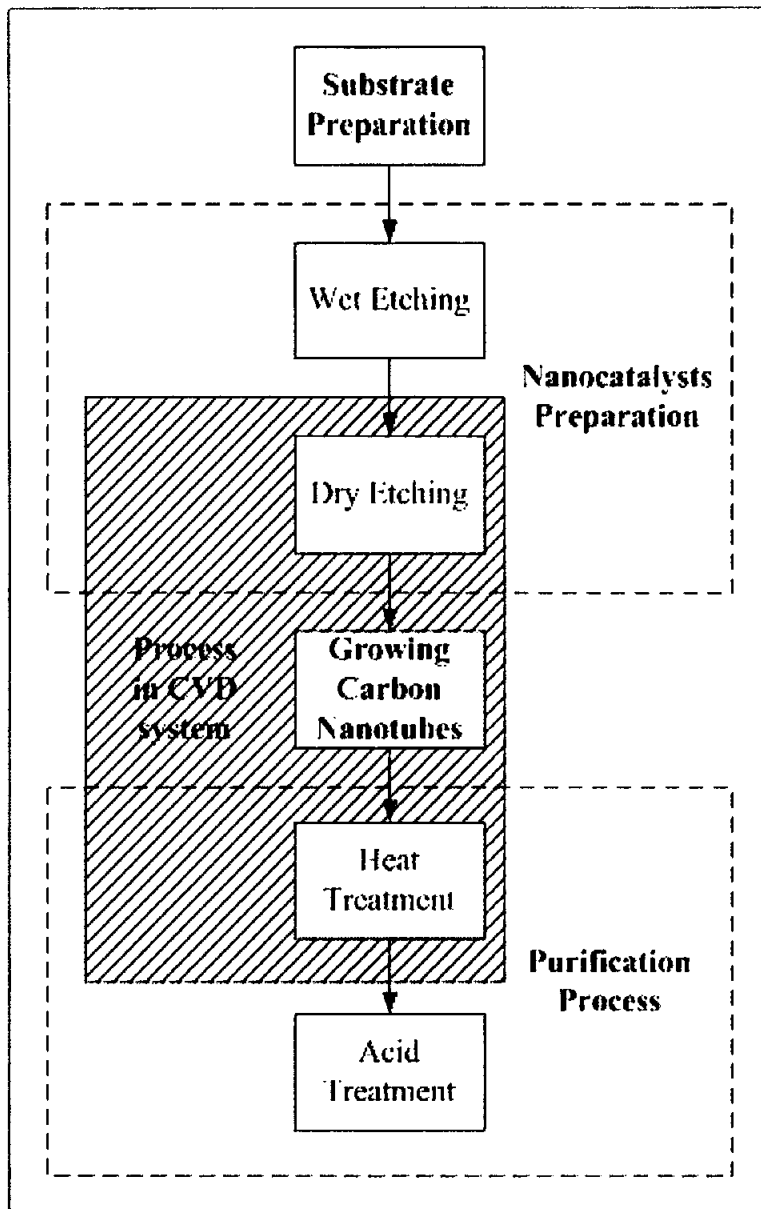


Figure 3.1: Schematic diagram of carbon nanotubes synthesis process.

## 3.2 Substrates Preparation

The silicon (Si) wafers used in this research is a P type with <100> orientation ShinEtsu silicon wafers. The size of the wafer is 150 mm in diameter. Resistivity is between 17.0 to 21.0  $\Omega$  cm.

### 3.2.1 Cutting of Silicon Wafers

Silicon wafers were first laid on a cutting board. The substrates were cut from big wafers into square pieces with sides of 20 mm with a diamond cutter and ruler. In order to get rid of possible impurities, it has to be cleaned, before it undergoes any other processing.

### 3.2.2 Cleaning of Silicon Wafer

Firstly, the silicon wafer cleaning process was done by using RCA cleaning method. This method was developed by Walter Kern in the mid 1960s and is widely used in the semiconductor industry to remove organic and inorganic residues from silicon wafers (Van Zant, 1997). RCA named after the company where Kern developed this process Radio Corporation of America.

As a safety precaution due to the corrosiveness of the solution, double layer of gloves were worn during the chemical mixing and cleaning process. The process was started by preparing two solutions, standard clean 1 (SC-1) and standard clean 2 (SC-2). The composition of each component in the solution is as shown in Table 3.1.

Cleaning was started by ultrasonically cleaning the Si substrates for 5 minutes in SC-1 solution with temperature controlled at about 75°C. Glass beaker should be used to contain SC-1

and SC-2 solution because of the corrosiveness. The substrates were taken out by tweezers and rinsed several times with deionised water (DI water).

After rinsing, the substrates were ultrasonicated in SC-2 solution for same period of time and temperature as SC-1 solution, followed by rinsing process. Then the substrates were soaked in a 2M-hydrofluoric acid solution for 5 minutes at 75°C. The beaker and tweezers for this solution should be made by polypropylene.

**Table 3.1:** RCA solution composition. (Reproduced from Van Zant, 1997).

| RCA Clean Solution                 | Volume Ratio   |
|------------------------------------|--|
| Standard Clean 1 (SC-1)<br>Process | 5 : 1 : 1<br>Deionised H <sub>2</sub> O : H <sub>2</sub> O <sub>2</sub> : NH <sub>4</sub> OH<br>75°C for 5 minutes |
| Standard Clean 2 (SC-2)<br>Process | 6 : 1 : 1<br>Deionised H <sub>2</sub> O : H <sub>2</sub> O <sub>2</sub> : HCl<br>75°C for 5 minutes                |



**Figure 3.2:** Desiccator that contain substrates.

The substrates were ensured clear of chemical solutions by soaking in deionised water for few minutes before being blown by nitrogen gas stream to dry the substrates. The Si

substrates were kept in clean plastic bag in a desiccator that contain silica gel drying agent. The substrate preparation procedures were summarised in Figure 3.3.

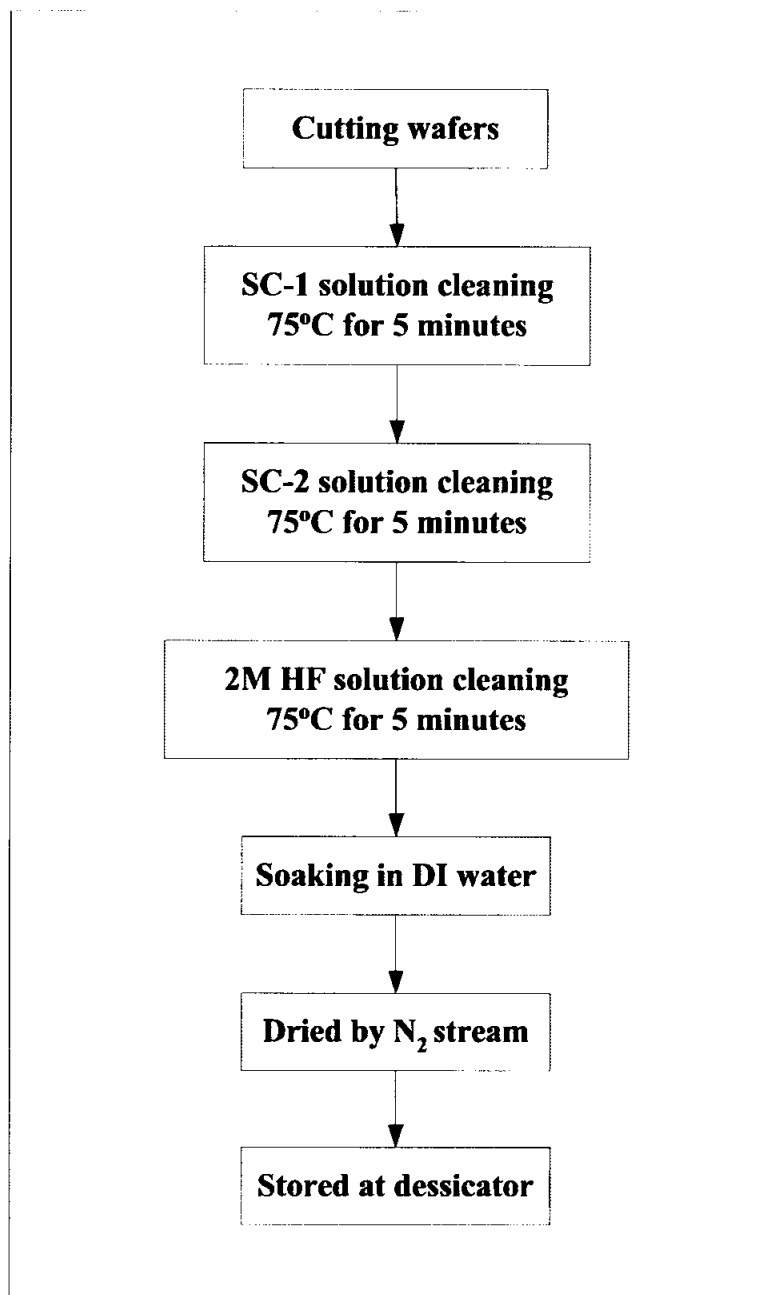


Figure 3.3: Flow chart that summarised substrate preparation procedures.

### 3.3 Nanocatalysts Preparation

Catalyst size is one of the most crucial factors in the synthesis of carbon nanotubes (CNTs), because only nano-sized catalysts are able to grow CNT. Consequently, catalysts preparation has become an important procedure in the synthesis of CNTs by catalytic method.

The synthesis of CNTs using thermal chemical vapour deposition (CVD) involved preparing three different catalytic metal powder particles, iron, nickel and cobalt in nano size.

#### 3.3.1 Wet Etching Process of Catalytic Particles

Approximately about 2.00 gram of catalytic metal powder (Fe, Co or Ni) was weighed into a 50 ml polypropylene beaker. Then the beaker was placed in a Hume cupboard. After that, 2M-hydrofluoric acid (HF) were poured into the beaker that contained metal powder until almost full. The metal powder was left in the 2M-hydrofluoric acid solution for various etching time at room temperature. In this research, 30, 60, 90 and 120 minutes are the etching time that were determined.

After that, the etched metal powder was rinsed by deionised water and filtered out from the solution. The rinsing and filtering process was repeated for about 10 times and litmus paper test was conducted to ensure the etching products are free from hydrofluoric acid. Then the etching product was dried in oven with controlled temperature of 80°C.

The wet etching procedure was repeated for each catalytic metal powder (Fe, Co or Ni) with difference etching time.

### 3.3.2 Dropping Wet Etched Product on Substrate

The dried wet etching product was mixed in approximately 20 ml ethanol by ultrasonic dispersion. The mixture was ultrasonicated for about 20 minutes.

Meanwhile, the substrates that were cleaned by RCA cleaning were rinsed with ethanol before used as substrate to support substrate. Then the substrates were dried in oven in controlled temperature of 80°C.

After that, several drops of the mixture were spread on a silicon substrate (see Figure 3.4) before drying out in the oven. This step is repeated until the total weight of the dried wet etched product on the substrate is 0.01 g. Then, the substrate was placed on a quartz boat. This technique of using ethanol droplets illustrated in Figure 3.5, will ensure an even spread of the wet etched catalytic particles on the substrate and to prevent agglomeration from occurring. The nanocatalysts preparation procedures were summarised in Figure 3.6.



**Figure 3.4:** Dropper dropping sonicating mixture of ethanol and catalyst particles on a silicon wafer.

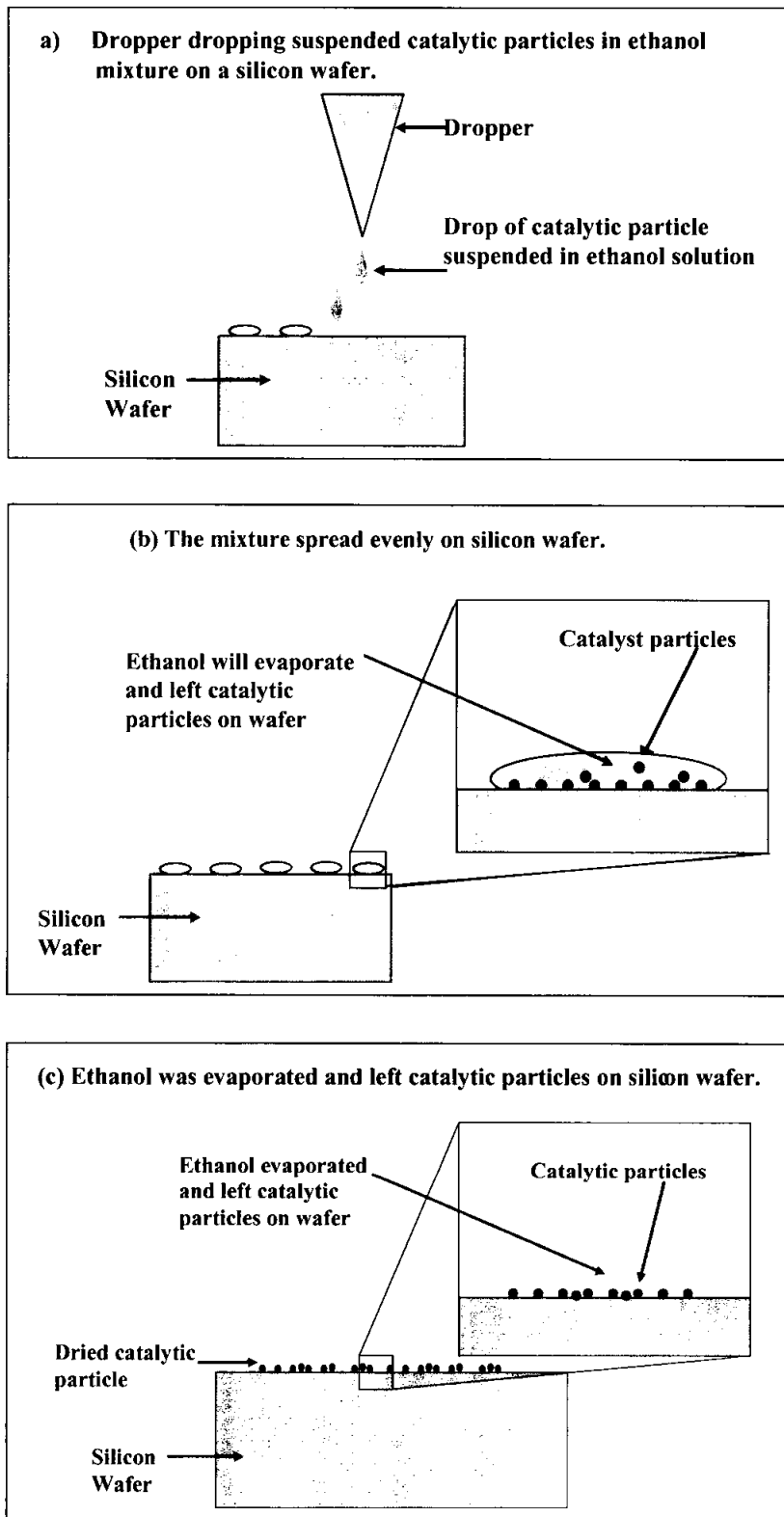


Figure 3.5: Spreading process of catalytic particles on a silicon wafer.

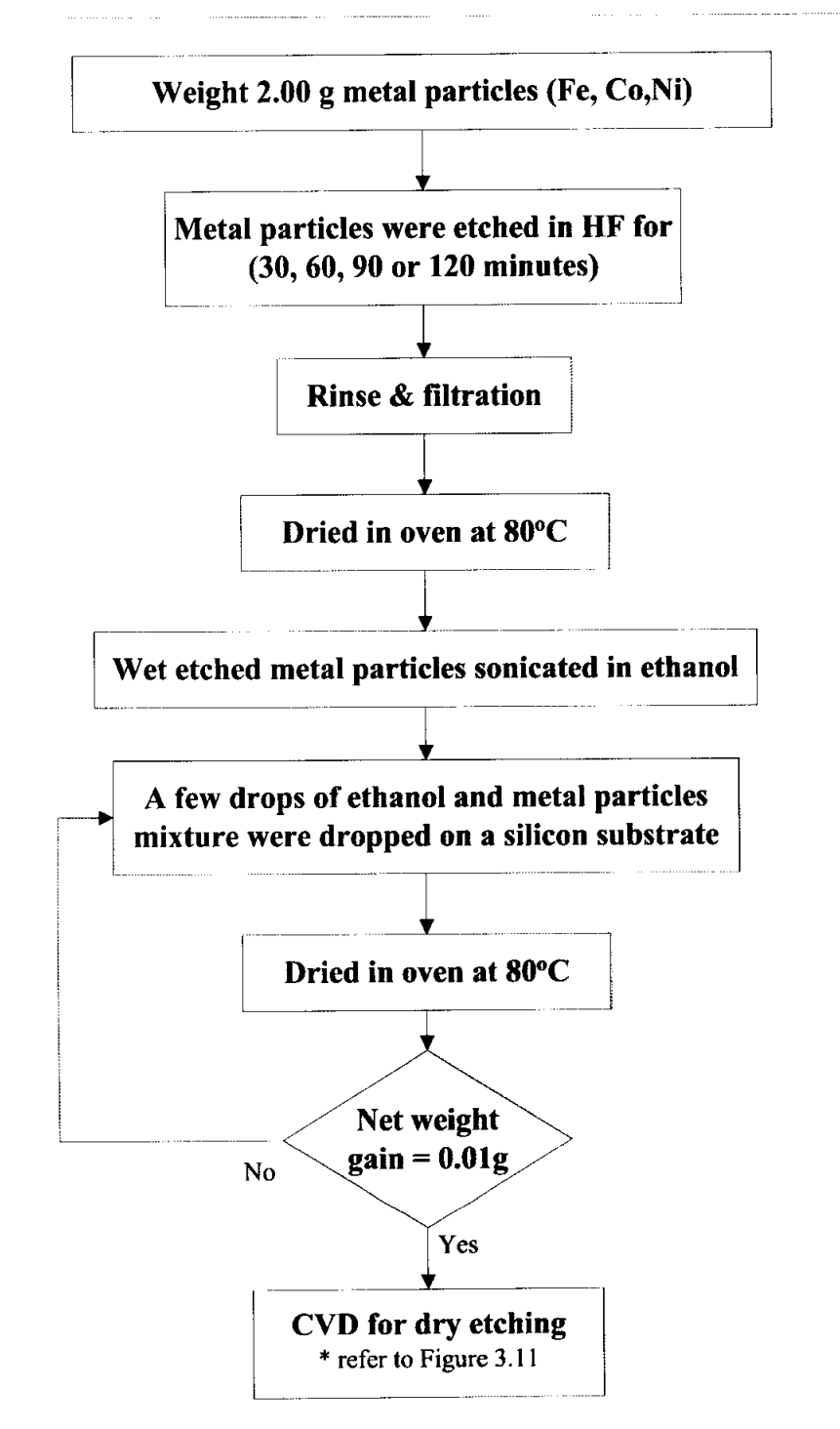


Figure 3.6: Flow chart that summarised nanocatalysts preparation procedures.

### 3.4 Growth of Carbon Nanotubes using Chemical Vapour Deposition

The chemical vapour deposition (CVD) technique was adopted from Dr Zhang Wei De at Institute of Materials Research and Engineering (IMRE), Singapore and referred to some literatures (Kong *et al.*, 1998 and Lee *et al.*, 2001). The CVD reaction process was carried out in an electrical tubular furnace as shown in Figure 3.8. The schematic diagram of thermal chemical vapour deposition (CVD) system is shown in Figure 3.9 and the entire CVD process was summarised in Figure 3.10.

After the wet and dry etching process, the ammonia ( $\text{NH}_3$ ) gas was stopped and carbon nanotubes (CNTs) were grown on these etched catalytic particles in methane ( $\text{CH}_4$ ) atmosphere flowed in at 40 sccm for an hour at  $950^\circ\text{C}$  (see Figure 3.11). The suggested possible reaction mechanism was discussed in section 2.4.

After that, the methane ( $\text{CH}_4$ ) gas was replaced by Argon (Ar) gas at 200 sccm. The CVD was programmed to cool down slowly at the rate of  $5^\circ\text{C}$  per minute to approximate  $400^\circ\text{C}$ . When the temperature reached  $400^\circ\text{C}$ , the CVD system will shut down automatically as programmed. Then the system was cooled down to room temperature without controlled environment. The Argon (Ar) gas was stopped when the system reached room temperature. The raw product obtained is shown in Figure 3.12.

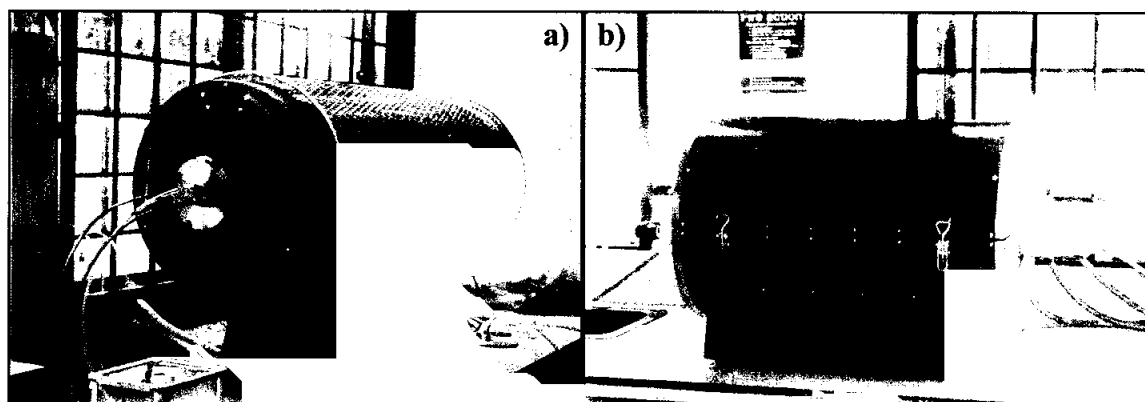


**Figure 3.8:** Thermal CVD system for carbon nanotubes growth. (a) Alumina tube electrical tubular furnace. (b) Quartz tube electrical tubular split furnace.

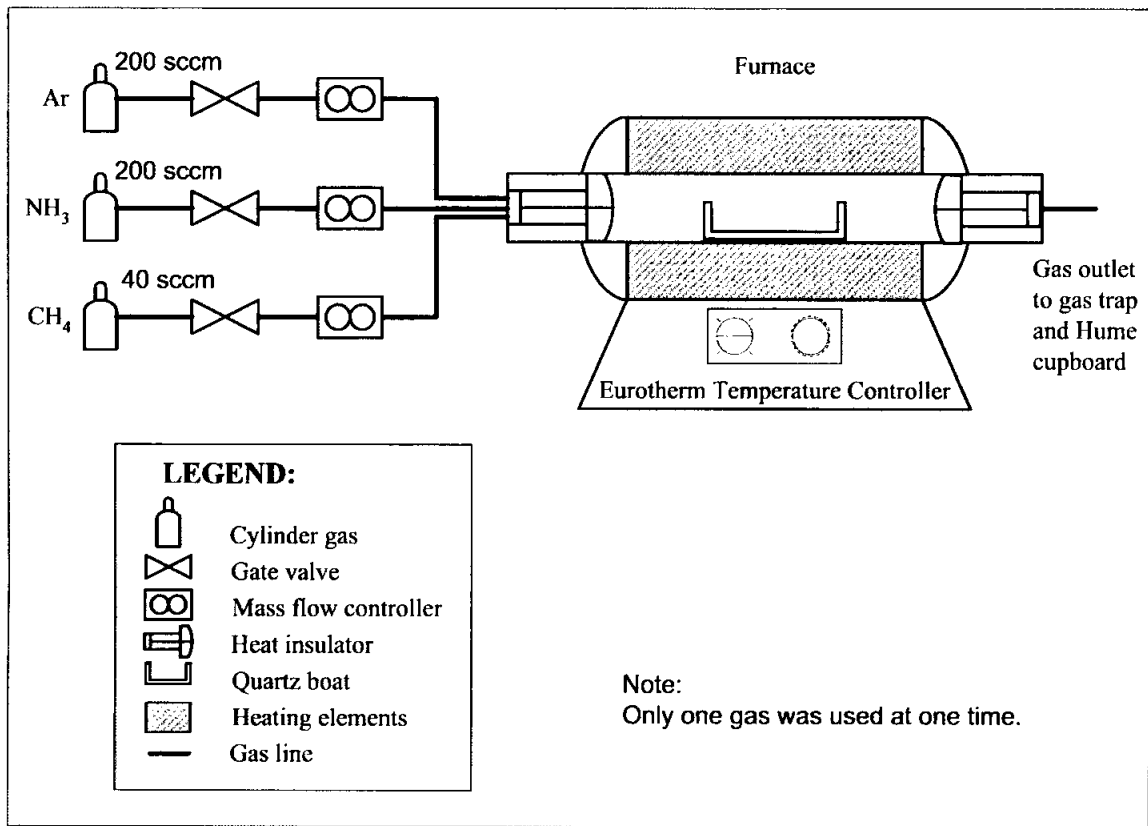


Figure 3.9: Schematic diagram of thermal chemical vapour deposition (CVD) system.

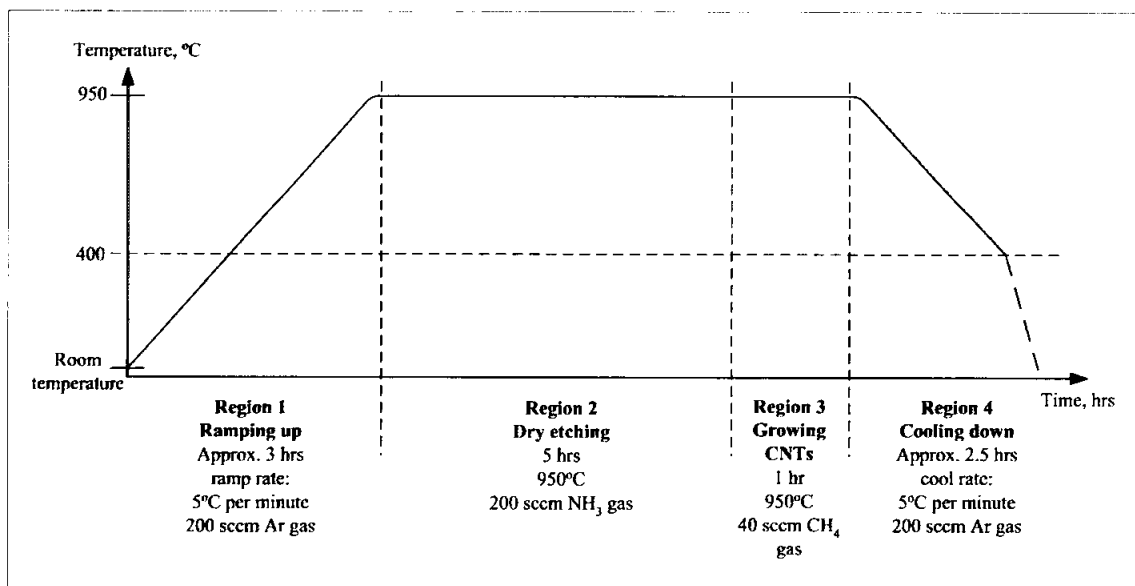


Figure 3.10: Thermal profile for the CVD process.

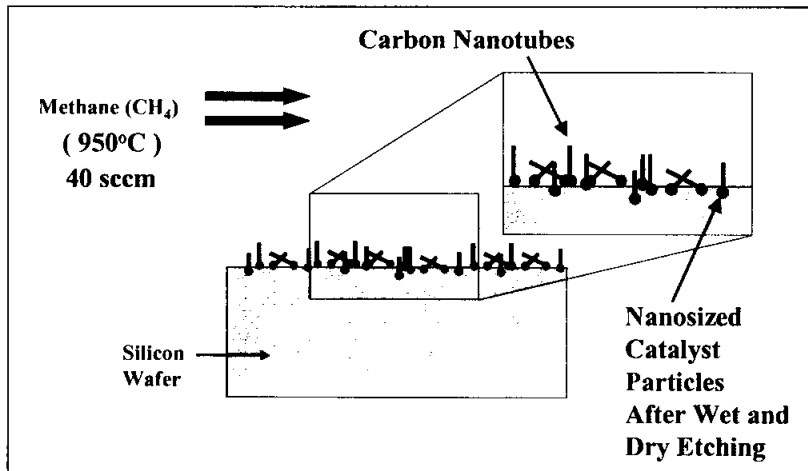


Figure 3.11: Carbon nanotubes were grown on Si wafer.

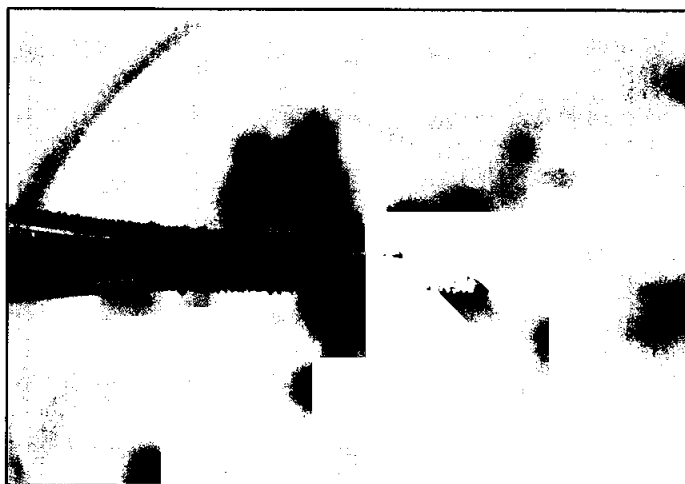


Figure 3.12: Non-purified carbon nanotubes held by tweezers.

## **3.5 Purification Procedure**

### **3.5.1 Thermal treatment**

After the CVD system was cooled to room temperature, the system was restarted before discharging the non-purified carbon nanotubes from the system. The temperature was set at 300°C with ramp rate of 5°C per minute. About an hour is needed for the system to reach 300°C. By heating up the system, the sealant of the furnace end cap would be soften. This would help to open the end cap. During the process, gas was flowed into from the system. Therefore, air was flowed in from the other end of the system.

The system was filled with air and allows the amorphous carbon and fullerene structure to gasify. When the end cap was opened, more air was flowed in and more amorphous carbon was gasified.

When the temperature reached 300°C, the system was shut and cooled to room temperature. Gasification process was continued during the cooling down. Approximately 3 hours was taken for the entire thermal treatment process from heating up to cooling down.

### **3.5.2 Acid treatment**

After thermal treatment, the carbon nanotubes were taken out from the CVD system and placed into a 250 ml beaker. Then approximate 250 ml 4M hydrochloric acid (HCl) was poured in the breaker and allows the carbon nanotubes to soak for 18 hours.

After that, the purified carbon nanotubes was rinsed by deionised water and filtered out from the solution. The rinsing and filtering process were repeated for about 10 times to ensure the etching products are free from hydrochloric acid. Then the purified products were dried in oven with controlled temperature of 80°C.

With this protective carbon coating weakened or removed, a mild acid treatment is then sufficient to remove most of the metal in the sample, leaving the nanotubes intact. The purification process procedures were summarised in Figure 3.13.

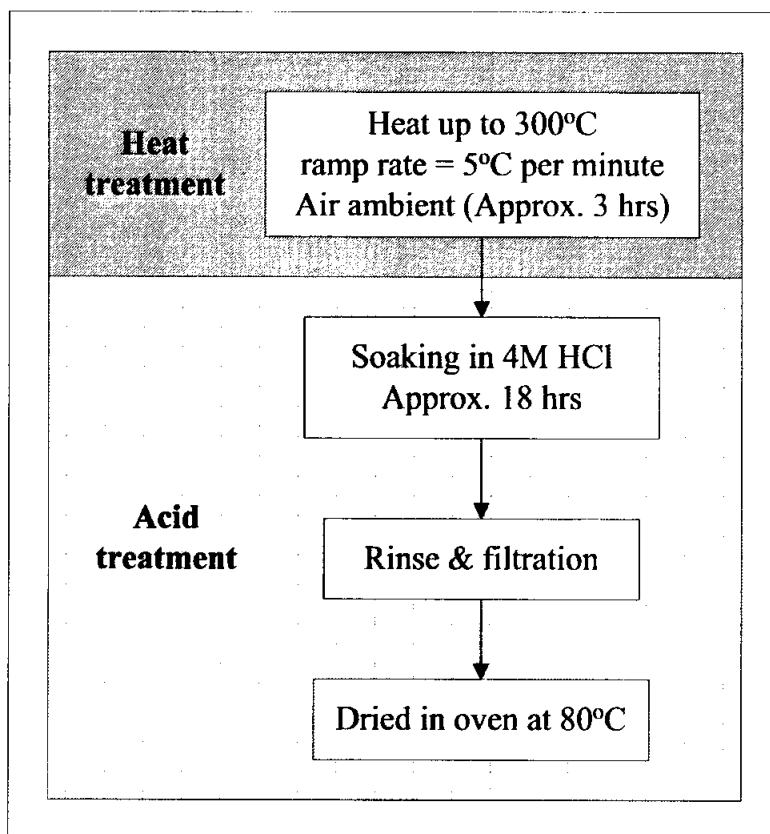


Figure 3.13: Flow chart that summarised purification process procedures.

## 3.6 Characterization Tests

### 3.6.1 Scanning Electron Microscopy (SEM)

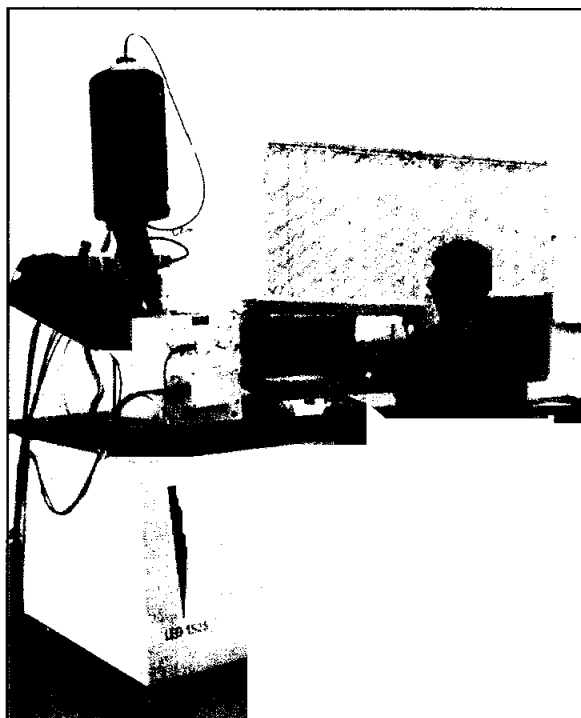


Figure 3.14: LEO 1525 Field Emission Scanning Electron Microscope.

Scanning electron microscopy (SEM) is frequently used to visualize the outer morphology catalytic materials. High resolution images of surface topography, with excellent depth of field are produced using a highly focused, scanning (primary) electron beam. The primary electrons enter a surface with energy of 0.5-1.5 keV, and generate many low energy secondary electrons. The intensity of this secondary electron is largely governed by the surface topography of the sample. An image of the sample surface can thus be constructed by measuring secondary electron intensity as a function of position of the scanning primary electron beam. High spatial resolution is possible because the primary electron beam can be focused to a very small spot ( $< 10$  nm). It is customary to use electron energies about 5 keV as they are much easier to focus and give rise to much secondary electron yields. Due to their much larger penetration depth of up to micrometer dimensions the apparent topographical contrast is not due to

surface features but represents a convolution of these features with the bulk in homogeneities in structure and composition that both modulate the secondary yield.

In addition to low energy secondary electrons, significant yields of backscattered electrons and X-rays are generated by primary electron bombardment at kinetic energies above 5 keV. The intensity of backscattered electrons of kinetic energies is significantly higher than their elements-specific threshold levels can be correlated to the atomic number of the element within the sampling volume. Hence, qualitative elemental information could be obtained.

The examination of scanning electron microscope images can yield information of the following material properties:

- (i) Topography - The surface features of an object or "how it looks", its texture; direct relation between these features and materials properties (hardness, reflectivity and etc.)
- (ii) Morphology - The shape and size of the particles making up the object; direct relation between these structures and materials properties (ductility, strength, reactivity and etc.)

Scanning electron microscopy (SEM) of the catalyst samples were conducted by LEO 1430VP scanning electron microscope model at Universiti Teknologi PETRONAS (UTP) while the carbon nanotubes (CNTs) samples were taken by LEO 1525 field emission scanning electron microscope (FESEM) model at Advance Materials Research Centre (AMREC), Kulim. For each of the specimens six sampling were taken for conducting SEM. The sample preparation involved pasted the specimen to a conductive carbon tape. Then the carbon tape was stuck on an aluminium stub as sample holder. After that, the specimens were coated by palladium gold with sputter coater. The coating provides a better conductive path for the electrons to return to earth, otherwise the specimen would charge up although the specimens are conductive

materials. The charging phenomena occur due to high accelerating voltages that are used for high-resolution application.

The specimens were mounted on a specimen stage that retractable from specimen chamber. Before imaging can start, air from within the chamber and column were pumped out. When a sufficiently good vacuum in the column has been achieved, the electron beam is switched on. High vacuum is required to prevent any electrical discharges occurring due to the high voltages that are used to generate the beam and to prevent the electron beam being diffused or absorbed by gas molecules.

The stage which specimens were mounted can be moved in a horizontal plane (x and y), raised or lowered (z), rotated and tilted so that each one in turn can be imaged from the most appropriate view. The operational parameters were applied as follow to optimise the quality of the micrograph images:

|                             |                                |
|-----------------------------|--------------------------------|
| Magnification               | : 5 to 400 kX                  |
| Accelerating voltage        | : 10 to 20 kV                  |
| Working distance            | : 4 to 6 mm                    |
| Final aperture              | : 30 $\mu\text{m}$             |
| Probe current               | : 10 to 200 pA                 |
| Secondary electron detector | : collector bias set to + 400V |
| Vacuum mode                 | : High vacuum                  |

Before every image was captured, focus wobble mode was used to check final aperture while astigmatism was corrected by using stigmation panel.

### 3.6.2 X-Ray Diffractometry (XRD)

XRD is one of the most frequently applied techniques in materials characterisation. X-rays have wavelengths in the Å range, are sufficiently energetic to penetrate solids and are well suited to probe their internal structure. XRD is used to identify bulk phases and to estimate particles size. Powder diffraction is able not only to identify but also to quantify the various crystalline phases present in a mixture.

X-ray diffraction is the elastic scattering of X-ray photons by atoms in a periodic lattice. The scattered monochromatic X-rays that are in phase give constructive interference. Figure 3.15 illustrates how diffraction of X-rays by crystal planes allows derivation of the lattice spacing,  $d$ , by measuring the angles,  $2\theta$ , under which constructively interfering X-rays with wavelength,  $\lambda$ , leave the crystal, by using the Bragg relation:

$$n\lambda = 2d \sin \theta \quad n = 1, 2, \dots \quad (3.1)$$

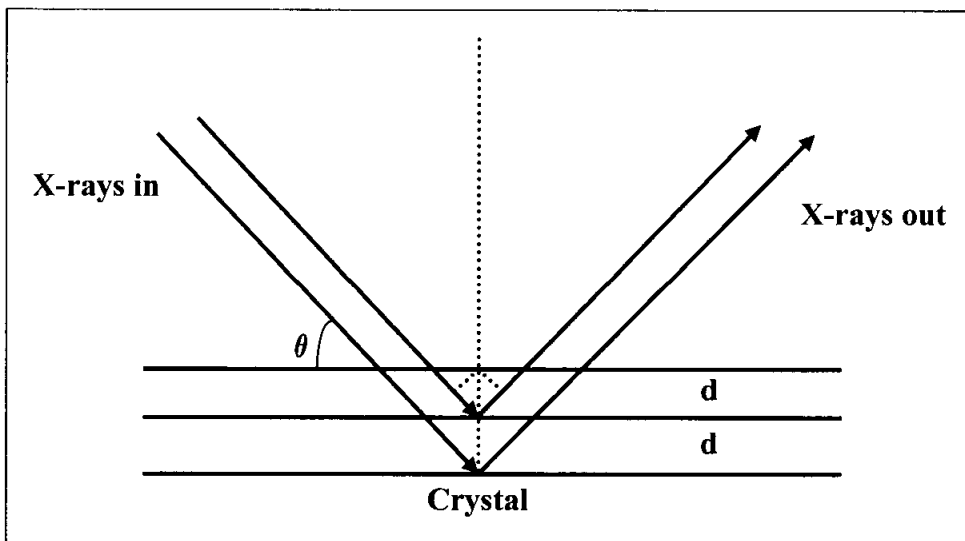


Figure 3.15: X-rays reflected by a series of atoms in a lattice plane interfere constructively in directions given by Bragg's Law.

The XRD pattern of a powder sample is measured with a stationary X-ray source (usually  $\text{CuK}_\alpha$ ) and a moveable detector, which scans the intensity of the diffracted radiations as a function of the angle  $2\theta$  between the incoming and the diffracted beams. When working with statistical oriented powder samples, diffracted intensity will be observed because fraction of the powder particles will be oriented such that a certain crystal plane (hkl) is at the right angle with the incident beam for constructive interference. Figure 3.16 illustrates a schematic layout of X-ray diffractometer.

The width of diffraction peaks carries information on the dimensions of the reflecting planes. Diffraction lines from perfect crystal are very narrow. For crystallite sizes below 100 nm, however, line broadening occurs due to incomplete destructive interference in scattering in directions where the X-rays are out of phase. The Scherrer formula relates crystal size to line width:

$$\langle L \rangle = K\lambda \beta \cos \theta \quad (3.2)$$

in which  $\beta$  is the peak width and  $K$  a constant (often taken unity). The linear dimension  $\langle L \rangle$  is a volume-averaged thickness of the crystallites, measured in a direction normal to the reflecting planes.

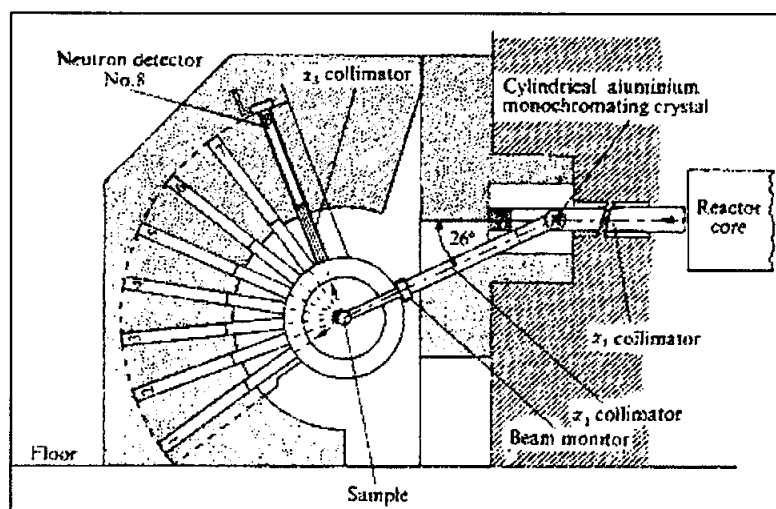


Figure 3.16: Schematic layout of X-ray diffractometer. (Reproduced from Bacon, 1975).

XRD is a basic characterisation technique for heterogeneous catalysts but it does have disadvantages. Because XRD is based on interference between reflecting X-rays from lattice from the support only a weak signal is received from the most relevant active phase. The surface region is where catalytic activity resides, but this part of the catalyst is virtually invisible for XRD (Warren, 1969; Klug *et al.*, 1974).

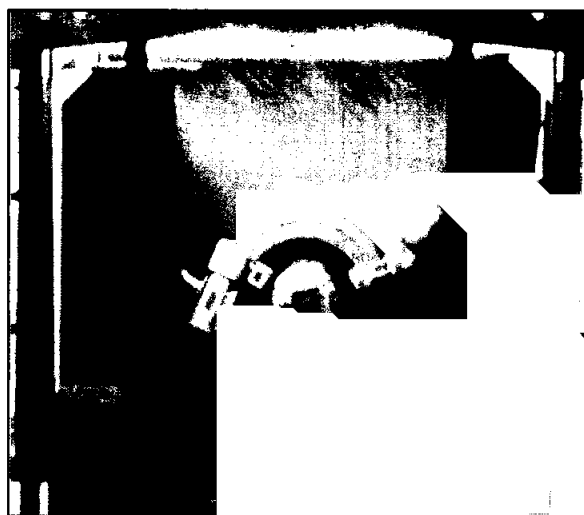


Figure 3.17: Bruker D8 Advance Powder X-ray diffractometer.

The sample was pressed into a sample holder. X-ray diffraction measurements were carried out using the Bruker D8 Advance Powder X-ray diffractometer and equipped with EVA Diffract software for data acquisition and analysis. The characterisation test was done at Advance Materials Research Centre (AMREC), Kulim. The crystal phases of the sample were identified by overlaying the standard JCPDS (Joint Committee on Powder Diffraction Standards) diffraction pattern of an expected compound; a match was based both upon peak position and relative intensity. Phase analysis, lattice parameters and particle size determination were conducted with a  $\text{CuK}_\alpha$  monochromatized radiation source operated at 40 kV and 40 mA. The intensity data were recorded by continuous scanning in a  $2\theta$  mode from  $20^\circ$  to  $70^\circ$  with a step size of  $0.04^\circ$  and 1 s counting time each step.

### 3.6.3 Transmission Electron Microscopy (TEM)

The principle of a Transmission Electron Microscope is given below (see Figure 3.18):

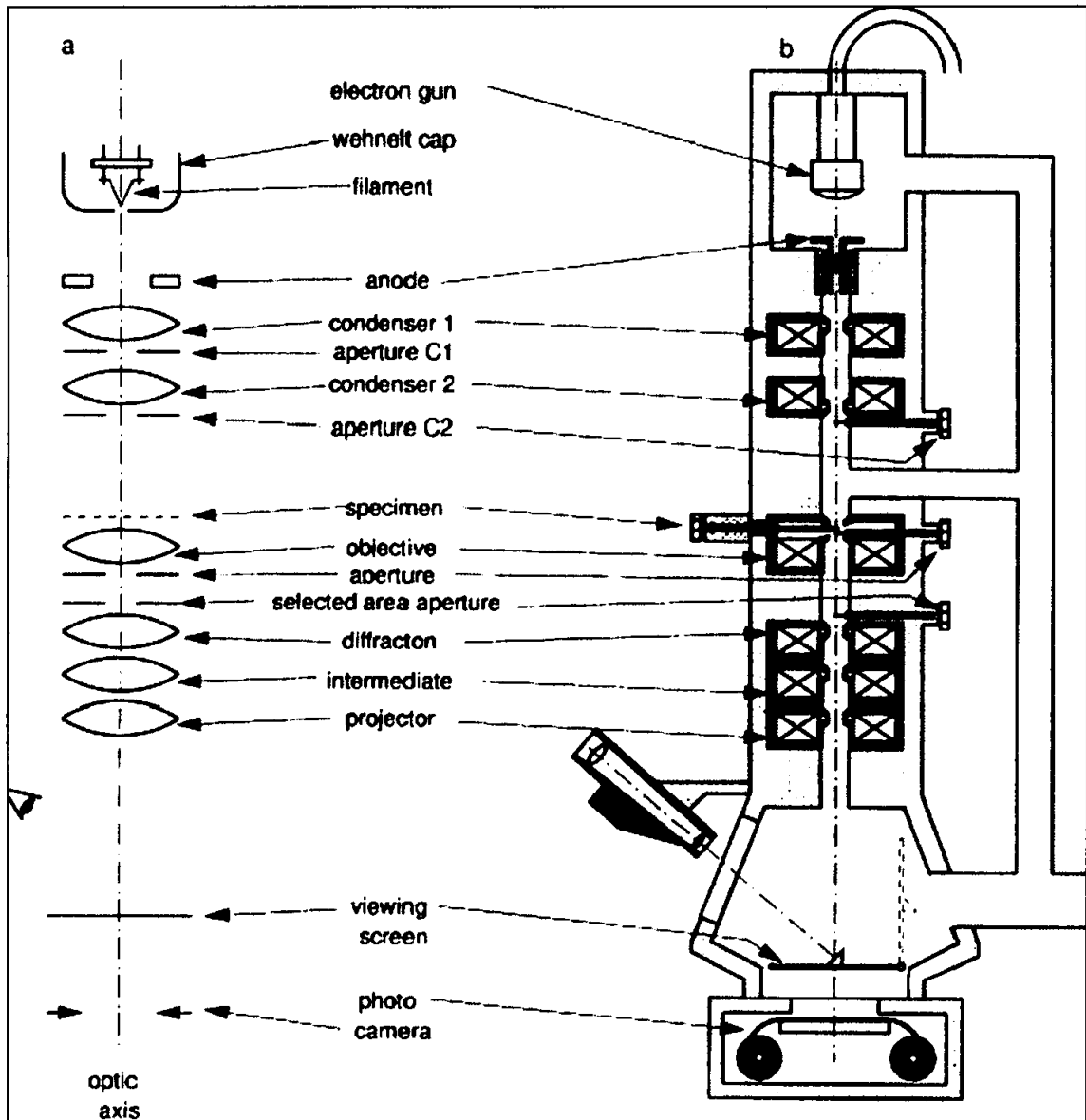
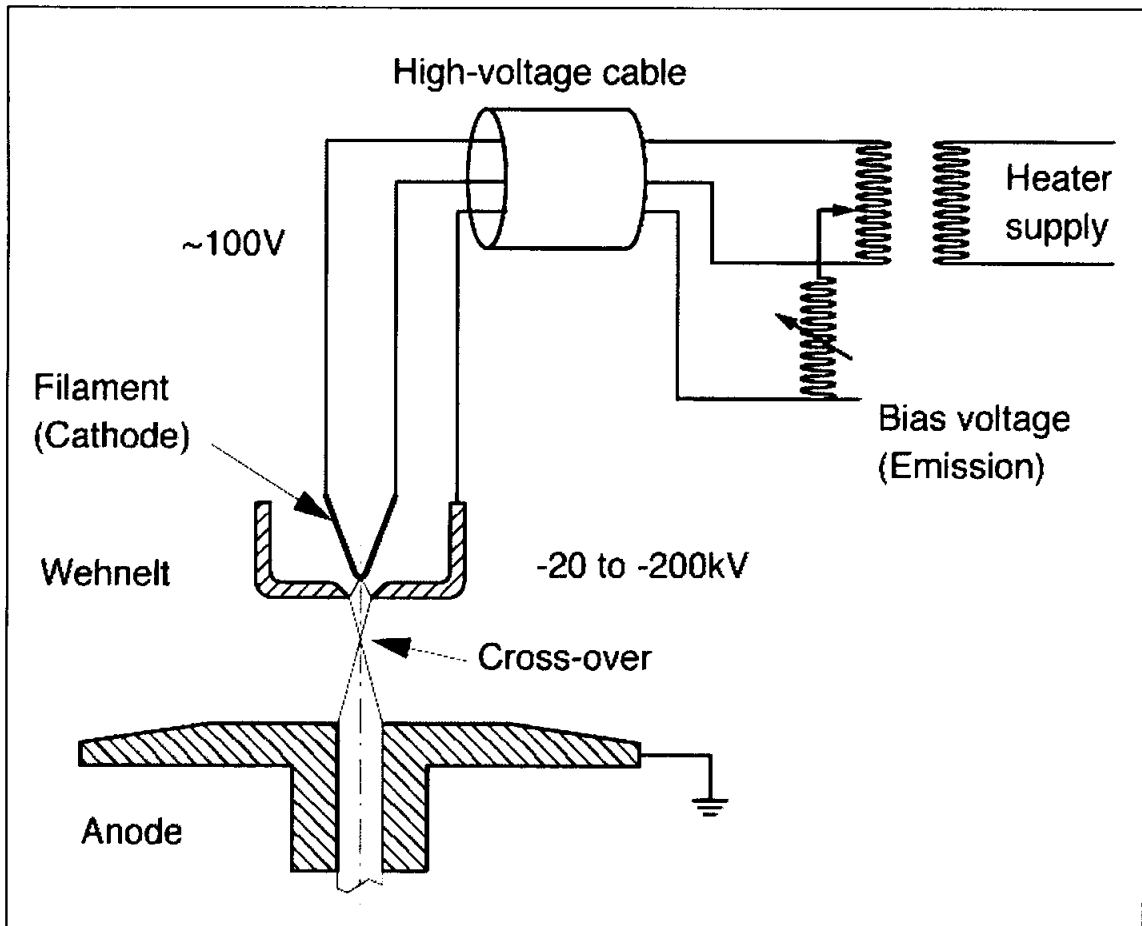


Figure 3.18: The principle of a transmission electron microscope. (Reproduced from Wat, 1997).

As the name of the instrument points out, the transmission electron microscope is a microscope, working in transmission. The electrons traverse the sample, which is inserted into the centre of the TEM column at the position labelled with “specimen”.

We therefore record images of the sample that are a projection of the whole sample volume, not only its surface. A complete three-dimensional reconstruction of the sample with its interior is possible.



**Figure 3.19:** The principle of the electron gun. (Reproduced from Wat, 1997).

The first component of an electron gun is a device that produces freely available electrons in the vacuum of the electron microscope. As illustrated in the Figure 3.19, the heated tungsten filament in the gun acts as the cathode. It “evaporates” electrons due to its temperature and the low energy barrier for electrons needed to leave the material. This filament is maintained at a high negative voltage, so that the electrons thermally emitted from this filament are attracted by the anode that is grounded and

hence highly positive with respect to the electron source. Thus, the electrons are highly accelerated by the potential difference between the cathode and the anode. In order to be able to adjust the quantity of electrons from the filament and produce a small electron source, a “cathode cap”, called Wehnelt cylinder, is positioned in front of the filament and kept a few hundred Volts more negative than the filament. A circular aperture in the Wehnelt acts as a converging electrostatic lens so that the electrons are focused into a “cross-over”. The electrons, after having passed this electrostatic lens, are then accelerated towards the anode aperture, which is at ground potential, by the high voltage. The high voltages used by current microscopes range between 100 to 400 kV.

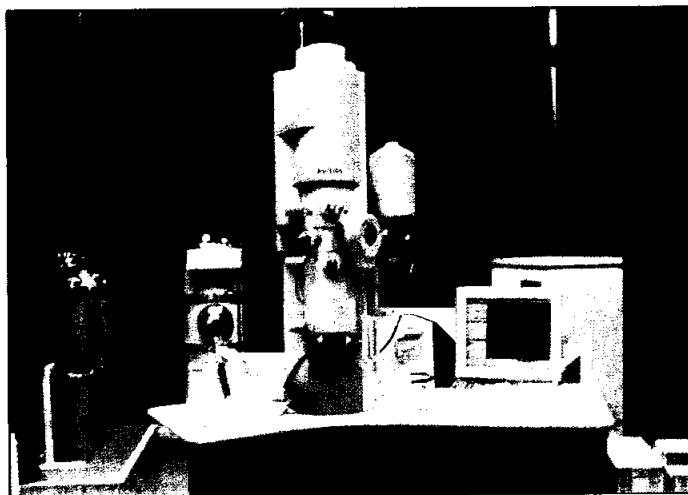


**Figure 3.20:** Phillips Tecnai 20 Transmission Electron Microscope (TEM).

Transmission electron microscopy (TEM) was performed on a Phillips Tecnai 20 model. The sample was not crushed and ground like conventional method because the sample is tiny enough to achieve the appropriate electron transparent.

For sample preparation, the samples were prepared by sonicating in isopropanol for 10 minutes followed by deposition of a few drops of the resulting suspension on the carbon grid supporting a perforated carbon film. Then the carbon grid was placed at specimen holder. Several magnifications were observed from low-resolution to

high-resolution transmission. During the high-resolution transmission working modes were used to monitor the morphology, the microscope was operating at 200 kV.

### 3.6.4 Thermal Gravimetry Analysis (TGA)

Temperature-programmed analysis refers to any technique, which measures the change of a curtail property such as the mass, the thermal conductivity or the size of a material under the influence of a linearly applied gradient in temperature.

The technique of thermal gravimetry analysis (TGA) originated in 1915, when K. Honda built the first “thermobalance”, a balance with weighing pan hanging inside a furnace for weighing sample at various temperatures. The instrument has evolved into one that could study the weight change of a sample, as it is exposed to heat. Two types of TGA may be performed:

- i. Isothermal TGA, which records the change in weight as a function of time at constant temperature.
- ii. Dynamic or non-isothermal TGA, which record the change in weight as a function of both temperature and time at programmed heating rate.

Any sample in the solid or liquid state can be studied by TGA. Typical sample weight ranges from 30 to 50 mg. One limitation of the technique is that it cannot be used for process that involves no weight change, for example, melting, crystallization and glass transition. Another severe limitation is the strong effect of the exchange properties between gas and reacting solid leading to transport-induced distortions of the TGA profile.

In addition to the actual TGA curves, the first derivative (differential thermal analysis (DTA) curve, rate of change of mass) is often used to support data analysis. Thermal events that are sampled by TGA include:

- i. Chemical reactions (decomposition and loss of water of crystallization, combustion and reduction)
- ii. Physical transitions (vaporization, evaporation, sublimation, desorption, drying)

Occasionally a gain in weight is observed. This can result from:

- i. Chemical reactions (reaction with gaseous substances in the purge gas such as oxygen, carbon dioxide with the formation of non-volatile or hardly volatile compounds)
- ii. Physical transitions (adsorption of gaseous substances on samples such as active charcoal)

The shape of the TGA curve is usually characteristic of the effect measured and can be used for identification purposes. The schematic and measured effects shown below illustrate many of the typical curve shapes observed in TGA.

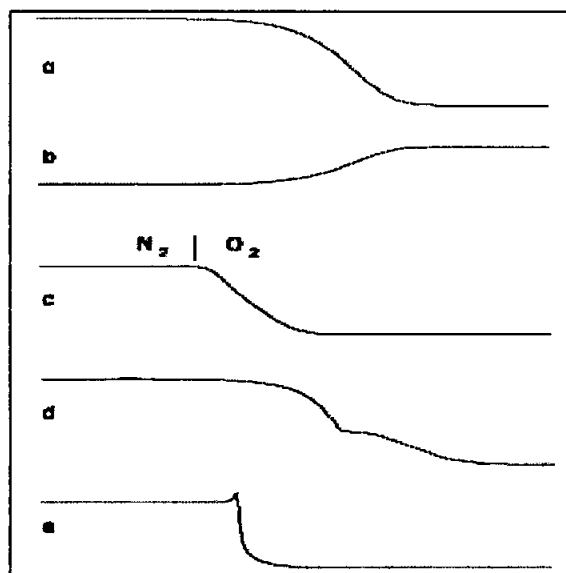
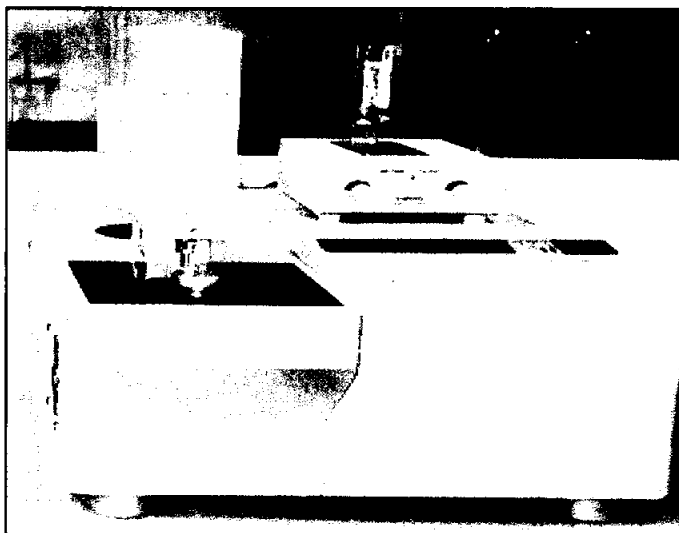


Figure 3.21: Typical TGA chemical reactions. (Reproduced from Spiewak *et al.*, 1997).

A typical weight loss step is about 100°C wide (for 1% to 99% conversion). The step usually develops slowly from the initially horizontal TGA curve. The point of inflection is at about 60% conversion. The radius of curvature is appreciably smaller at

the end of the reaction than at the beginning (see Figure 3.21(a)). Corrosion or oxidation of metals (see Figure 3.21(b)). Diffusion-controlled reactions, in which the transport of starting materials or products is restricted, proceed at an almost constant rate (i.e. the slope of the TGA curve is almost constant, see Figure 3.21(c)). Several steps often occur (see Figure 3.21(d)). Explosive substances sometimes decompose so rapidly that the force of the recoil disturbs the TGA signal (see Figure 3.21(e)). This problem can be avoided by using smaller sample quantities or by diluting the sample with an inert substance.



**Figure 3.22:** METTLER TOLEDO TGA/SDTA851<sup>°</sup> thermal gravimetry analyser.

A METTLER TOLEDO TGA/SDTA851<sup>°</sup> with the heating facilities up to 1600°C was used for the measurements. The balance was purged with 50 ml/min of nitrogen as protective gas. The results were evaluated with the V7.01 STAR<sup>°</sup> software package. The DTA curves are calculated as derivatives of the TGA curves. Samples of about 40 to 50 mg were measured in an open alumina oxide standard crucible of 70  $\mu$ l volume. The TGA temperature program operated dynamically from 30 to 800°C at a heating rate of 10°C/min; with air was used as a reactive gas flowing at the rate of 50 ml/min.

### 3.6.5 Raman Spectroscopy

Raman spectrometer is a tool used Raman effect as means of determining molecular structure in chemical analysis. The effect was discovered by an Indian scientist, Sir C.V. Raman (1888 - 1970).

Raman effect is a type of scattering of electromagnetic radiation in which light suffers a change in frequency and phase as it passes through a material medium. The intensity of Raman scattering is about one-thousandth of that in Rayleigh scattering in liquids. For this reason it was not used until the development of laser that the effect was put to use.

In Raman spectroscopy, light from a laser is passed through a substance and the scattering is analysed spectroscopically. The new frequencies in the Raman spectrum of monochromatic light scattered by a substance are characteristic of the substance. Both inelastic and super elastic scattering occurs.

In the scattering process the photon can either absorb energy or transfer energy to the molecule, but in either case information about the energy levels of the molecule under study can be inferred by examining the scattered light. This has proven a powerful tool indeed in chemistry, and is also extremely valuable in the study of carbon nanotubes.

When Raman Spectroscopy is used in the investigation of carbon nanotube properties, typical spectra obtained look like Figure 3.23. The radial breathing mode (RBM) peak is a result of a single type of scattering process between the incoming photons and the nanotubes. In this process the photon excites a vibrational mode like the one shown in Figure 3.23. The energy involved in this process can be shown to be proportional to  $1/d_{\text{tube}}$  (Saito *et al.*, 2001) and although the exact constant of proportionality is still being debated, a Raman investigation of a sample of nanotubes and their RBM-frequencies can provide information about the diameter distribution. The analysis is not straightforward however a careful statistical analysis of the RBM-peak is needed for accurate results even if a less rigorous treatment still yields an estimate for the

diameter distribution (Kuzmany 2001). It is this latter method, which have been employed by the Oxford group, as the only information needed was whether the majority of the nanotubes were large enough for filling while the exact distribution was not important.

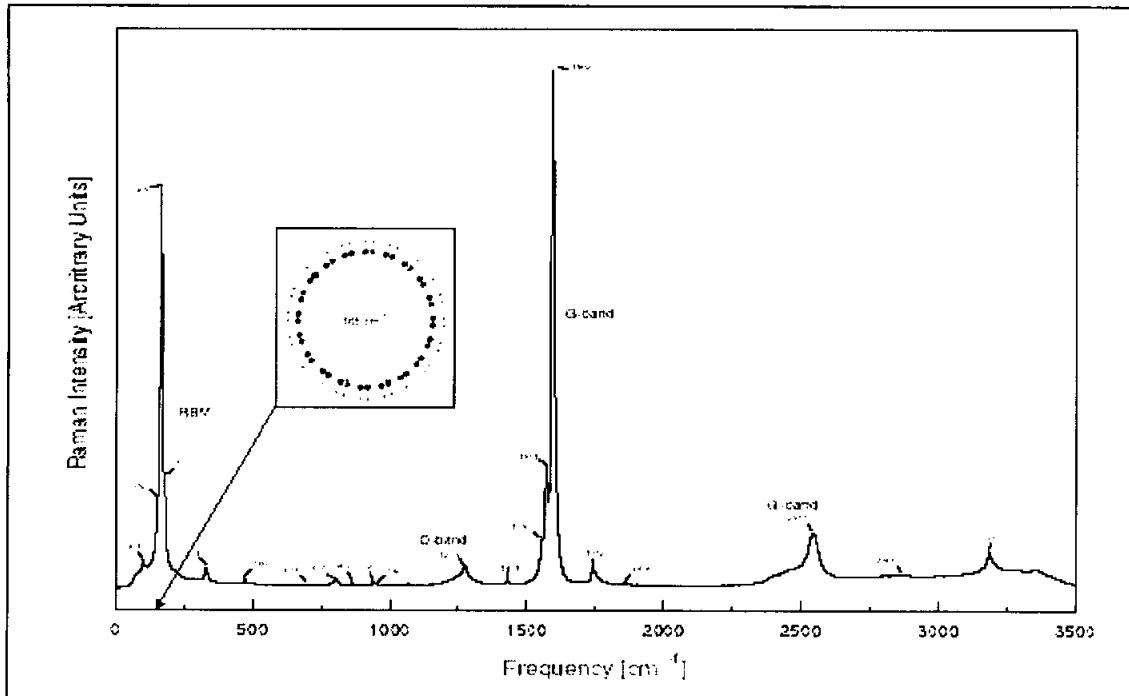


**Figure 3.23:** A CNTs Raman spectrum. Reproduced from (Saito *et al.*, 2001).

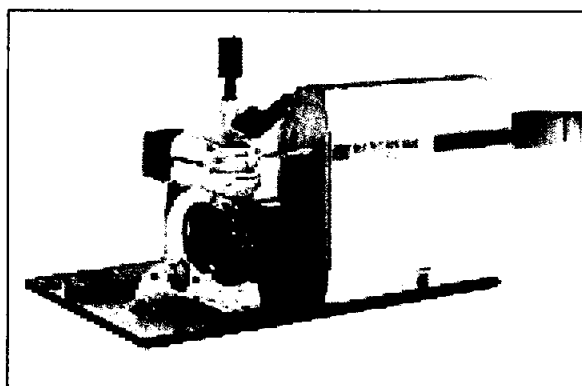


**Figure 3.24:** Renishaw inVia Raman Reflex microscope. (Reproduced from Renishaw, 2001.).

Raman spectroscopy was conducted on Renishaw inVia Raman Reflex microscope (see Figure 3.24). The samples were given to Renishaw plc, Wotton-under-Edge, UK for performs Raman characterisation.

Raman analysis was performed using both 514.5 nm and 632.8 nm laser excitation from an Ar<sup>+</sup> and He-Ne laser, respectively. A power density of 1 mWcm<sup>-2</sup> was used. In this case relatively low laser power were utilised to avoid sample degradation. Calibration was performed with the Si peak at 520.7 cm<sup>-1</sup>.

The samples were compacted in a sample holder before being placed on the microscope sample stage. Raman spectrum was recorded in the spectral range at 200 to 3000 cm<sup>-1</sup>. Then curve fitting with Lorentzian lineshape were performed.

## **Chapter 4: RESULTS AND DISCUSSION**

### **4.1 Introduction**

The discovery of carbon nanotubes and recognition of their exceptional physical properties have generated a great deal of interest and engendered much speculation as to possible applications in numerous fields. In order to retain the excellent intrinsic properties and the optimal performance of carbon nanotubes, understanding about the materials are very important. Therefore, intensive characterisation tests on the materials are required.

In overall view, three different types of samples were used on this study; there are catalyst samples, non-purified CNT samples and purified CNT samples. A total of twelve catalyst specimens were obtained by different wet etching time and type of catalyst as mentioned in section 3.3.1. However, out of twelve different catalysts, only six catalysts are able to grow CNTs. Consequently, only six non-purified CNT samples and six purified CNT samples were obtained by using thermal chemical vapour deposition (CVD) method. For each of the specimens six sampling were taken for conducting scanning electron microscopy (SEM).

The most common analytical techniques used are scanning electron microscope and X-ray diffractometry. These techniques have been adapted in the current work, with emphasis on standardizing measurements to facilitate easy comparison of results. Furthermore, the availability of analytical tools and methods for monitoring the results of a purification procedure, such as the purity and the structure of the CNTs

themselves, allows the procedure to be objectively assessed and shall reveal insights, which might leads to a new experiments hypothesis for the future development.

Three purified CNT samples (FeD3, CoB3 and NiC3) were chosen for further in-depth characterization. The investigation of particular interest would be to study the influence of synthesis method on crystallinity of CNTs by deriving the structural, thermal and molecule vibration information.

**Table 4.1:** Description and coding for each individual synthesised samples.

| Sample treatment   | Code |
|--|------|
| 1) Fe catalyts with 30 minute etching time                             | FeA1 |
| 2) Fe catalyts with 60 minute etching time                             | FeB1 |
| 3) Fe catalyts with 90 minute etching time                             | FeC1 |
| 4) Fe catalyts with 120 minute etching time                            | FeD1 |
| 5) Non-purified CNTs grown by Fe catalyts with 120 minute etching time | FeD2 |
| 6) Purified CNTs grown by Fe catalyts with 120 minute etching time     | FeD3 |
| 7) Co catalyts with 30 minute etching time                             | CoA1 |
| 8) Co catalyts with 60 minute etching time                             | CoB1 |
| 9) Non-purified CNTs grown by Co catalyts with 60 minute etching time  | CoB2 |
| 10) Purified CNTs grown by Co catalyts with 60 minute etching time     | CoB3 |

Table 4.1: Continued.

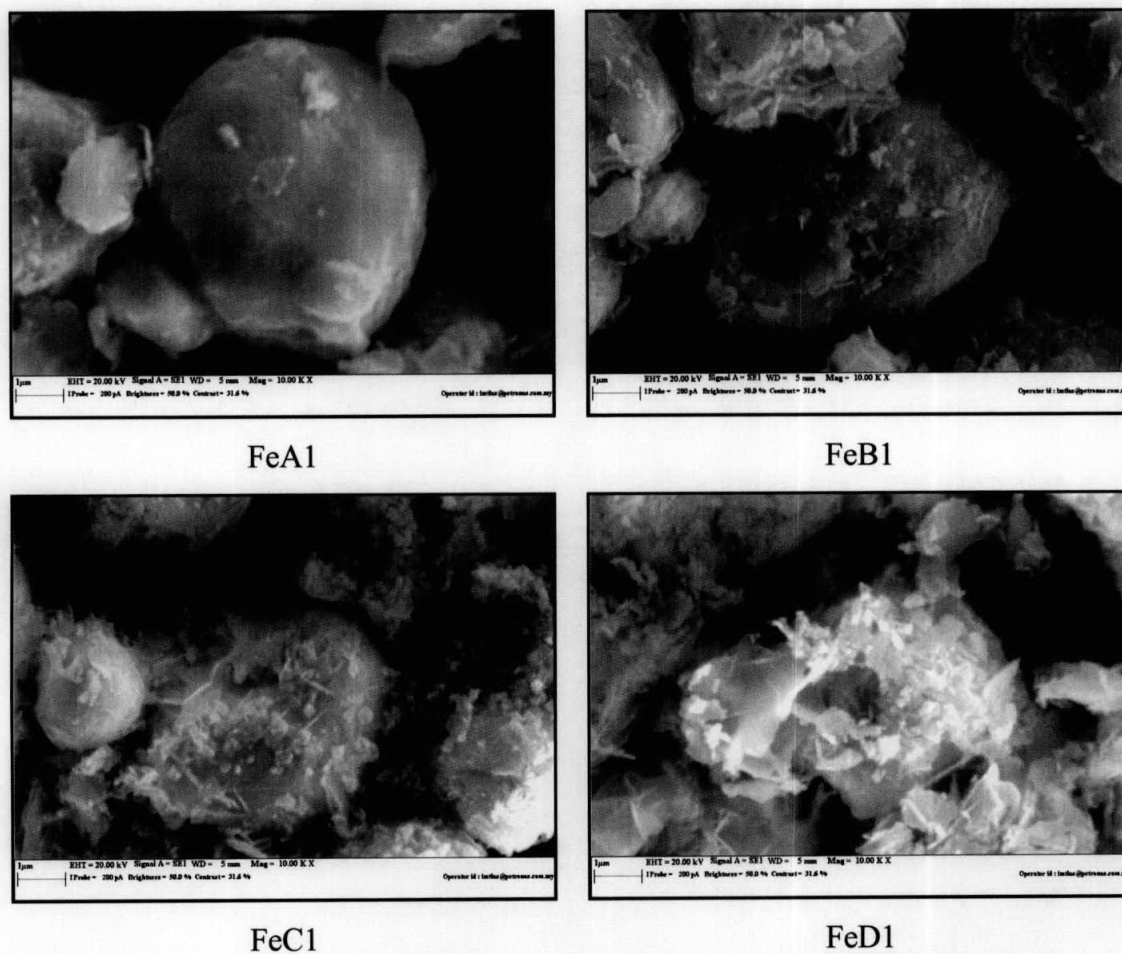
| Sample treatment   | Code |
|--|------|
| 11) Co catalysts with 90 minute etching time                             | CoC1 |
| 12) Non-purified CNTs grown by Co catalysts with 90 minute etching time  | CoC2 |
| 13) Purified CNTs grown by Co catalysts with 90 minute etching time      | CoC3 |
| 14) Co catalysts with 120 minute etching time                            | CoD1 |
| 15) Non-purified CNTs grown by Co catalysts with 120 minute etching time | CoD2 |
| 16) Purified CNTs grown by Co catalysts with 120 minute etching time     | CoD3 |
| 17) Ni catalysts with 30 minute etching time                             | NiA1 |
| 18) Ni catalysts with 60 minute etching time                             | NiB1 |
| 19) Ni catalysts with 90 minute etching time                             | NiC1 |
| 20) Non-purified CNTs grown by Ni catalysts with 90 minute etching time  | NiC2 |
| 21) Purified CNTs grown by Ni catalysts with 90 minute etching time      | NiC3 |
| 22) Ni catalysts with 120 minute etching time                            | NiD1 |
| 23) Non-purified CNTs grown by Ni catalysts with 120 minute etching time | NiD2 |
| 24) Purified CNTs grown by Ni catalysts with 120 minute etching time     | NiD3 |

## 4.2 Scanning Electron Microscopy (SEM)

In this research, scanning electron microscopy was conducted by two type of scanning electron microscope. A common scanning electron microscope (LEO 1430VP) was used to observe wet etched catalyst samples while FESEM (LEO 1525) with higher resolution was used to observe CNTs samples.

### 4.2.1 Wet Etched Catalyst Samples

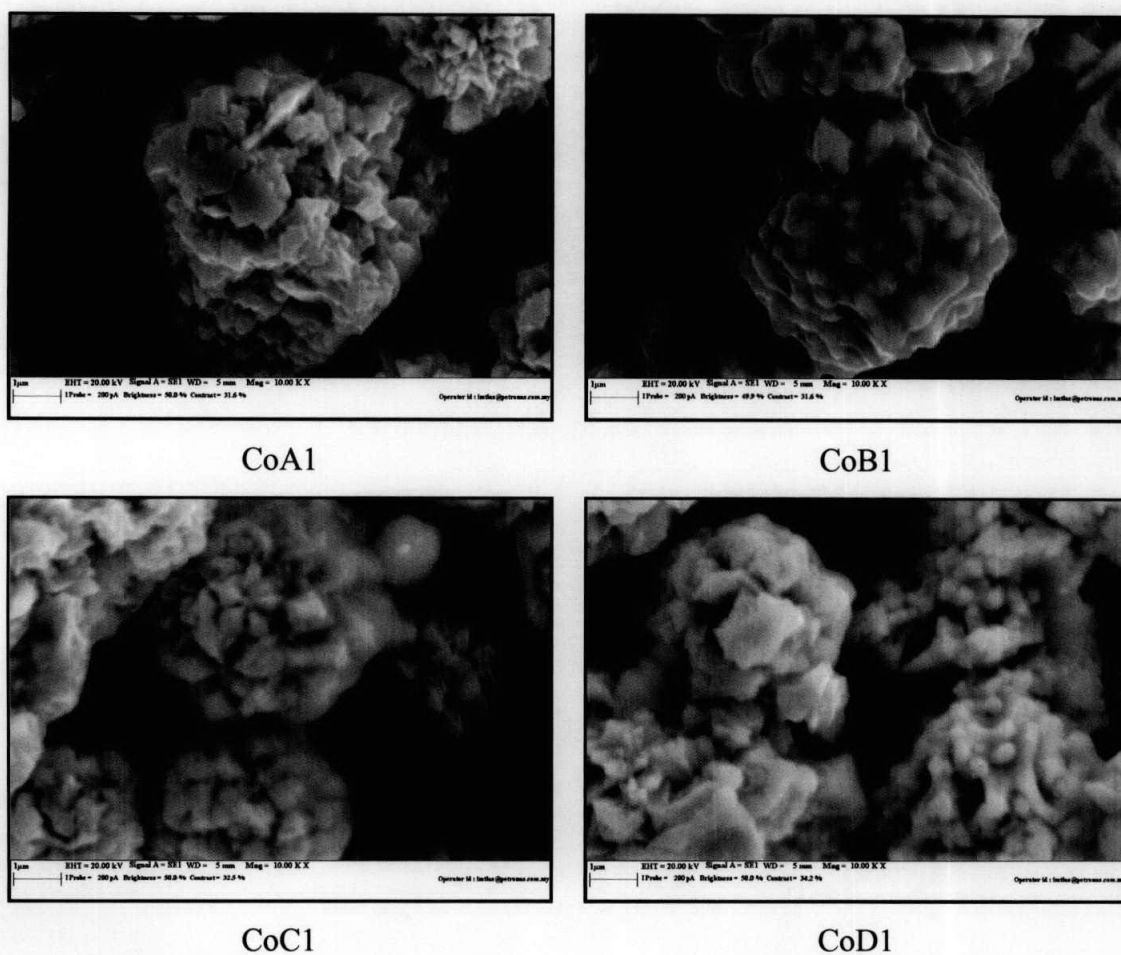
The effect of wet etching time on catalyst samples was studied by scanning electron microscope. Figures 4.1 to 4.3 are SEM images of iron, cobalt and nickel catalyst respectively under different etching time varying from 30 to 120 minutes. These micrographs show the morphology of the catalyst which and going to be used in growing process of CNTs. The wet etched catalyst is known to be inhomogeneous and contain a variety of impurities due to wet etching process. As indicated in Figure 4.1, 4.2 and 4.3 the particles of the prepared catalyst have uniform size but of irregular shapes. It is observed that these catalyst particles have some planar facets on the surface; indicating their crystalline nature. The initial particles size of Fe and Co is 10  $\mu\text{m}$  while Ni is 2  $\mu\text{m}$ .



**Figure 4.1:** SEM images of FeA1, FeB1, FeC1 and FeD1 under different etching time varying from 30 to 120 minutes at magnification of 10 000x. Scale bar 1  $\mu\text{m}$ .

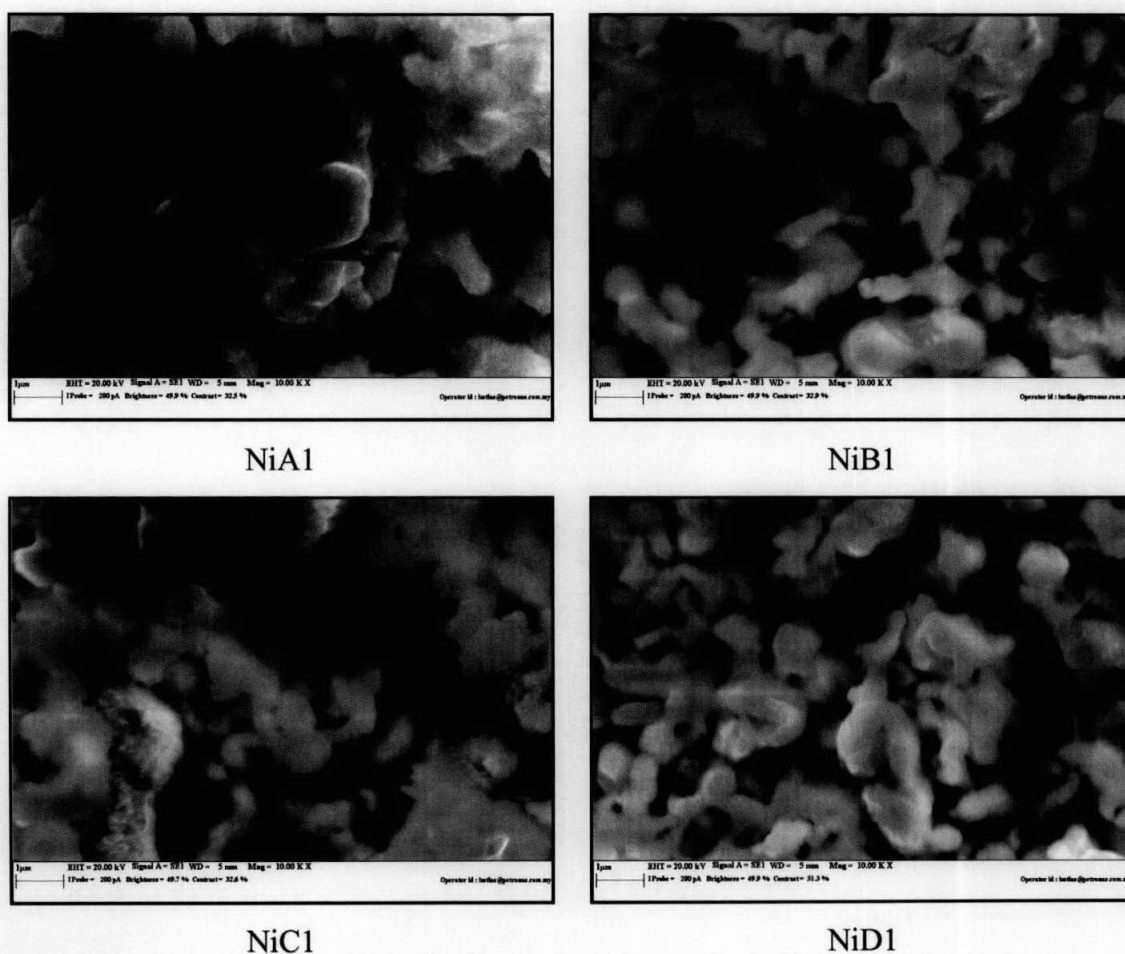
The particles size of the catalyst shown in Figure 4.1 was determined by using analysis software of Carl Zeiss AxioVision 3.1. The value obtained ranges from 6.40  $\mu\text{m}$  for 30 minutes etching time with sample (FeA1) to 4.62  $\mu\text{m}$  for 120 minutes with sample (FeD1).

Figure 4.2 describes micrographs of cobalt catalyst under different etching time varying from 30 to 120 minutes. Particles size of Co catalyst is observed to be slightly smaller than iron catalysts, about  $6.00\ \mu\text{m}$  for 30 minutes etching time with sample (CoA1) to  $4.59\ \mu\text{m}$  for 120 minutes with on sample (CoD1).



**Figure 4.2:** SEM images of CoA1, CoB1, CoC1 and CoD1 under different etching time varying from 30 to 120 minutes at magnification of 10 000x. Scale bar  $1\ \mu\text{m}$ .

Micrographs of nickel catalyst using different etching time varying from 30 to 120 minutes are shown in Figure 4.3. The particles size of Ni catalyst was observed to be much smaller than iron and cobalt catalyst. Values obtained are in the range of 1.37  $\mu\text{m}$  for 30 minutes etching time with sample (NiA1) to 1.12  $\mu\text{m}$  for 120 minutes with sample (NiD1). The catalyst particles size obtained are summarised in Table 4.2.



**Figure 4.3:** SEM images of NiA1, NiB1, NiC1 and NiD1 under different etching time varying from 30 to 120 minutes at magnification of 10 000x. Scale bar 1  $\mu\text{m}$ .

It is observed in Figure 4.1 that the iron catalyst samples exhibit some flakes like structure and the amount been mean as etching time prolonged, the more flake like structure observed in Fe catalyst with longer wet etching time is attributed to the longer dissolution by hydrofluoric acid. A clear image of the flake structure has been captured

in Figure 4.4. The morphologies of the cobalt catalysts for etching time are almost the same except for the varying particle size from bigger to smaller as the etching time prolonged. As for Ni catalyst, agglomerating appears more as the etching time prolonged (see Figure 4.3). The example of how to measure particles size is shown in Appendix B.

**Table 4.2:** Summary of wet etched samples under different etching time.

| Description                                   | Coding | Particles Size ( $\mu\text{m}$ ) |
|---|--------|----------------------------------|
| 1) Fe catalyts with 30 minutes etching time   | FeA1   | $6.40 \pm 0.58$                  |
| 2) Fe catalyts with 60 minutes etching time   | FeB1   | $5.78 \pm 0.52$                  |
| 3) Fe catalyts with 90 minutes etching time   | FeC1   | $5.33 \pm 0.48$                  |
| 4) Fe catalyts with 120 minutes etching time  | FeD1   | $4.62 \pm 0.42$                  |
| 5) Co catalyts with 30 minutes etching time   | CoA1   | $6.00 \pm 0.54$                  |
| 6) Co catalyts with 60 minutes etching time   | CoB1   | $5.28 \pm 0.48$                  |
| 7) Co catalyts with 90 minutes etching time   | CoC1   | $4.88 \pm 0.34$                  |
| 8) Co catalyts with 120 minutes etching time  | CoD1   | $4.59 \pm 0.32$                  |
| 9) Ni catalyts with 30 minutes etching time   | NiA1   | $1.37 \pm 0.12$                  |
| 10) Ni catalyts with 60 minutes etching time  | NiB1   | $1.31 \pm 0.12$                  |
| 11) Ni catalyts with 90 minutes etching time  | NiC1   | $1.23 \pm 0.11$                  |
| 12) Ni catalyts with 120 minutes etching time | NiD1   | $1.12 \pm 0.09$                  |

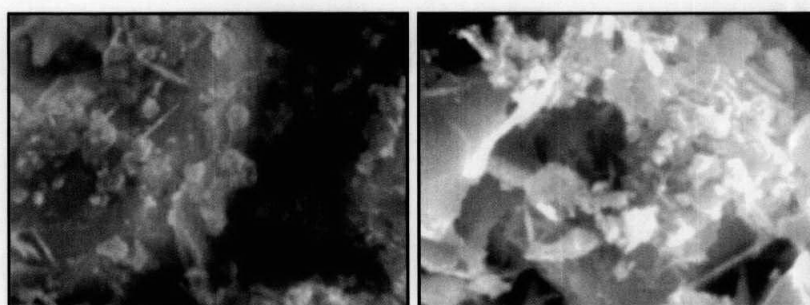


**Figure 4.4:** Flakes like structure exhibit by Fe catalyts.

The above results indicated that the longer the wet etching time the smaller would be the particles size of the catalyst. Different in the value can be clearly illustrates in the Table 4.2 and the graph seen in Figure 4.5. Figure 4.5 illustrates that particle size of iron catalyst is the largest among the catalysts. Cobalt catalyst is slightly smaller than iron catalysts but much larger than nickel catalyst. The etching rates for these three catalysts seem to have same trend where the initial rate is higher than etching rate after 60 minutes.

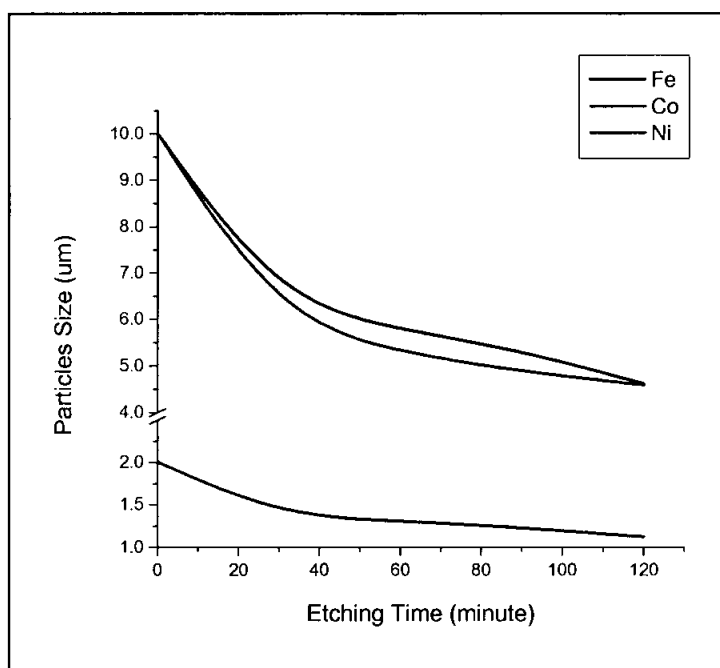


Figure 4.5: Graph of particles size (µm) versus etching time (minute).

### 4.2.2 Non-purified Samples

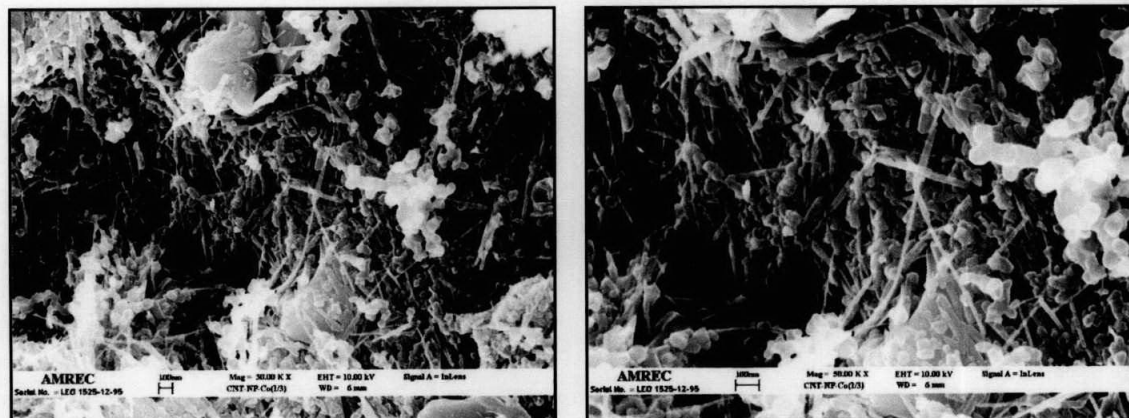
The CNTs prepared by catalytic methods contain metallic impurities such as Fe, Co and Ni in addition to various forms of carbon such as graphite, amorphous carbon, multishell carbon nanocapsules and nanoparticles. Such impurities are a serious impediment to detailed characterization of the properties of the carbon nanotubes. This is also why the non-purified samples were observed under scanning electron microscope.

Figures 4.6 to 4.11 show SEM images of the non-purified CNTs grown on Fe, Co and Ni catalysts. A total of six out of twelve catalysts have exhibited the ability of growing CNTs. The description and coding of each non-purified CNTs samples are as shown in Table 4.3. The example of how to measure diameter size is shown in Appendix B.



**Figure 4.6:** SEM images of FeD2 under magnification of (a) 30 000x and (b) 50 000x.

Scale bar 100 nm.



(a)

(b)

**Figure 4.7:** SEM images of CoB2 under magnification of (a) 30 000x and (b) 50 000x.

Scale bar 100 nm.

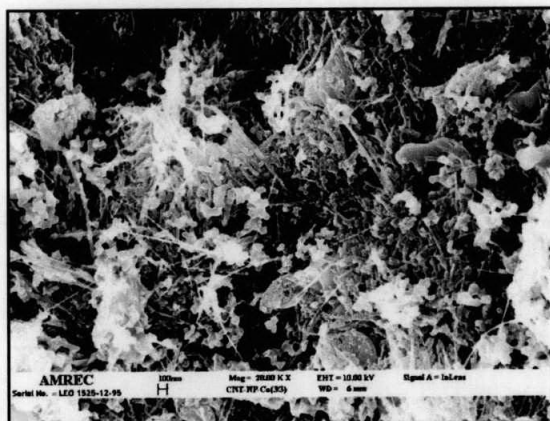


**Figure 4.8:** SEM image of CoC2 under magnification of 20 000x. Scale bar 100 nm.

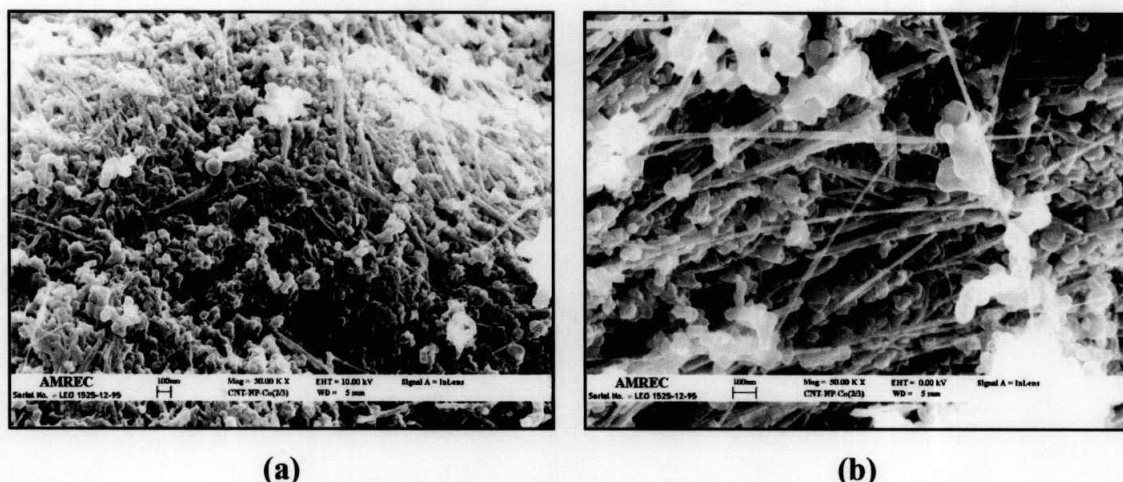
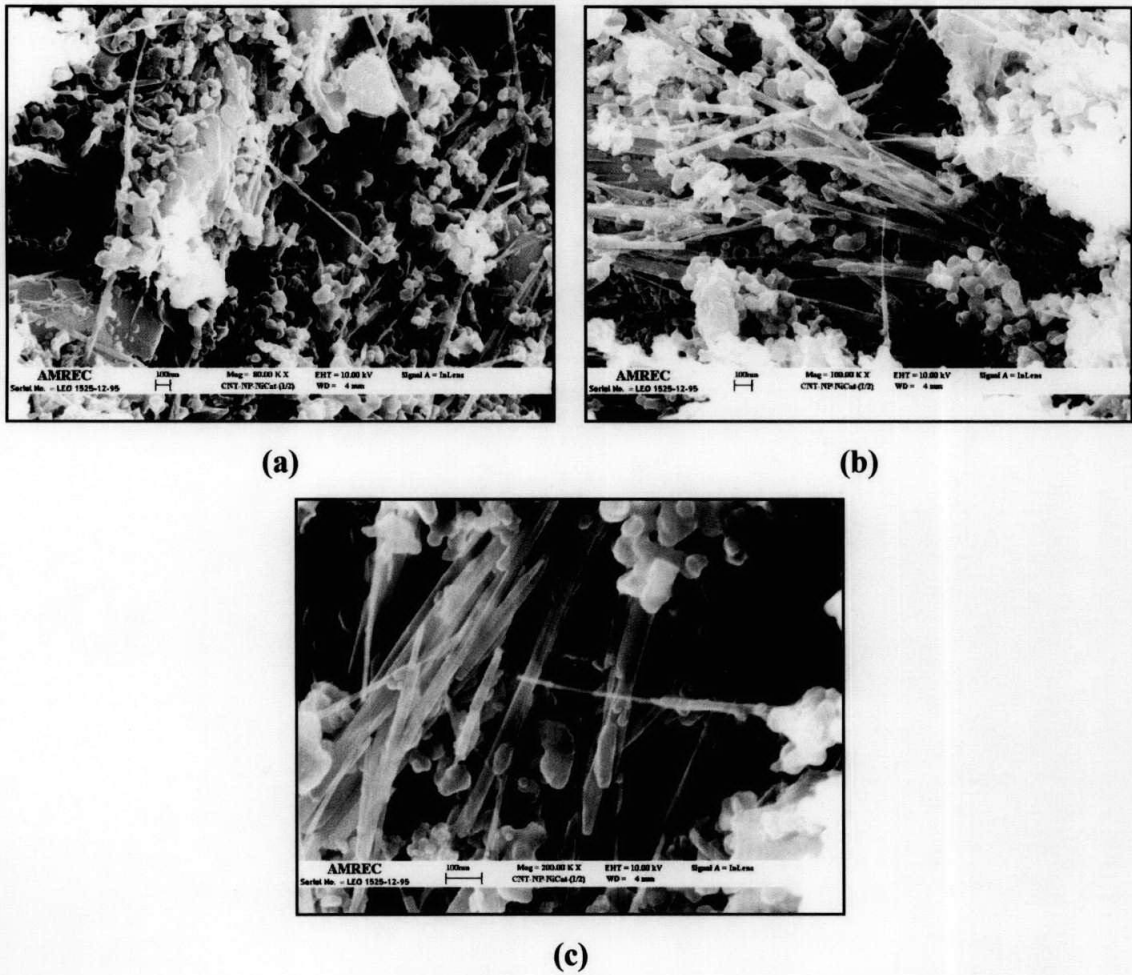


Figure 4.9: SEM images of CoD2 under magnification of (a) 30 000x and (b) 50 000x.

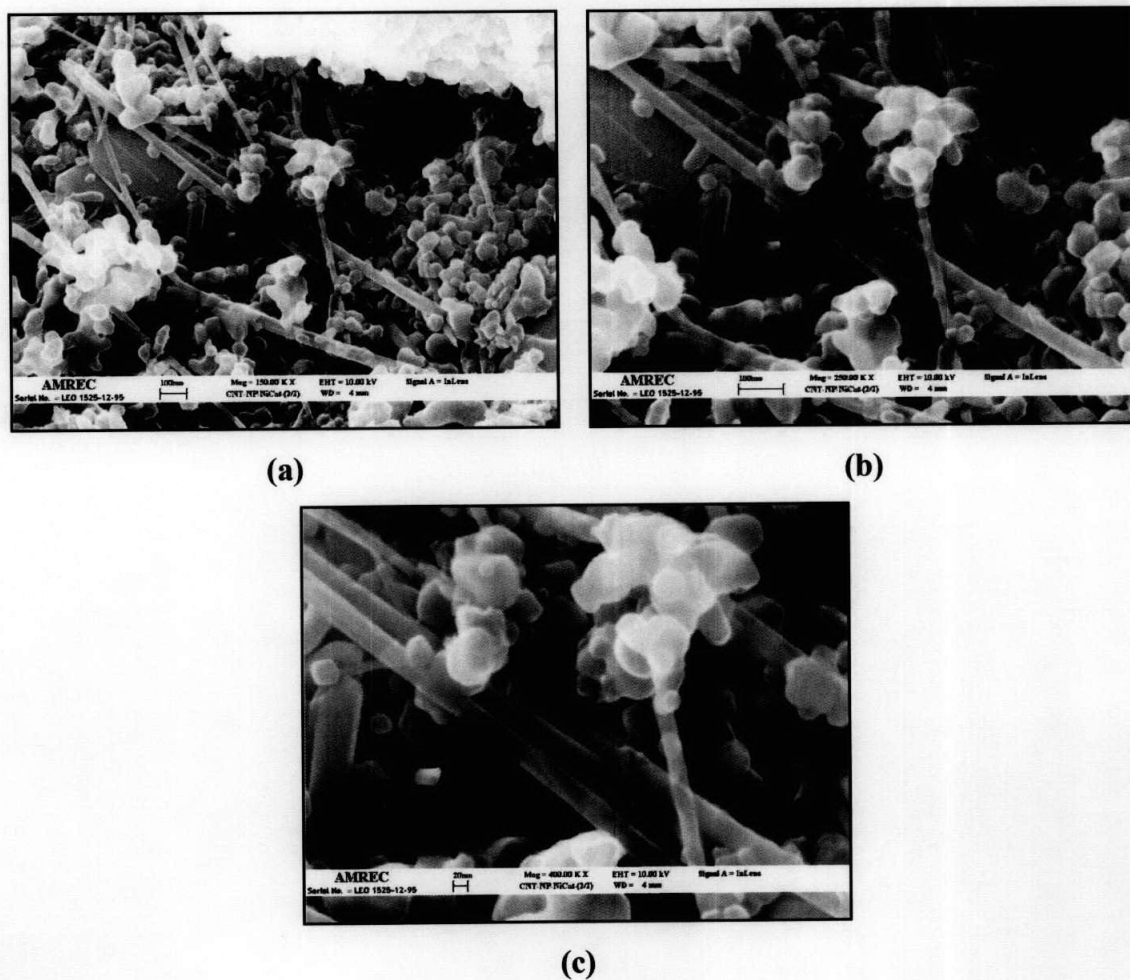
Scale bar 100 nm.

Table 4.3: The effect of dry etching process to the catalysts size.

| Description                                   | Coding | Catalyst size before dry etching ( $\mu\text{m}$ ) | Catalyst size after dry etching (nm) |
|---|--------|--|--------------------------------------|
| 1) Non-purified CNTs grown by FeD1 catalysts. | FeD2   | $4.62 \pm 0.42$                                    | $466 \pm 42$                         |
| 2) Non-purified CNTs grown by CoB1 catalysts. | CoB2   | $5.28 \pm 0.48$                                    | $537 \pm 48$                         |
| 3) Non-purified CNTs grown by CoC1 catalysts. | CoC2   | $4.88 \pm 0.34$                                    | $381 \pm 34$                         |
| 4) Non-purified CNTs grown by CoD1 catalysts. | CoD2   | $4.59 \pm 0.32$                                    | $285 \pm 25$                         |
| 5) Non-purified CNTs grown by NiC1 catalysts. | NiC2   | $1.23 \pm 0.11$                                    | $209 \pm 19$                         |
| 6) Non-purified CNTs grown by NiD1 catalysts. | NiD2   | $1.12 \pm 0.09$                                    | $143 \pm 13$                         |



**Figure 4.10:** SEM images of NiC<sub>2</sub> under magnification of (a) 80 000x, (b) 100 000x and (c) 200 000x.  
Scale bar 100 nm.



**Figure 4.11:** SEM images of NiD<sub>2</sub> under magnification of (a) 150 000x, (b) 250 000x and (c) 400 000x. Scale bar 100 nm for (a) and (b) while scale bar 20 nm for (c).

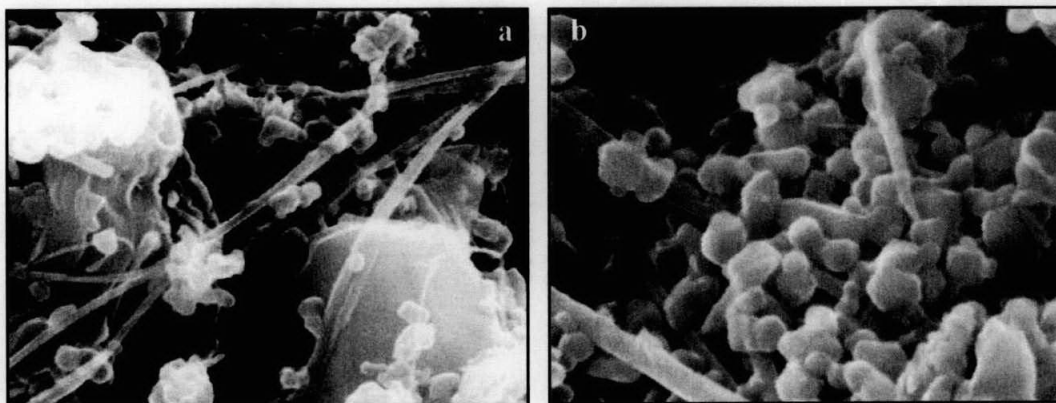


**Figure 4.12:** (a) Irregular shaped catalysts particles surrounded by CNTs and (b) polyhedral nano particles (disordered carbon).

The morphologies of non-purified CNTs are almost the same regardless of the catalyst used. It is observed that the non-purified products exhibit some polyhedral nano particles and fairly straight CNTs around irregular shaped particles. It is reported by Ebbesen *et al.* (1993) that the polyhedral structure might be some disordered carbon (see Figure 4.12 (b)), which is co-product of the process. All the non-purified samples that exhibit polyhedral structures were the size range of 60 nm to 80 nm.

The irregular shaped particles might be nano catalysts used to grow CNTs (see Figure 4.12 (a)). The size of the catalyst particles was determined by using analysis software of Carl Zeiss AxioVision 3.1. Values obtained are in the range of 466.01 nm to 142.92 nm and are summarised in Table 4.3. The results imply that the 5 hours dry etching process (refer to section 3.3.3) has actually reduced the catalysts size approximately ten times smaller than the size before dry etching for the same catalysts. The catalysts size obtained has also proven that the diameter size of the CNTs will not be the same as the catalyst particles size. Similar phenomenon has been reported by Ivanov *et al.* (1995). This is because CNTs will only grow on particular growing sites of the catalysts. This growth mechanism has been suggested by some of the researchers (Bethune *et al.*, 1993 and Iijima *et al.*, 1993). It was explained that the narrow diameter

range of CNT is resulted from the presence of more homogenous growing sites in the smaller catalyst used.

### 4.2.3 Purified Samples

The micrographs of non-purified samples have shown the existence of impurities in the samples due to catalytic method used during synthesise CNTs. The purification procedure which employed oxidation heat treatment followed by acid wash was straightforward, inexpensive and fairly effective (refer to section 2.3). The purification procedure is found to be able to eliminate the impurities completely by first oxidising the non-nanotube carbon and metal catalyst and second by removing the metal oxide, leaving relating pure CNTs. Thus this simple and effective method of carbon nanotubes purification has the ability to provide a stable, high quality source of carbon nanotubes for use in multiple applications.

Here, a purification scheme (refer to section 3.5) was designed to remove all of these undesired impurities. In a typical purification experiment reported by Strong, 2003, about 100 mg raw materials was mixed with 5 ml of hydrofluoric acid and 15 ml of water to dissolve the metallic impurities. It was stirred for 18 hours and then centrifuged to remove hydrofluoric acid. However, the carbon nanotubes obtained still contained many metal particles, presumably because some of the nano-sized catalysts coated with carbon layers were protected from the acid attack.

Thus, in this research a two-step purification technique was adopted. The technique involved oxidation in furnace and acid washing. The oxidation process was carried out at 300°C in furnace for 3 hours and then the sample was soaked in diluted 2M-hydrochloride acid for 18 hours to dissolve the metal oxides that formed during the oxidation process. Such oxidation steps burned the carbon coating on the catalyst particles, making them exposed to acid attack, while leaving the nanotubes unaffected because of their higher stability against oxidation compared with the defect-rich amorphous carbon.

First of all, changes in surface morphologies of purified CNTs have been carefully examined by scanning electron microscope. Figures 4.13 to 4.18 shows the typical SEM images of CNT after purification. The micrographs clearly illustrated that the efficiency of the purification process has lead to an obvious decrease of impurities content.

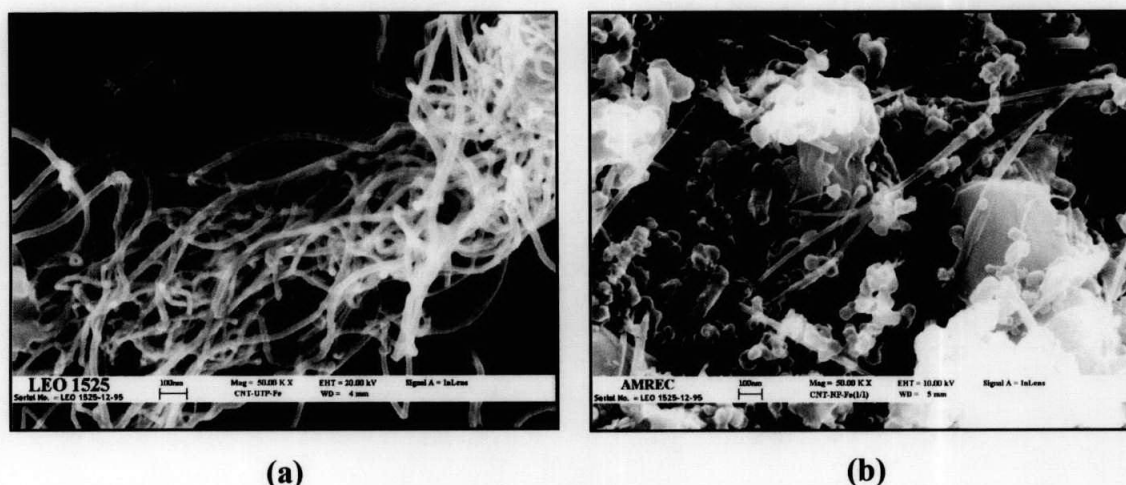


**Figure 4.13:** Micrograph of (a) purified CNTs grown on Fe catalyst ( $\text{FeD}_3$ ) and (b) non-purified CNTs grown on Fe catalyst ( $\text{FeD}_2$ ) under magnification of 50 000x. Scale bar 100 nm.

However, all the purified samples relatively are curvier than non-purified samples. It is believed that the purification process has disturbed the force equilibrium between CNTs and impurities. Before the samples purified, the Van der Waals force between molecules and stresses created during growing CNTs are in equilibrium. However, after purification, the CNTs may adjoin by Van der Waals interactions and deformed at certain sites (Ruoff *et al.*, 1993). The Van der Waals force has bigger effect when CNTs no longer on stress between catalysts. Besides, oxidising environment during oxidation may lead to gasification on certain sites of CNTs, which are defect-rich. These have cause deformation of the nanotubes structure.

Measurements on the external diameter of CNTs have been conducted using surface analysis software on the image derived from SEM. The average value obtained ranges from 35 nm for sample  $\text{FeD}_3$  to 19 nm for sample  $\text{NiD}_3$ . The results obtained were

summarised in Table 4.4. The example of how to measure average diameter and diameter range is shown in Appendix B. It is observed that the average diameter of CNTs follows the order of  $\text{FeD3} > \text{CoB3} > \text{CoC3} > \text{NiC3} > \text{CoD3} > \text{NiD3}$ . This outcome is attributed to the effect of the particle size of the catalyst, which is in the same order before the synthesis. It is predicted that the particle size of the catalyst is one of the factors determining the diameter of the CNTs produced.

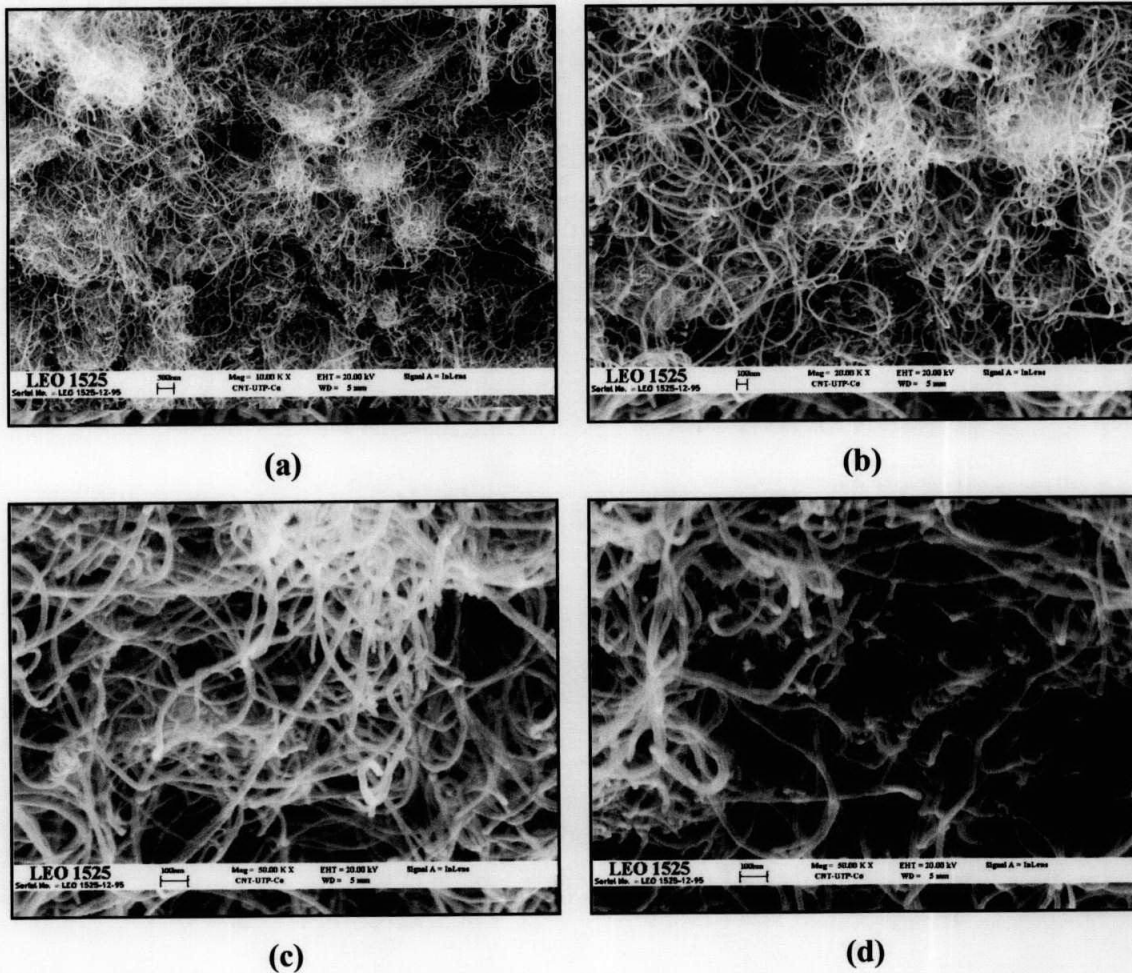


**Figure 4.14:** Micrograph of purified CNTs grown on Co catalyst (CoB3) under magnification of (a) 10 000x, (b) 20 000x, (c) 50 000x and (d) 50 000x. Scale bar 100 nm.

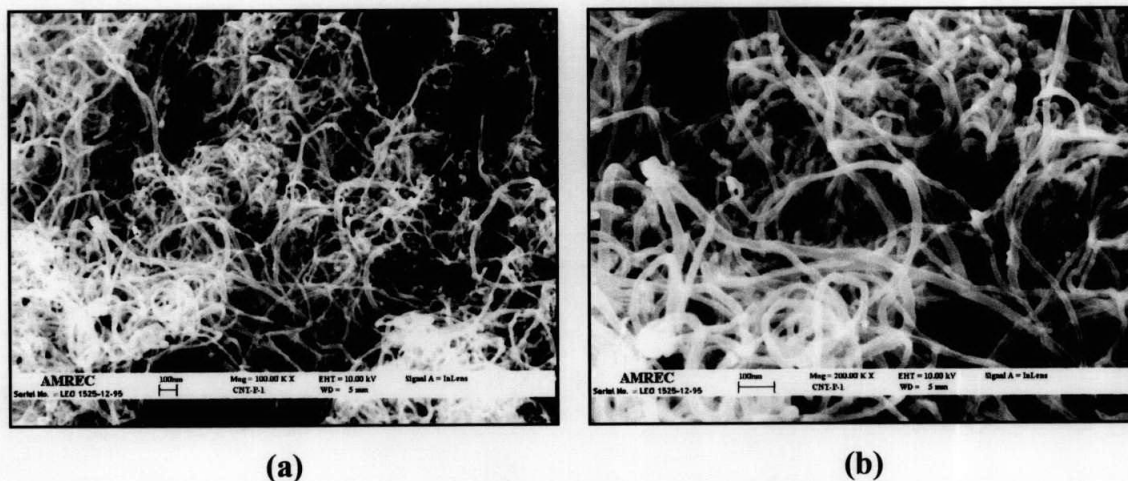


**Figure 4.15:** Micrograph of purified CNTs grown on Co catalyst (CoC3) under magnification of (a) 100 000x and (b) 200 000x. Scale bar 100 nm.

**Table 4.4:** Diameter measurement of CNTs.

| Description                               | Coding | Diameter range (nm) | Average external diameter (nm) | Structure                                | Diameter range obtained by Lee <i>et al.</i> , 2002 (nm) |
|---|--------|---------------------|--------------------------------|--|--|
| 1) Purified CNTs grown by FeD1 catalysts. | FeD3   | 31-38               | $35.16 \pm 3.12$               | Fairly straight with some curled ones.   | 80-200   |
| 2) Purified CNTs grown by CoB1 catalysts. | CoB3   | 23-26               | $25.32 \pm 1.24$               | Curled nanotubes with some helical ones. | 80-130   |
| 3) Purified CNTs grown by CoC1 catalysts. | CoC3   | 21-25               | $23.45 \pm 1.37$               |  |  |
| 4) Purified CNTs grown by CoD1 catalysts. | CoD3   | 18-22               | $20.62 \pm 1.22$               |  |  |
| 5) Purified CNTs grown by NiC1 catalysts. | NiC3   | 19-24               | $21.30 \pm 1.47$               | A lot of curled nanotubes.               | 90-110   |
| 6) Purified CNTs grown by NiD1 catalysts. | NiD3   | 17-23               | $19.17 \pm 1.52$               |  |  |

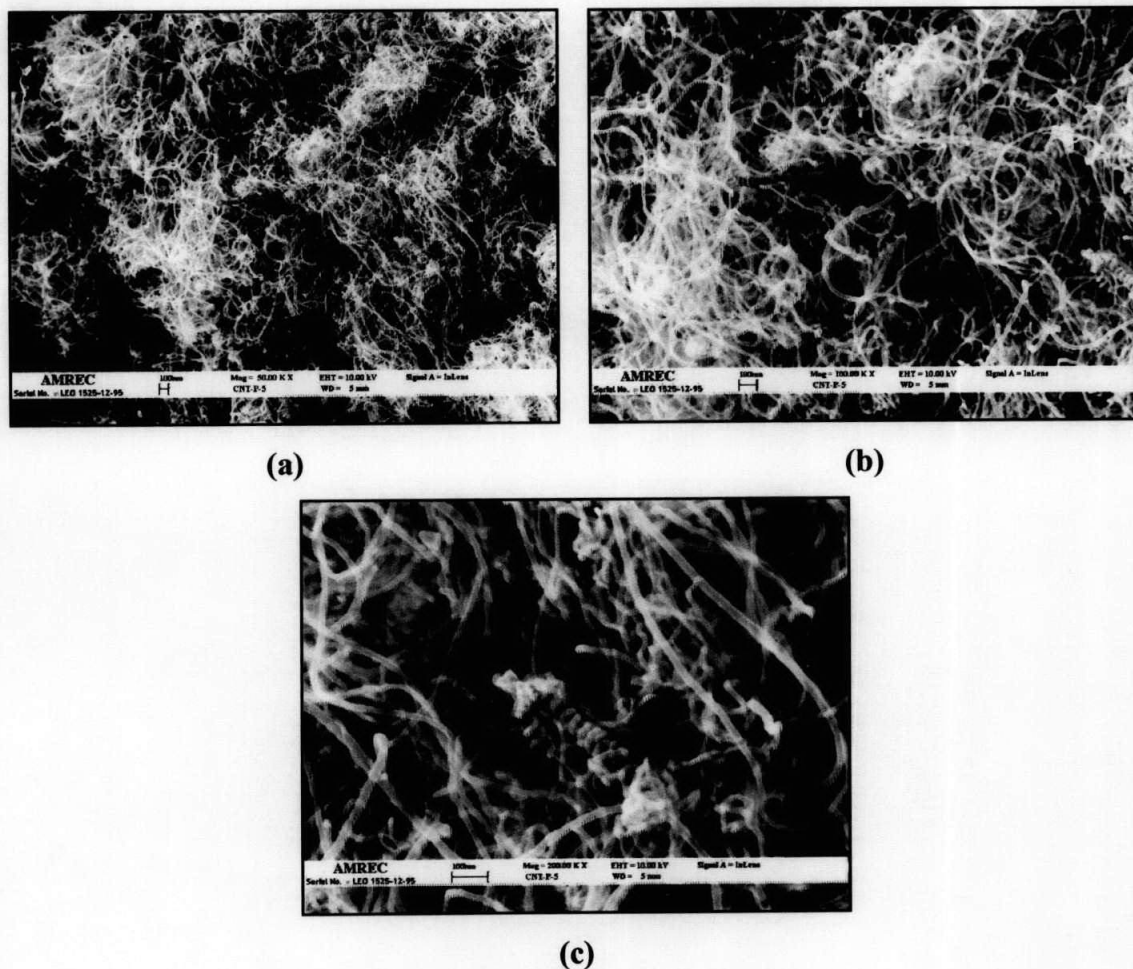


**Figure 4.16:** Micrograph of purified CNTs grown on Co catalyst (CoD3) under magnification of (a) 50 000x, (b) 100 000x and (c) 200 000x. Scale bar 100 nm.

The results indicated that CNTs grown on Fe catalyst have larger diameters compared to the ones on Co and Ni. Similar order in the size of CNTs grown catalytically on the catalyst particles has been reported by Lee *et al.*, 2002. This can be explained by the size effect of catalyst particles on the CNT growth. It is believed that the size of catalyst particles is in the order of Fe > Co > Ni before CNT growth. Lee has also reported the highest growth rate with Ni particles because being the smallest particle the rate of adsorption of carbon at the growth sites is faster, resulting in a faster growth rate.

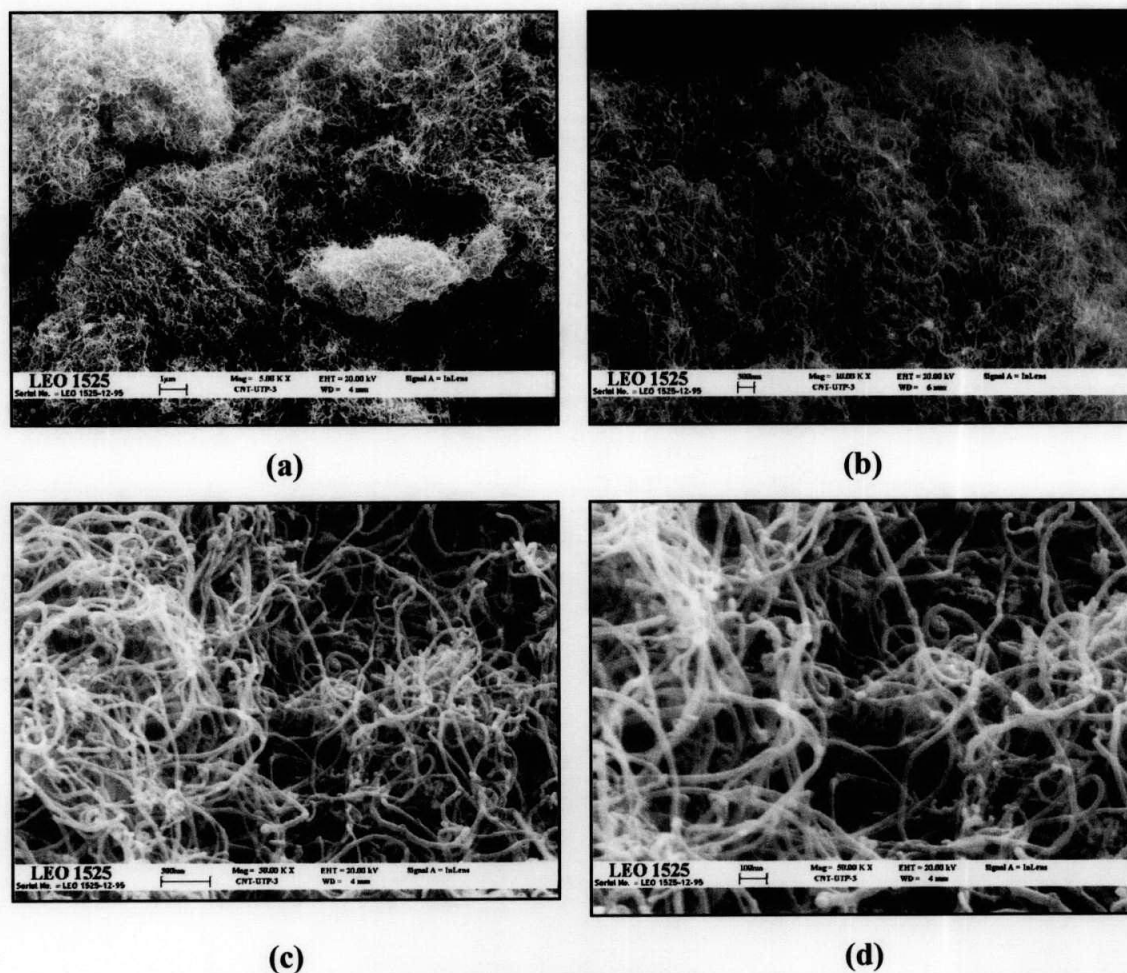


**Figure 4.17:** Micrograph of purified CNTs grown on Ni catalyst (NiC3) under magnification of (a) 5 000x, (b) 10 000x, (c) 30 000x and (d) 50 000x. Scale bar 100 nm.

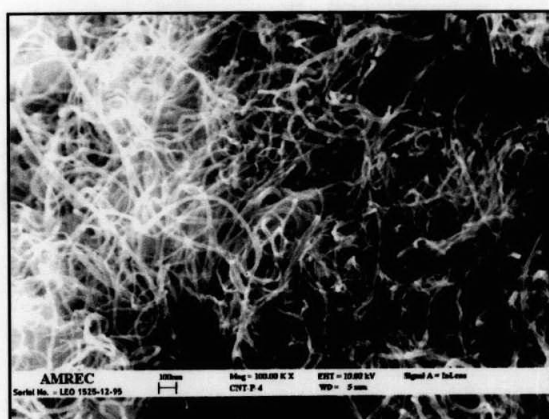


**Figure 4.18:** Micrograph of purified CNTs grown on Ni catalyst (NiD3) under magnification of 100 000x. Scale bar 100 nm.

CNTs grown on Fe are found to have the largest diameter range compared to the ones on Co and Ni catalysts (see Table 4.4), while CNTs grown on Co exhibit the narrowest diameter range compared to the others catalysts. Lee *et al.*, 2002 had reported similar order in the diameter range of CNTs grown. The comparison between the value obtained by Lee *et al.*, 2002 and this research is also exhibited in Table 4.4. This is explained by the size effect of catalyst particles on the growth of CNT where before the growth (see Table 4.3). The diameter range obtained here seems to be much smaller than others (Lee *et al.*, 2002, Pradhan *et al.*, 2002). This is believed to be due to the longer period and higher gas flow rate of ammonia pre-treatment prior to the growth of nanotubes, resulting in very much smaller nanosized catalyst particles (refer to section 3.3.3).

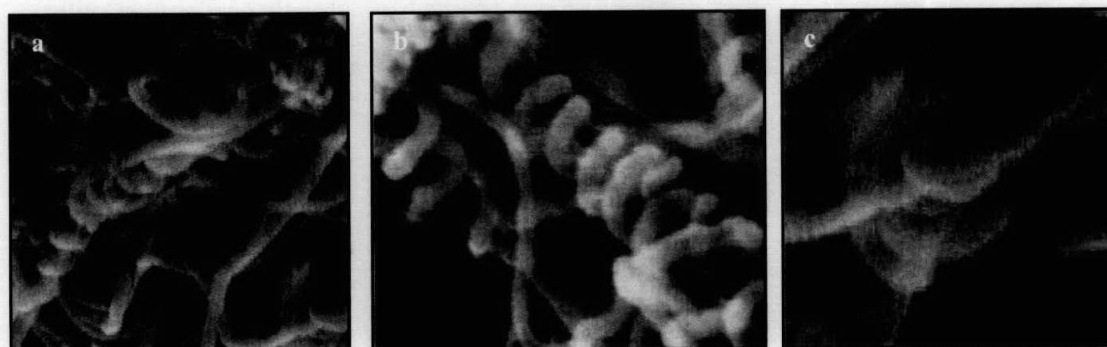


**Figure 4.19:** Images of helical structure of CNT grown on Co catalyst.

It appears that the morphologies of CNTs on all catalyst particles are almost the same. However, closer inspection of the images shows a distinction between CNTs on different catalyst particles. Nanotubes grown on Fe particles seem to have fairly straight structure whereas a lot of curled ones can be observed in CNTs image grown on Ni. Some helical tubes can even be identified amongst the curled ones grown on Co (see Figure 4.19). Similar shaped nanotubes have been reported by Bernaerts *et al.*, 1995.

Detailed model on curled and helical nanotubes is given by Amelinckx *et al.*, 1994. The growth of these nanotubes is discussed in terms of a locus of active sites around the

periphery of the catalytic particle, and growth velocity vectors. In the simplest case the locus sites is circular and the extrusion velocity is constant, producing a straight tube propagating at a constant rate as can be seen in some of the tubes grown on Fe catalyst particles. In reality, the locus of active sites may not be circular, which introduces some complexity in the shape of the tubes. It has been shown that a catalytic activity, which varies around the ellipse, will produce helical growth.

In this work, the successful procedures have been developed to grow carbon nanotubes catalytically in powder form using thermal CVD. The effect of using different catalyst particles on the size and shape of CNTs has also been investigated. It was found that the particle size of the catalyst which is in the order of  $Fe > Co > Ni$  produced CNTs with diameters in the same order. The size effect of catalyst particle is concluded to be the main factor determining the diameter of CNTs grown. Structurally, CNTs grown on Fe are fairly straight whereas CNTs grown on Ni and Co reveals some curled and even helical shaped tubes.

Since SEM images observation is focused on a tiny part of the sample, the understanding of the material morphologically does not reflect an overall characterisation. Thus further investigations are needed, especially bulk characterisation like X-ray diffraction (XRD), thermal gravimetry analysis (TGA) and Raman spectroscopy. Therefore, the next section will be discussing on X-ray diffraction characterisation on non-purified and the purified samples

### 4.3 X-Ray Diffractometry (XRD)

The phases and structural integrity of the 6 samples were evaluated using powder X-ray diffraction. The radiation source is  $\text{CuK}\alpha$  where the wavelength is 0.15418 nm. Reference materials such as graphite and pure metals together with Joint Committee on Powder Diffraction (JCPDS) citation are tabulated in Table 4.5. For all the XRD results, diffraction pattern of graphite and pure metal will be included for the purpose of comparison.

**Table 4.5:** Main diffraction peaks related to graphite and pure metal Fe, Co and Ni.

| Compound                                | Plane [hkl] | Diffraction angle ( $2\theta$ ) | Intensity |
|---|-------------|---------------------------------|-----------|
| <b>Graphite</b><br>(JCPDS 23-64)        | [002]       | 26.5                            | 100       |
|   | [100]       | 42.4                            | 10        |
|   | [101]       | 44.6                            | 50        |
|   | [004]       | 54.7                            | 80        |
| <b>Pure metal Fe</b><br>(JCPDS 6-696)   | [110]       | 44.7                            | 100       |
|   | [200]       | 65.0                            | 20        |
| <b>Pure metal Co</b><br>(JCPDS 89-4308) | [100]       | 41.6                            | 270       |
|   | [002]       | 44.3                            | 286       |
|   | [101]       | 47.4                            | 999       |
| <b>Pure metal Ni</b><br>(JCPDS 3-1051)  | [111]       | 44.8                            | 100       |
|   | [200]       | 52.2                            | 54        |

X-ray beam would give a hexagonal diffraction pattern when perpendicular to a flat graphite sheet. A similar pattern will result, if a beam impinging on a multiwalled nanotube in which all the tubes have an identical structure as represented in Figure 4.20(a). By tilting the beam in a direction perpendicular to the tube axis, the same diffraction pattern will be obtained (Zhang *et al.*, 1994). Therefore, in reciprocal space the spots become circles situated in planes normal to nanotube axis, as shown in Figure 4.20(b). This has explained that all the obtained XRD pattern shows a significant peak at an angle of  $26.5^\circ$ . Since the graphitic (002) diffraction are locally tangent to successive cylinders, distance between lattice fringe of CNTs can be determined by calculating the interlayer spacing of plane (002) diffraction peak. Figure 4.20(b)

illustrate that diffraction of CNT would be very close to graphite diffraction. Since JCPDS do not have diffraction file for CNT, researchers would normally use other carbon allotrope diffraction file as a reference especially graphite (Zhang *et al.*, 1994, Pradhan *et al.*, 2002, Strong *et al.*, 2003).

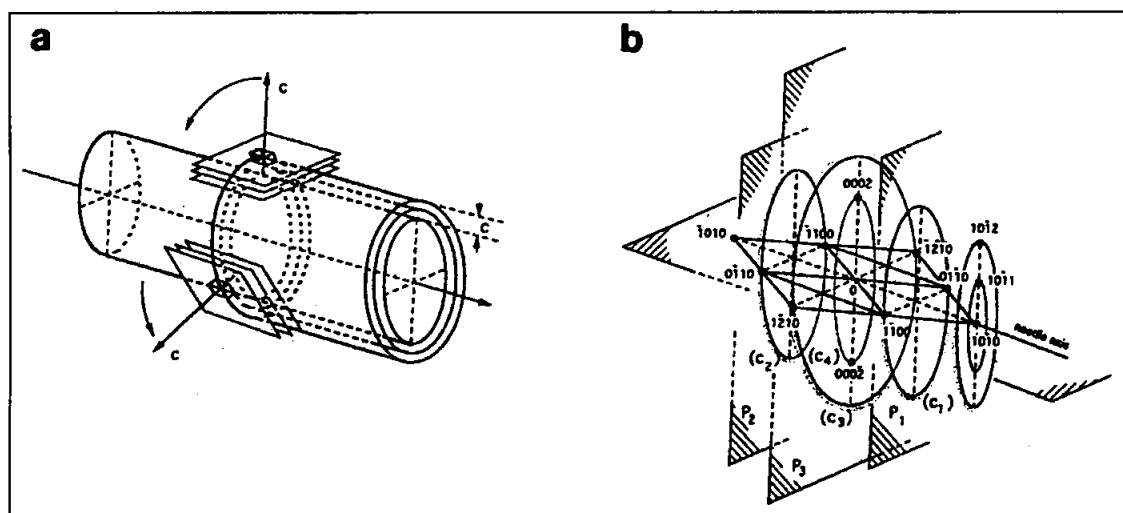


**Figure 4.20:** (a) Schematic drawing of multiwalled nanotube illustrating graphite c-planes.  
(b) Reciprocal space construction for a tube. (Reproduced from Zhang *et al.*, 1994).

### 4.3.1 Non-purified Samples

Figure 4.21 to 4.23 show XRD pattern of non-purified CNTs grown on Fe, Co and Ni respectively. As mention in previous section, the CNTs diffraction pattern is dominated by the graphitic (002) diffraction peak. However, the angle of plane (002) peak for most of the specimen is slightly smaller than graphite ( $26.5^\circ$ ). This is due to the stacking of CNTs, which is in the form of turbostratic structure rather than ABABAB type (Saito *et al.*, 1993). Besides, other diffraction peak of CNT is difficult to identify because the catalysts diffraction peak is close to CNT diffraction peak especially at angle around  $42^\circ$  to  $45^\circ$ .

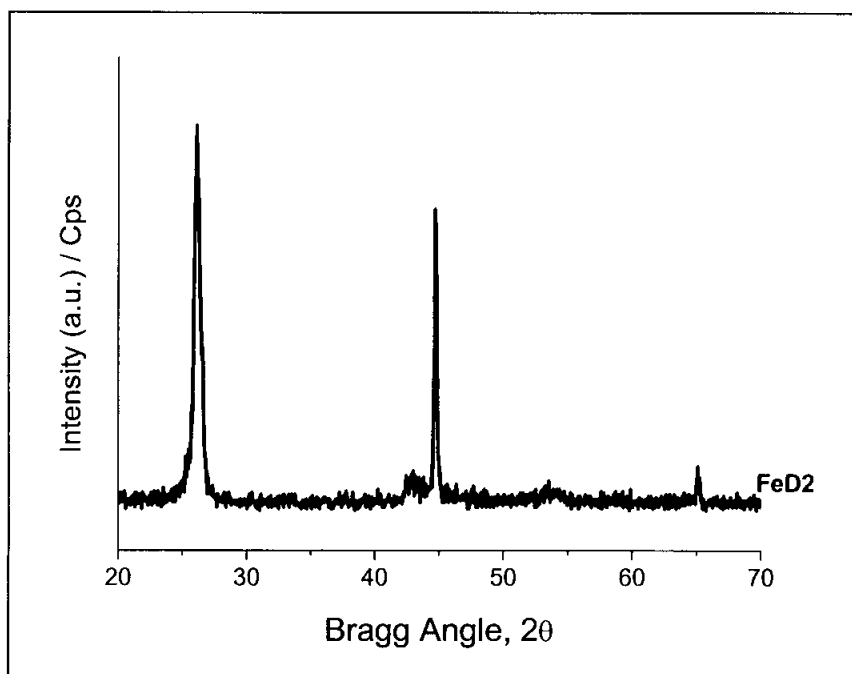


Figure 4.21: XRD diffractogram of FeD2.

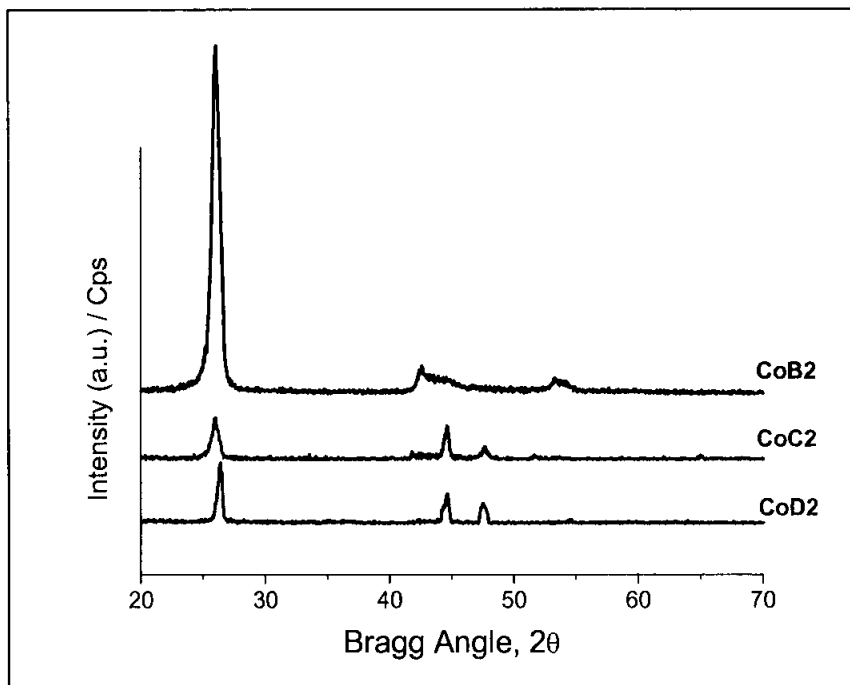


Figure 4.22: XRD diffractogram of CoB<sub>2</sub>, CoC<sub>2</sub> and CoD<sub>2</sub>.

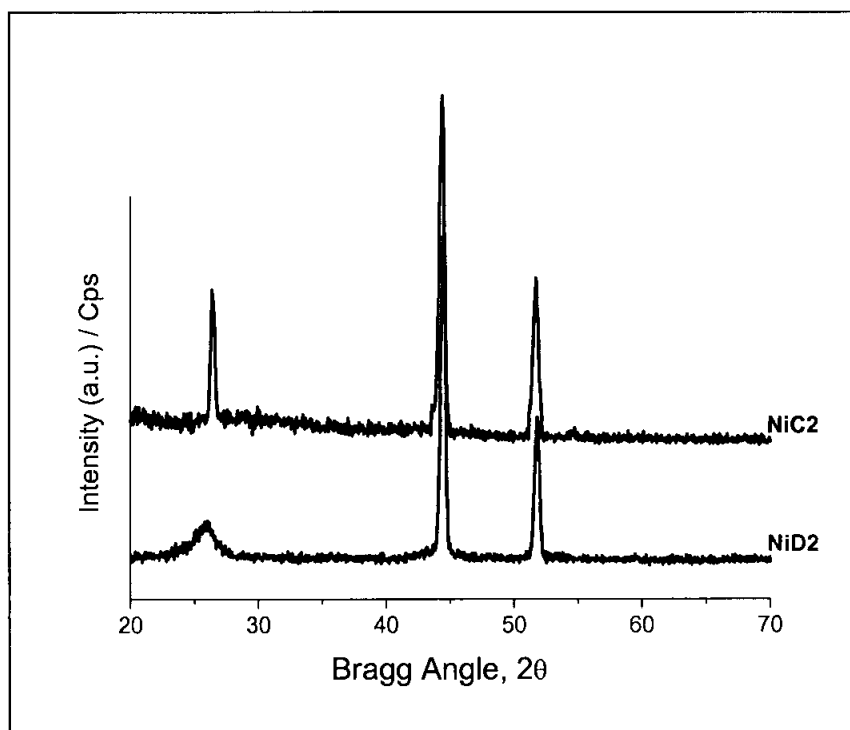


Figure 4.23: XRD diffractogram of NiC<sub>2</sub> and NiD<sub>2</sub>.

The interlayer spacing for CNTs would be bigger compare to graphite because Van der Waals force between interlayer for turbostatic is weaker. Therefore, the interlayer spacing that obtained for non-purified CNTs are bigger than graphite (3.34 Å). The values are in the range 3.37 Å to 3.47 Å and were tabulated in Table 4.6. Corresponding peak reflections together with observation on each diffraction pattern was recorded in Table 4.6.

**Table 4.6:** XRD summary of non-purified samples.

| <b>Specimen</b> | <b>Main peak</b>             | <b>Plane (002)<br/>Interlayer Spacing<br/>(Å)</b> | <b>Observation</b>  |
|-----------------|------------------------------|---|---|
| FeD2            | 26.12°,<br>44.73°,<br>65.06° | 3.41  | Crystallite material. Graphitic (002) diffraction shows a sharp peak at 26.12°. A sharp peak shows reflection of CNT and Fe at 44.73° while a small peak shows Fe reflection at 65.06°.             |
| CoB2            | 25.96°,<br>42.66°,<br>53.64° | 3.43  | Crystallite material. Graphitic (002) diffraction shows a sharp peak at 25.96°. A broad peak shows reflection of CNT and Co at 42.66° while a small broad peak shows graphite reflection at 53.64°. |
| CoC2            | 25.96°,<br>44.53°,<br>47.67° | 3.43  | Crystallite material. Graphitic (002) diffraction shows a sharp peak at 25.96°. A sharp peak shows reflection of CNT and Co at 44.53° while a small broad peak shows Co reflection at 47.67°.       |

Table 4.6: Continued.

| Specimen | Main peak                    | Plane (002)<br>Interlayer<br>Spacing<br>(Å) | Observation   |
|----------|------------------------------|---|---|
| CoD2     | 26.36°,<br>44.53°,<br>47.54° | 3.38  | Crystallite material. Graphitic (002) diffraction shows a sharp peak at 26.36°. A sharp peak shows reflection of CNT and Co at 44.53° while a small broad peak shows Co reflection at 47.54°. |
| NiC2     | 26.44°,<br>44.34°,<br>51.82° | 3.37  | Crystallite material. Graphitic (002) diffraction shows a sharp peak at 26.44°. Sharp and high peaks show reflection of Ni at 44.34° and 51.82°.  |
| NiD2     | 25.64°,<br>44.34°,<br>51.69° | 3.47  | Crystallite material. Graphitic (002) diffraction shows a sharp peak at 25.64°. Sharp and high peaks show reflection of Ni at 44.34° and 51.69°.  |

Figure 4.21 shows diffraction pattern of FeD2, the non-purified CNTs grown on FeD1. The graphitic (002) diffraction peak is shown at 26.12° and was identified the interlayer spacing,  $d_{002}$  is 3.41 Å. The interlayer spacing obtained based on Bragg's law, which is mentioned in Equation 3.1 and the calculation working is presented in Appendix C. Another sharp peak is shown at 44.73°, which is believed to be the reflection of CNT and Fe since their peak overlapped each other. At 65.06° there is a small peak, attributed Fe.

Figure 4.22 depicts diffractions pattern of non-purified CNTs grown on Co catalyst, there are CoB2, CoC2 and CoD2. The latter illustrate graphitic (002) diffraction at  $26.36^\circ$  and  $3.38 \text{ \AA}$  of interlayer spacing. While CoB2 and CoC2 have graphite (002) diffraction at  $25.96^\circ$  with  $3.43$  of interlayer spacing. CoC2 and CoD2 have shown weaker crystallinity than CoB2 by comparing the intensity of the diffraction plane (002). For CoB2, a broad peak shows reflection of CNT and Co at  $42.66^\circ$  while a small broad peak shows CNT reflection at  $53.64^\circ$ . Specimen CoC2 and CoD2 have second peak at  $44.53^\circ$  indicating the presence of CNT and Co while a small broad peak appearing at  $47.67^\circ$  and  $47.54^\circ$  respectively is the characteristic of Co alone.

NiC2 and NiD2, the non-purified CNTs grown on Ni catalyst diffraction pattern were shown in Figure 4.23. The (002) diffraction peak at  $26.44^\circ$  and  $25.64^\circ$  with  $3.37 \text{ \AA}$  and  $3.47 \text{ \AA}$  were shown respectively. Both specimens show two significant peaks at  $44.34^\circ$  and around  $52^\circ$ , which is Ni reflection.

In this section, FeD2, CoB2 and NiC2 have exhibit higher crystallinity compared to the rest of non-purified CNT specimens because the ratio between the graphitic peak and metal diffraction peaks are higher compare to the rest of the specimens. From the interlayer spacing results, CoB2 has shown to have the biggest spacing followed by FeD2 and NiC2. This may implies that the one with bigger interlayer spacing may have weaker Van der Waals force between the layers.

### 4.3.2 Purified Samples

XRD patterns of purified CNTs samples are compared in Figure 4.24 to 4.26. The diffraction pattern is dominated by the graphitic (002) diffraction peak.

From the XRD pattern in Figure 4.24, apart from the CNT peak, the strong Fe peaks were observed. However, these Fe peaks seem to be of lower intensity compared to the non-purified ones. This indicates that FeD3 contained some residual metal, which are not totally eliminated after the purification process. However the graphite peak is more prominent revealing the condition of nanotube with amorphous carbon being totally eliminated by oxidation reaction.

The XRD patterns of the CoB3, CoC3 and CoD3 in Figure 4.25 show that the metal Co peak was very weak and broad in intensity. Among these three samples, CoB3 exhibit higher graphitisation degree. The graphitic (002) peak of CoB3 is much more prominent than CoC3 and CoD3.

From the XRD pattern in Figure 4.26, apart from the graphitic (002) peak, the strong metal Ni peak was observed in NiD3. Comparative between NiC3 and NiD3, relatively pure CNT were obtained by NiC3 although a very broad metal Ni peak was observed at  $41^\circ$  to  $45^\circ$ . However, the peak might be CNT reflection of plane (100) and (101).

The interlayer spacing of CNTs sample shows the same result as the non-purified sample except specimen FeD3, which exhibit the interlayer spacing reduced by  $0.01 \text{ \AA}$  and NiD3 reduced by  $0.1 \text{ \AA}$ . This may be caused by the changes in Van der Waals forces among the layer after the catalyst particles have been eliminated. The interlayer spacing results for purified sample are presented in Table 4.7. The diffraction pattern observations are also summarised in Table 4.7.

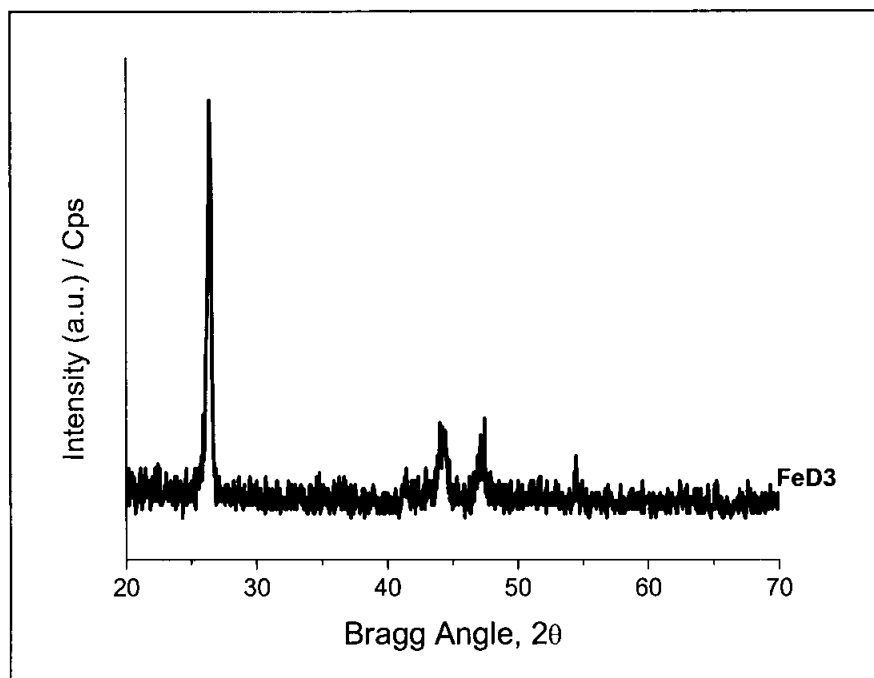


Figure 4.24: XRD diffractogram of FeD<sub>3</sub>.

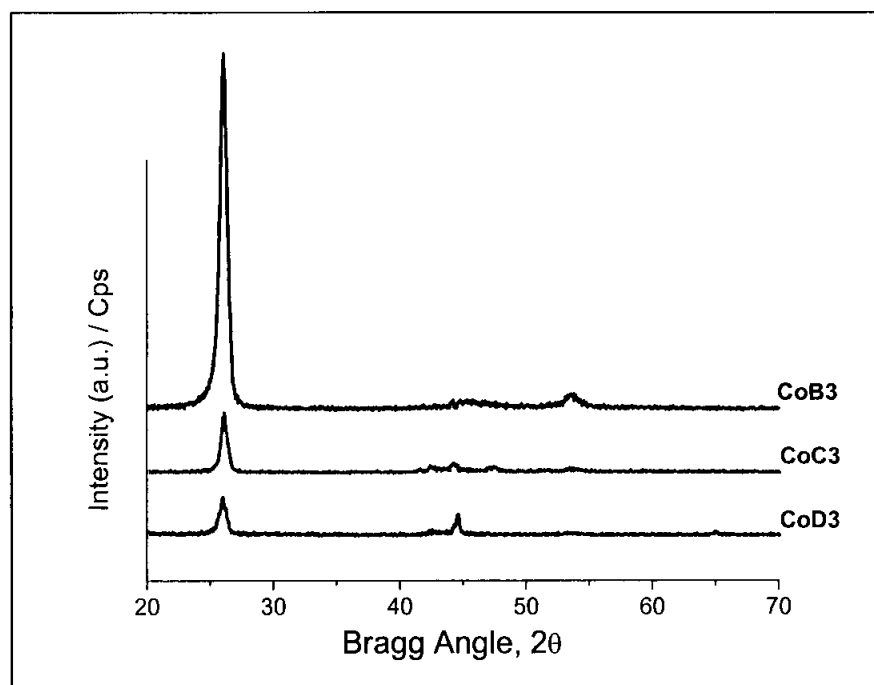


Figure 4.25: XRD diffractogram of CoB<sub>3</sub>, CoC<sub>3</sub> and CoD<sub>3</sub>.

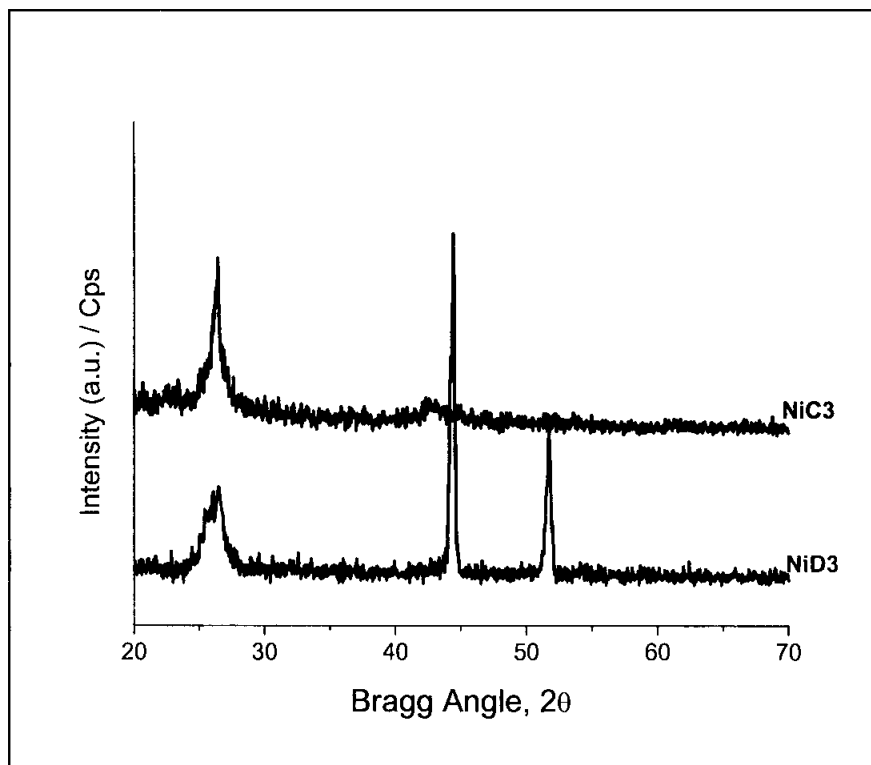


Figure 4.26: XRD diffractogram of NiC3 and NiD3.

Based on all the XRD results obtained for purified and non-purified CNTs, specimen FeD3, CoB3 and NiC3 are the best specimens for further investigation on crystallinity of CNTs. This is because the three specimens exhibited high degree of graphitisation from the observation of the XRD results. Since the characterisation needed sophisticated techniques such as equipments transmission electron microscope, thermal gravimetry analysis (TGA) and Raman spectroscopy, the analysis would be very costly and time consuming. Therefore, only three specimens are selected, there are FeD3, CoB3 and NiC3.

Table 4.7: XRD summary of purified samples.

| Specimen | Main peak                               | Plane (002)<br>Interlayer<br>Spacing<br>(Å) | Observation  |
|----------|---|---|--|
| FeD3     | 26.32°,<br>44.03°,<br>47.47°,<br>54.34° | 3.39  | Crystallite material. Sharp peaks show reflection of CNT at 26.32° and 44.03° followed by a small peak at 54.34°. A small sharp peak shows reflection of Fe at 47.47°. |
| CoB3     | 25.95°,<br>53.48°                       | 3.43  | Crystallite material. Sharp peaks show reflection of CNT at 25.95° and 53.48°. A small broad peak shows reflection of CNT and Co at 42.3° to 47.8°.                    |
| CoC3     | 25.94°,<br>44.39°                       | 3.43  | Crystallite material. A Sharp peak shows reflection of CNT at 25.94° and a small sharp peak shows reflection of Co at 44.39°.  |
| CoD3     | 25.94°,<br>44.66°                       | 3.43  | Crystallite material. Sharp peak shows reflection of CNT at 25.94. A small sharp peak shows reflection of Co at 44.66°.  |
| NiC3     | 26.42°                                  | 3.37  | Crystallite material. Broad tail peak shows reflection of CNT at 26.42°. A very broad peak shows reflection of CNT and Ni at 41° to 45°.                               |
| NiD3     | 26.42°,<br>44.40°,<br>51.60°            | 3.37  | Crystallite material. A Broad peak shows reflection of CNT at 26.42° and sharp peaks show reflection of Ni at 44.40° and 51.60°.                                       |

## 4.4 Further Investigation of Selected Samples

### 4.4.1 Introduction

Three purified CNTs samples were chosen for further investigation into their degree of crystallinity, purity, tube wall structure and buckling behaviour in purification. TEM, TGA and Raman spectroscopy were used to characterise these selected samples. One sample will be selected from each type of catalyst. FeD3 was selected because it is the only purified CNTs sample grown by Fe catalyst. While CoB3 and NiC3 were chosen due to high crystallinity and less impurities based on XRD results. The descriptions of the three specimens were tabulated in Table 4.8.

**Table 4.8:** Description of purified samples for the investigation of TEM and TGA techniques.

| <b>Description</b>             | <b>Code</b> |
|--------------------------------|-------------|
| 1) Purified CNTs grown by FeD1 | FeD3        |
| 2) Purified CNTs grown by CoB1 | CoB3        |
| 3) Purified CNTs grown by NiC1 | NiC3        |

### 4.4.2 Transmission Electron Microscopy (TEM)

The typical SEM images in Figures 4.13 to 4.18 show the configuration of the purified samples. Abundant threadlike entities can be seen clearly. Further TEM observations (see Figures 4.27, 4.28 and 4.29) provide evidence that the twisting and winding entities are carbon nanotubes. It is difficult to make out the accurate length of the MWNTs from the SEM observation due to the twisting, but the length is assumed to be more than several tens of micrometers.

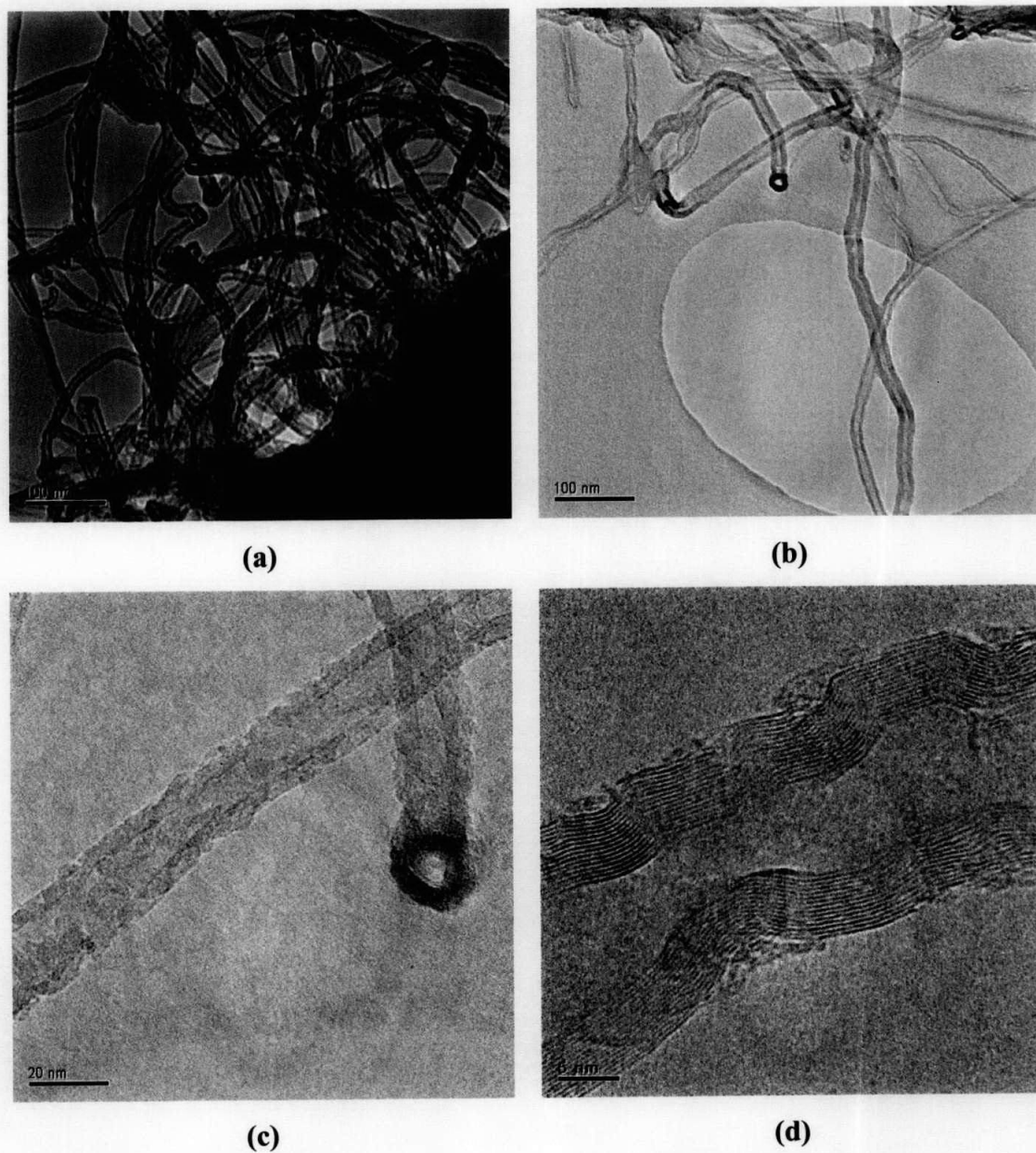


**Figure 4.27:** (a) to (c) TEM images of FeD3 under different magnification. (d) Higher resolution image of FeD3. Scale bar 100 nm for (a) and (b) while (c) scale bar is 20 nm and scale bar for (d) is 5 nm.

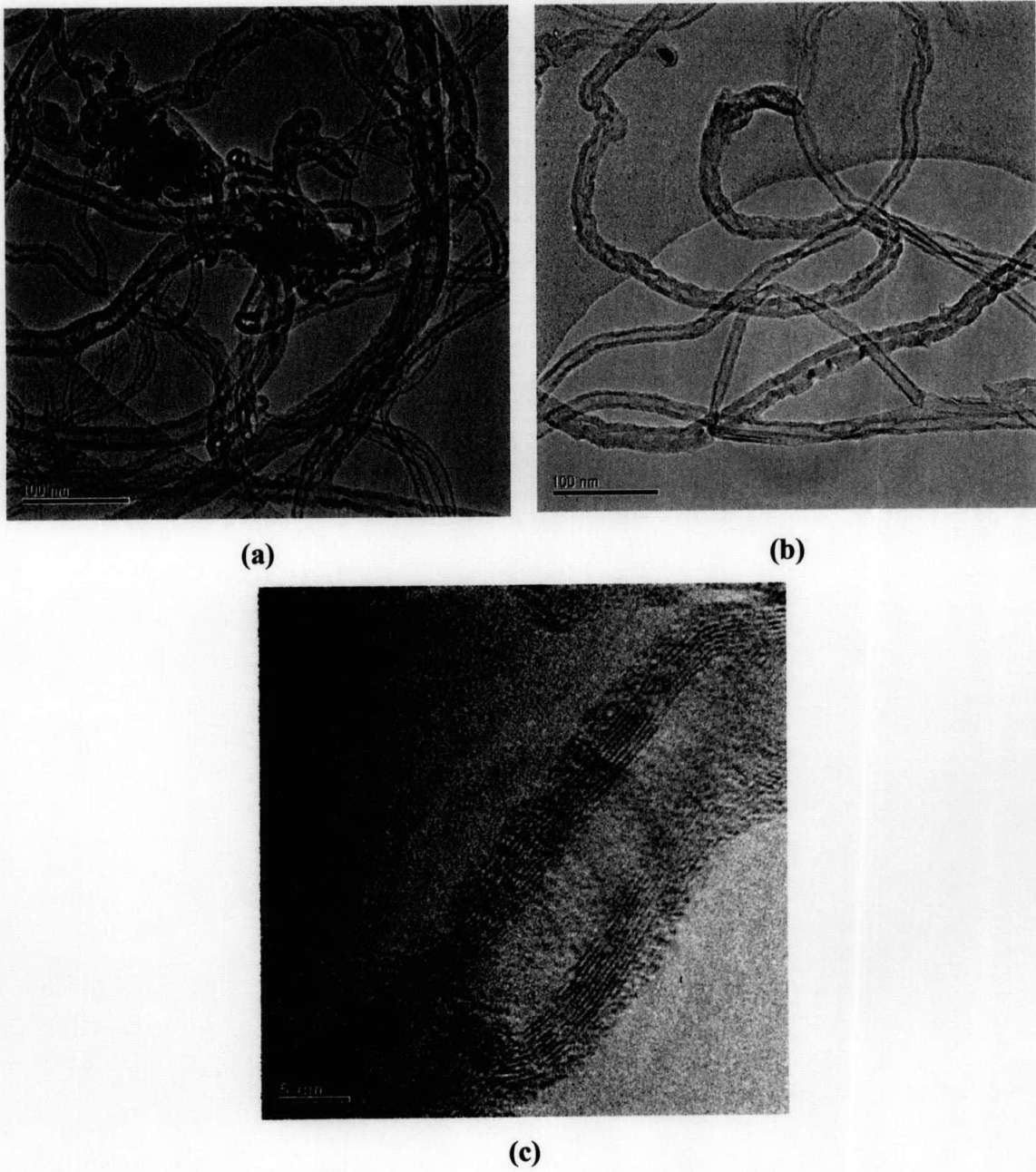


**Figure 4.28:** (a) and (b) TEM images of CoB3 under different magnification. (c) Higher resolution image of CoB3. Scale bar 100 nm for (a) and (b) while scale bar for (c) is 5 nm

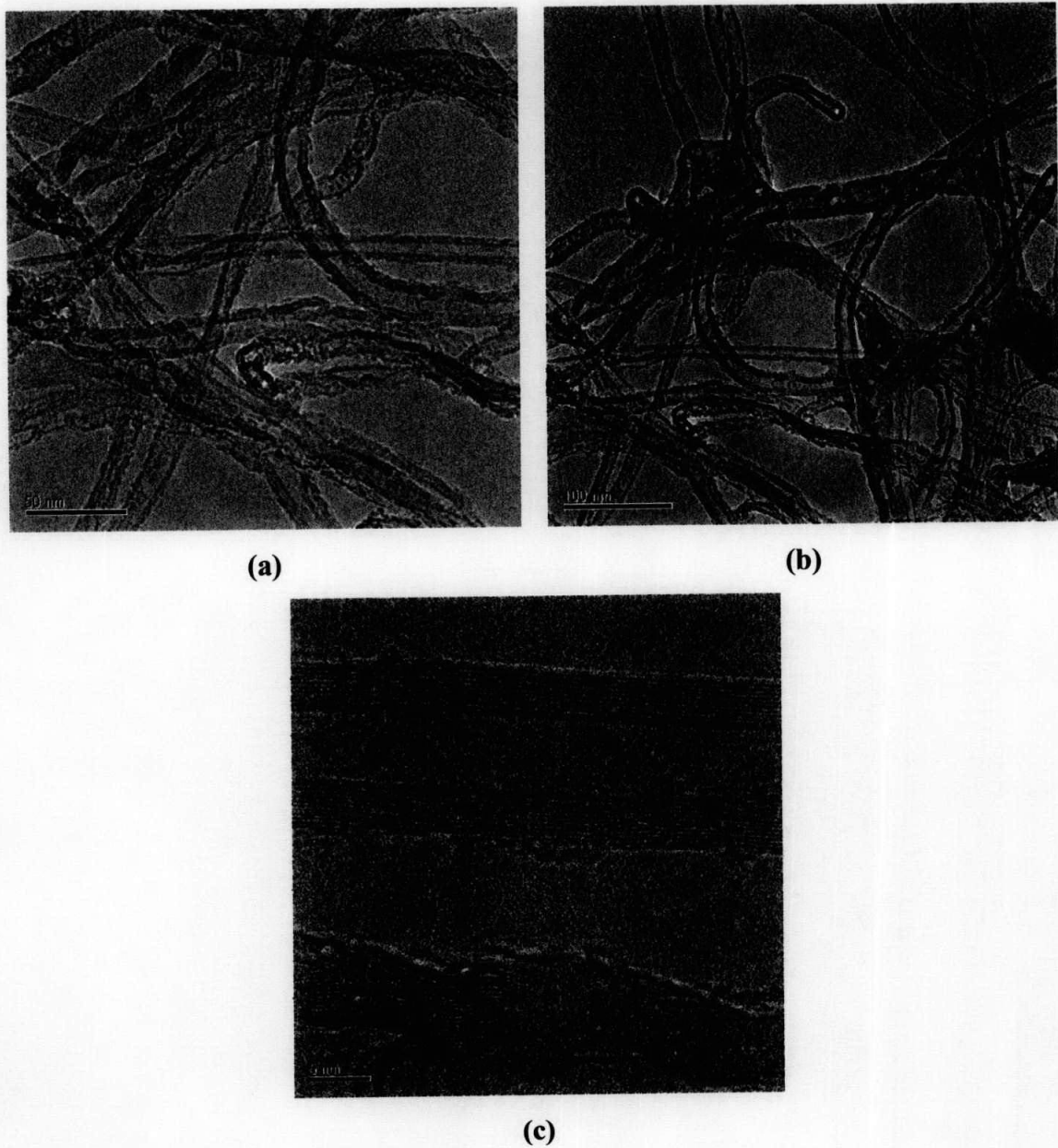


**Figure 4.29:** (a) to (b) TEM images of NiC<sub>3</sub> under different magnification. (c) Higher resolution image of NiC<sub>3</sub>. Scale bar 100 nm for (a) and (b) while scale bar for (c) is 5 nm.

In addition to catalyst particles, catalytically prepared CNT sample contains various kinds of by-products, such as fullerenes, polyaromatic hydrocarbons, polyhedral carbon, amorphous carbon etc. Dissolving metal particles in HCl can be done with ease in a laboratory scale experiment. Selective oxidation of undesirable carbon means a real challenge, since there is only a slight difference in the reactivities in CNTs and other

carbonaceous materials. This suggests that during oxidation purification, competitive oxidation always takes places whereby CNTs and amorphous carbon react simultaneously, with different rates. The structure of polyhedral carbon, amorphous carbon, etc is full of reactive edges that are exposed directly to oxidizing agents that can results in faster oxidation compared to CNTs. At the same time, straight CNTs can be oxidized only from the ends. Of course, the structure of different CNTs has indisputable effect on their oxidation rate. Fullerene can be oxidized more easily and its reactivity is increasing with decreasing diameter. The oxidation rates of structures strained by pentagons or heptagons, such as end caps or spiral nanotubes, are definitely higher compared to cylindrical surfaces. Thus, some open-ended CNTs were produced as the by-product of oxidation purification procedure. In the TEM images, open-ended CNTs were observed (see Figure 4.30). Structural defects in CNTs would also become the sites of preferential etching during oxidation.

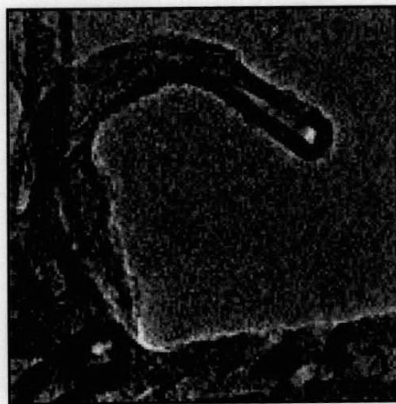


**Figure 4.30:** Open-ended CNT.

TEM analysis reveals that the synthesised CNTs are multiwalled. A careful survey by TEM studies enabled carbon nanotubes tips to be identified and as expected, the proportion of opened ends was greater in the purified CNTs sample than in the raw sample. The tips were typically hemispherical with no catalyst particle at the tip but other less symmetrical structures were also observed (see Figures 4.27, 4.28 and 4.29). However, in some cases a catalyst particle was found attached to the tube end. These features are characteristics of 'base-growth' and 'tip-growth' mechanism respectively

(refer to section 2.1.2). Defects such as tube layer mismatch and corrugated or discontinued tube walls are very common. Overall the tubes are less well defined, few carbonaceous impurities are observed. Catalyst particles are embedded in the tubular structure, a common feature of tubes synthesized by CVD. Tubes with higher crystallinity can better retain structural integrity (refer to section 4.4.3).

A long-standing issue involving the complete elimination of the metal catalysts, namely Fe, Co and Ni, from MWNT soot remains to be addressed. After purification most of the metal catalyst was removed. However, there is still some remaining catalyst particles surrounded by large masses of carbon (see Figure 4.31). As can be seen, the typical impurity in the samples is the catalyst; which is randomly distributed throughout the sample. Metal catalyst particles are evident at the nanotube tips and metal inclusions are seen in the tube cores. The black areas are possibly due to agglomerated catalyst particles. These magnetic impurities are entrapped inside the individual nanotubes or incorporated as carbide like material along graphitic walls. Residual catalyst has also been reported to nest in between tubes of MWNT bundles (Tsang et al., 1994).

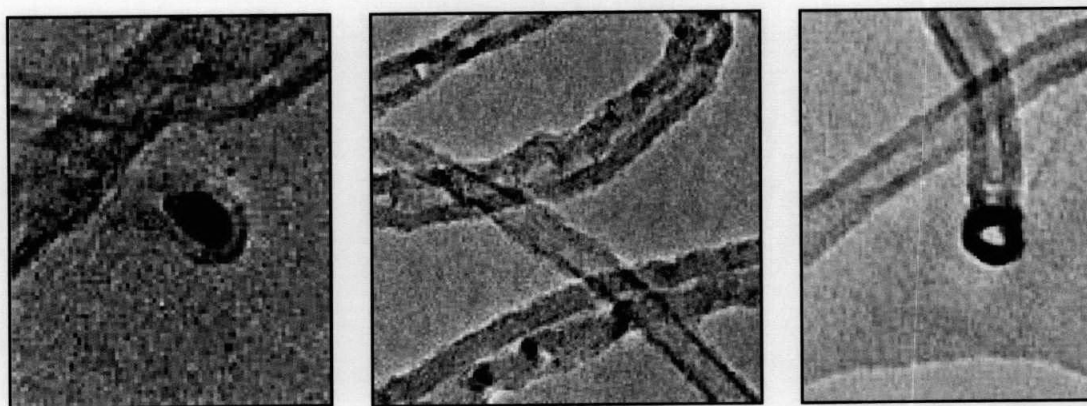


**Figure 4.31:** TEM images that illustrate the presence of metal catalyst in purified samples.

Figure 4.27(d), 4.28(c) and 4.29(c) show higher resolution transmission electron microscope images of CNTs grown on Fe, Co and Ni catalysts respectively. It is observed that CNTs grown on all catalysts exhibit multiwalled structure. In general,

CNTs exist in two variations, graphitic multiwalled carbon nanotubes (MWNTs) and single-walled carbon nanotubes (SWNTs). The former may be considered to be single-crystal nanosized ideal graphite fibres while the latter are true elongated fullerene tubes. Here, it was observed that the lattice fringes of the CNTs are evenly spaced with an almost equal number of fringes on either side of the central hollow core. Such result lead to the idea that these nanotubes are of Russian doll like structure (see Figure 4.32(a)) The average interlayer spacing for all CNTs are found to be in the range of 0.32 nm to 0.34 nm, which is very similar to the values found from XRD results (refer to section 4.3) and turbostratic graphites (Saito *et al.*, 1993).

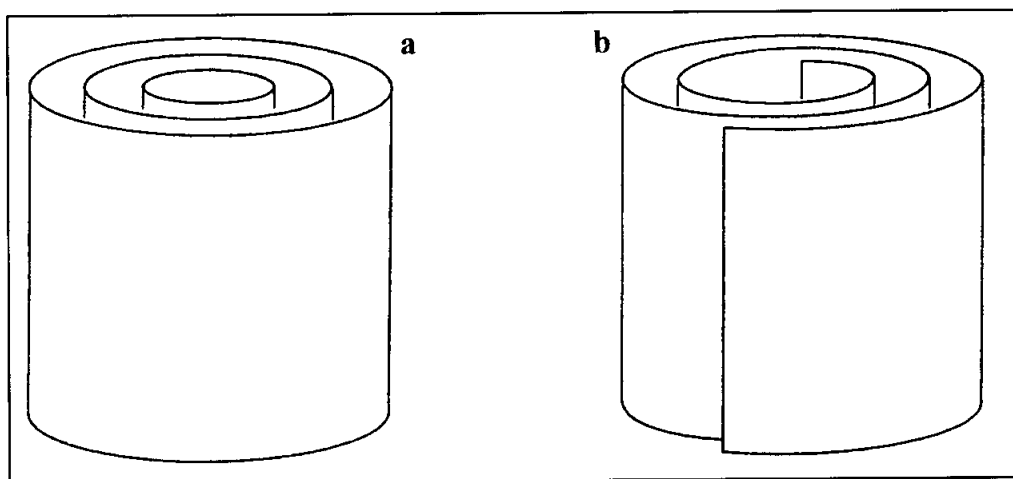


**Figure 4.32:** Schematic illustration of (a) 'Russian doll' and (b) 'Swiss roll' models for multiwalled nanotubes. (Reproduced from Harris, 1999).

Close examination of TEM images (see Figure 4.27(d), 4.28(c) and 4.29(c)) showing the walls of CNTs would allow one to determine the catalyst effect on the crystallinity of the grown CNTs. The well-defined graphene layers of CNTs grown on Fe catalyst indicate a highly ordered crystalline structure. The defective structure in the form of short-range layers can be seen in CNTs grown on Ni catalyst indicating a lower degree of crystalline perfection compared to that of Fe catalyst. More defects can be observed in CNTs grown on Co catalyst. This structural observation of TEM images indicates that the highest degree of crystalline perfection is shown by CNTs grown on Fe followed by that on Ni and Co catalyst.

The TEM images revealing the intricate structure of multiwalled nanotube can give a reasonable understanding of the main structural features of multiwalled nanotubes. All CNTs grown on Fe, Ni and Co have shown to be of multiwalled type with evenly spaced graphene layers.

#### 4.4.3 Thermal Gravimetry Analysis (TGA)

Presently, there is no conclusive method by which the purity of CNTs can be directly evaluated. In this work, TGA was used to estimate the purity of the MWNTs in terms of metal and metal oxide contents. It should be noted that there is a minor discrepancy between the impurity content of the MWNTs and the residual weight percent from the oxidation of the catalyst in TGA measurements. But the discrepancy is small and can be reasonably neglected when the metal content is very low in the samples.

Oxidation temperature ( $T_o$ ) of the sample in TGA (see Figure 4.33) can serve as a measure of thermal stability of CNTs in air. It depends on a number of parameters. For example, smaller diameter and high helicity CNTs are believed to oxidize at lower temperature due to higher curvature strain (Amelinckx *et al.*, 1994). Defect and derivatisation moiety in nanotube walls can also lower the thermal stability. Active metal particles present in the nanotube samples catalyse carbon oxidation, so the amount of metal impurity in the sample can have a considerable influence on the thermal stability. It is impossible to distinguish these contributions, but nevertheless thermal stability is a good measure of the overall quality of nanotube sample. Higher oxidation temperature is always associated with purer, less defective samples. Note that oxidation temperature can be defined alternatively as an onset (deflection point) temperature, or as a maximum in the derivative weight curve, also known as differential thermal analysis (DTA) curve (see Figure 4.34). In the case of CNTs samples, onset temperature is poorly defined since transitions are rather broad and initial mass loss is attributed to the oxidation of amorphous carbon impurities rather than nanotubes themselves. Maximum in the DTA curve, on the other hand, can be defined and measured precisely and is associated with burning of nanotubes rather than impurities. Therefore, oxidation temperature,  $T_o$  was define as a DTA maximum.

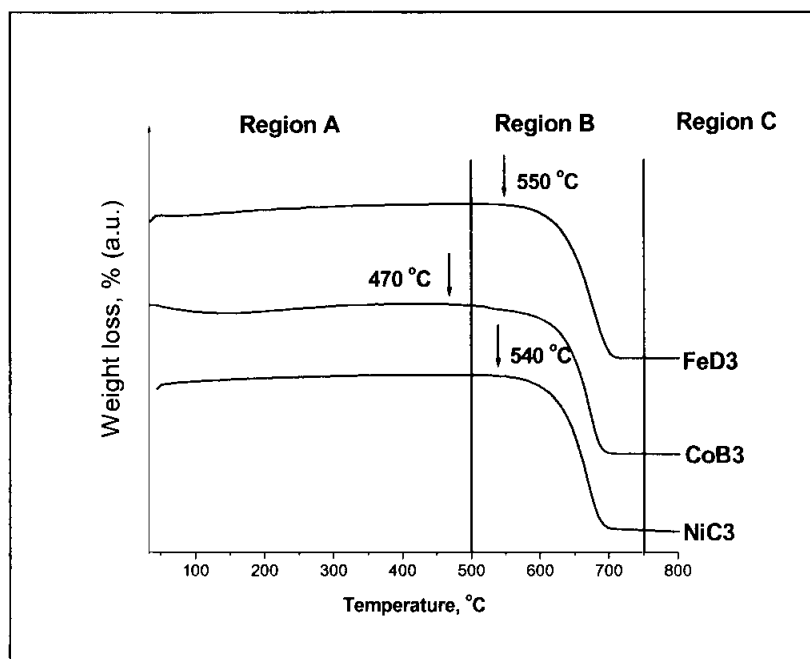


Figure 4.33: TGA plot of percentage weight against oxidation temperature for FeD<sub>3</sub>, CoB<sub>3</sub> and NiC<sub>3</sub>.

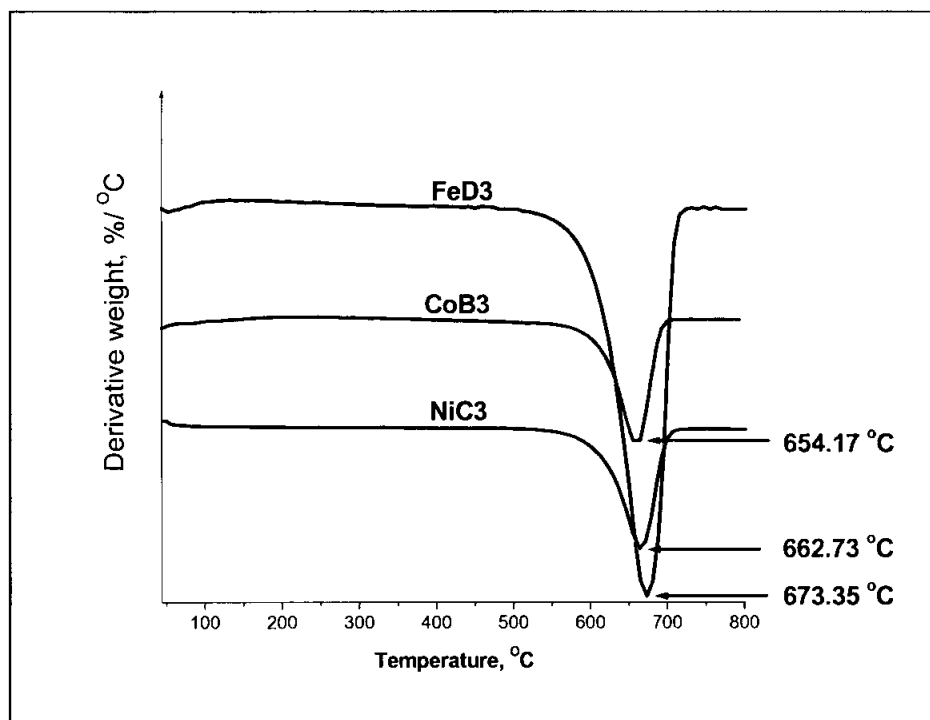


Figure 4.34: DTA plot of FeD<sub>3</sub>, CoB<sub>3</sub> and NiC<sub>3</sub>.

Table 4.9: Summary of TGA results of FeD3, CoB3 and NiC3.

| Specimen | TGA   |                |   |                |   |
|----------|---|----------------|---|----------------|---|
|          | Region A                                    |                | Region B  |                | Region C  |
|          | T <sub>R</sub> and T <sub>min</sub><br>(°C) | wt loss<br>(%) | T <sub>R</sub> and T <sub>max</sub><br>(°C)         | wt loss<br>(%) | M <sub>r</sub> (%)                                |
| FeD3     | T <sub>R</sub> = 30-500                     | + 5.82         | T <sub>R</sub> = 500-750<br>T <sub>o</sub> = 673.35 | -89.16         | M <sub>r</sub> =16.66<br>T <sub>R</sub> = 750-800 |
| CoB3     | T <sub>R</sub> = 30-500                     | -1.53          | T <sub>R</sub> = 500-750<br>T <sub>o</sub> = 654.17 | -85.65         | M <sub>r</sub> =12.82<br>T <sub>R</sub> = 750-800 |
| NiC3     | T <sub>R</sub> = 30-500                     | +5.05          | T <sub>R</sub> = 500-750<br>T <sub>o</sub> = 662.73 | -89.93         | M <sub>r</sub> =15.12<br>T <sub>R</sub> = 750-800 |

T<sub>R</sub> = weight loss temperature range

T<sub>o</sub> = DTA maximum

M<sub>r</sub> = residue mass, %

The thermal gravimetry analysis (TGA) data shown in Figure 4.33 indicated weight consumption for the purified sample. The TGA of the purified sample FeD3 and NiC3 have an initial weight gain commencing at approximately from 30 to 500°C reflecting the oxidation of the metallic elements. This could be due to oxygen introduced through the purification steps into carbon nanotubes structures in the form of functional groups such as -COH, -COOH, etc. This is presumably the uptake of oxygen by the iron and nickel catalyst. Note that without the oxidation cycle, extraction of the catalyst is ineffective; Fe and Ni remains in the sample, which is oxidized during TGA.

The initial weight loss been observed for the CoB3 sample, this may be caused by the release of tenaciously held solvent in the tiny crystallites structure. This could be due to the initial oxidation of the remaining cobalt in the sample such that no additional oxygen uptake is seen between 30 to 500°C. Significant weight loss starts to occur at 500°C. The weight loss continued to increase rapidly with temperature elevation until a stable plateau region appeared at nearly 750°C.

From the DTA curve in Figure 4.34, the temperature of the maximum rate of weight loss is 673.35°C for FeD3 (89.16 %), 654.17°C for CoB3 (85.65 %) and 662.73°C for NiC3 (89.93 %). CoB3 has the lowest temperature of maximum rate of weight loss

among the three samples. Also interesting to note in the NiC<sub>3</sub> and FeD<sub>3</sub>, there is a delay of the onset of oxidation compared with CoB<sub>3</sub>.

The DTA showed that an apparent differential peak structure was obtained, which indicated that the metal catalyst partially oxidized the tubes, to form amorphous carbon and multi shell carbons. Oxidation of carbon nanotubes and amorphous carbon occurs simultaneously even at moderate temperature, whereas amorphous carbon is more rapidly oxidized than carbon nanotubes. So it is possible to remove the amorphous carbon quantitatively with minimal losses of carbon nanotubes. But it was found that graphitic nanoparticles have highest stability against oxidation and could therefore not be quantitatively removed by this method without the complete destruction of carbon nanotubes. Therefore, the CVD process has to be a controlled process for minimum production of graphitic nanoparticles to obtain a material with a high content of carbon nanotubes.

Effective purification of CNTs can occur since CNT has better oxidation resistance compare to amorphous carbon and multishell carbon nanocapsules. Owing to the removal of amorphous carbon and multishell carbon nanocapsules, catalyst particles enclosed in the amorphous carbon and multishell carbon nanocapsules were exposed, and can be dissolved in the hydrochloric acid. The tip of the carbon nanotubes is the most reactive area and can be opened, which can be observed from the TEM image. However not all tips of carbon nanotubes are opened and then the catalyst particles embedded in them cannot be totally removed, a few percent of metal particles still remained in the sample, which is consistent with the result of TGA.

The temperature programmed oxidation technique is adopted in order to determine the relative amounts of defective and crystalline constituents in the CNTs grown on Fe, Co and Ni catalysts. CNTs with less crystalline structure will react preferentially with the oxidant and lose weight at a lower temperature compared to the more highly crystalline CNTs. Plots of the weight loss percentage against the oxidation temperature for CNTs grown on Fe, Co and Ni is shown in Figure 4.33. CNTs grown on Fe, Co and Ni

catalyst start to gasify at approximately 550°C, 470°C and 540°C, respectively. TGA plots in Figure 4.33 indicate that the crystallinity of the CNTs grown on Fe catalyst is slightly better than CNTs grown on Ni, with the least crystalline structure shown by CNTs grown on Co. This result supported the observation made by TEM. Lee *et al.*, 2002 had also reported similar findings on the crystallinity of CNTs grown on Fe, Ni and Co.

Considering the relationship between the SEM microstructure of CNTs and its thermal stability, the results of TGA is consistent whereby smaller diameter and higher helicity CNTs are believed to oxidise at lower temperature. However, CoB3 oxidised at lower temperature than NiC3 even though CoB3 has bigger diameter than NiC3. Thus it can be concluded that the helical structure of CoB3 may have more curvature strain than curled structure of NiC3 (Amelinckx *et al.*, 1994).

#### 4.4.4 Raman Spectroscopy

Raman spectroscopy has shown to be a powerful tool for characterising CNTs. The characteristic peaks occur due to the radial breathing mode (RBM), disordered carbon (D band), and an out of phase graphene sheet like vibrations (G band) (Saito *et al.*, 2001, Souza Filho *et al.*, 2002). These peaks occur at approximately  $170\text{ cm}^{-1}$  to  $325\text{ cm}^{-1}$ ,  $1330\text{ cm}^{-1}$  and  $1585\text{ cm}^{-1}$ , respectively (refer to section 3.6.5).

The Raman analysis was performed with a Renishaw Raman microscope to investigate the change in crystallinity with change in catalyst used. Laser light at  $514.5\text{ nm}$  and  $632.8\text{ nm}$  from an  $\text{Ar}^+$  and He-Ne lasers respectively were used for excitation. A power density of  $1\text{ mW cm}^{-2}$  (10% of maximum power) was used over the spectral range  $200$  to  $3000\text{ cm}^{-1}$ . The laser power density is extremely important for analysis of CNTs, as sample degradation effects can often be subtle but significant. When comparing the Raman spectra of different samples it is also important that no structural modification has taken place.

CNTs samples are susceptible to modification through thermal effects induced by high laser densities. This is an unwanted consequence of having too high laser power on the sample when collecting Raman information. Figure 4.35 shows an example of the differences in laser power on the same sample. The real effects in this case are:

- Significant increase in fluorescent background
- Reduction in signal to noise ratio (lower quality data)
- Shifting of the D band and G band resulting from structural changes

To ensure the integrity of such samples is maintained the use of lower laser power density is required. This results in a lower Raman intensity, as the laser power at the sample is directly proportional to the Raman intensity. The use of line focus optics has dramatically improved this problem area in Raman spectroscopy, where full laser power is utilised, but the power is focused into a line rather than a spot. This has the

advantage of maintaining the low power densities necessary whilst increasing the amount of Raman being collected. For example the laser power at each point has not increased, but the number of point increase by approximately 20 times.

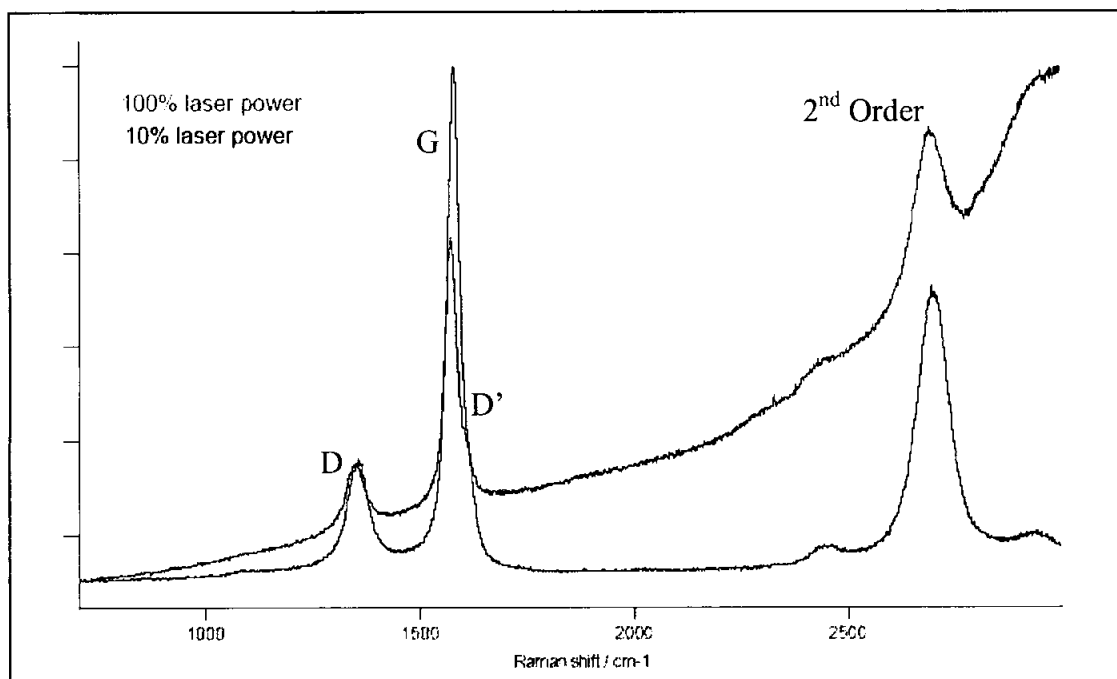


**Figure 4.35:** Comparison of CNTs spectra collected using different laser powers.

The crystallinity of CNT is determined through comparison of the D (disordered) band, and G (graphite) band. Broadly speaking the D band is located at approximately  $1348\text{ cm}^{-1}$ , and the G band at approximately  $1574\text{ cm}^{-1}$ . The exact position of the bands depends very much on the crystallinity of the nanotubes, as the D and D' band ( $\sim 1613\text{ cm}^{-1}$ ) increase in relative intensity with decreasing crystallinity. So, the higher the ratio ( $I_D / I_G$ ) the less crystalline the sample would be. It is worth nothing that, as might be expected, a perfectly crystalline graphite sample has no D band.

Figure 4.36 shows the Raman spectra collected with 514.5 nm laser excitation and the results confirmed that all the samples are multiwalled carbon nanotubes (MWNT) because RBM peak region is not visible. The D band ( $\sim 1348\text{ cm}^{-1}$ ) could be resulted from the defective outer graphite sheets of multiwalled CNTs. However, the D' band

( $\sim 1613 \text{ cm}^{-1}$ ) is too near to G band ( $\sim 1574 \text{ cm}^{-1}$ ) and appears as a small bump of G band. As the result, the intensity of G band ( $I_G$ ) is higher than actual value. Thus, the actual G band intensity can only be quantified by Lorentzian curve fitting to allow the crystal nature of each to be compared. Figure 4.37 shows a typical example of NiC3 Raman spectrum with Lorentzian curve fit, where the D band, G band and D' band are easily identified. The curve fit in this case allows effective G band or D' band deconvolution for highly accurate  $I_G$  values.

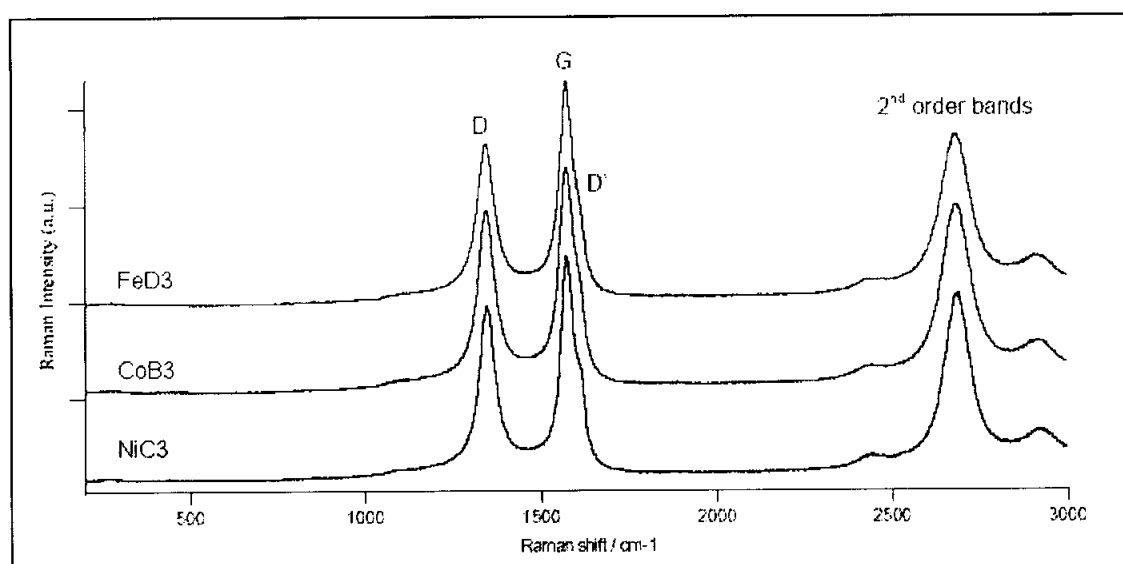


Figure 4.36: 514.5 nm excitation Raman spectra of CNT.

Table 4.10: Raman intensity value for carbon nanotubes at 514.5 nm excitation.

| Specimen | $I_D$ | $I_G$ | $I_D / I_G$ |
|----------|-------|-------|-------------|
| FeD3     | 13588 | 18246 | 0.745       |
| CoB3     | 16652 | 20248 | 0.822       |
| NiC3     | 13921 | 17774 | 0.783       |

The ( $I_D / I_G$ ) values are calculated in Table 4.10 for each of the samples analysed at 514.5 nm excitation. In Table 4.10, the ( $I_D / I_G$ ) values for specimens FeD3, CoB3 and NiC3 are 0.745, 0.822 and 0.783 respectively. These imply that the degree of

crystallinity perfection for FeD3 is the highest among the three specimens, while CoB3 is the lowest.

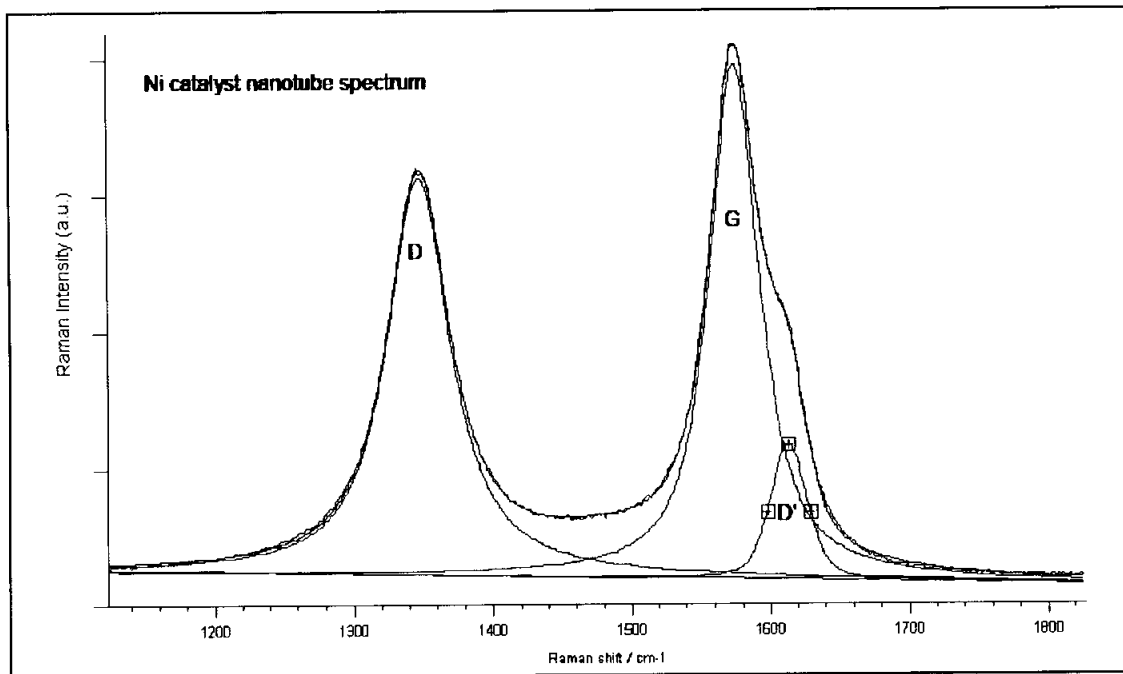
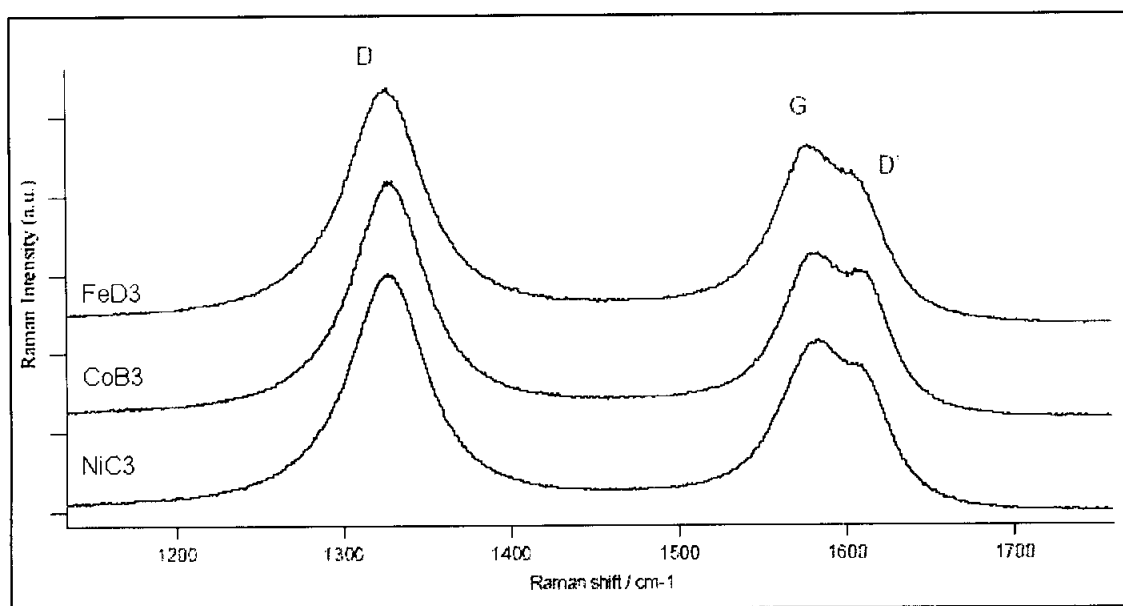


Figure 4.37: Lorentzian curve fit example of CNT spectrum.

Figure 4.38 illustrates Raman spectra of three CNT specimens grown by different catalyst at 632.8 nm laser excitation. The band positions are different at 632.8 nm (see Figure 4.38) compared to those previously collected at 514.5 nm (see Figure 4.36). The observed shifting is thought to relate to the extent of the resonance of  $sp^2$  and  $sp^3$  sites at different laser wavelengths. For example,  $sp^3$  sites are more resonant at lower wavelengths.

The separation between the G band and D band is larger than 514.5 nm, and the effect of this is shown as D' band is more distinctive as a result of the increased separation with the G band. Figure 4.38 clearly shows the shift in D band position with sample, and D' band contribution to the overall spectrum. It is also illustrates the greater dominance of D band in this spectral series, where the D band intensity at times is

greater than the G band intensity. Indeed the D' band intensity is close to the intensity of the G band itself.



**Figure 4.38:** 632.8 nm excitation Raman spectra of CNT.

The crystallinity trends observed at 632.8 nm (see Table 4.11) are consistent with those previously observed at 514.5 nm (see Table 4.10). However, due to D band intensity is higher than G band the ( $I_D / I_G$ ) values are more than 1. The values for specimens FeD3, CoB3 and NiC3 are 1.454, 1.538 and 1.483 respectively.

**Table 4.11:** Raman intensity value for carbon nanotubes at 623.8 nm excitation.

| Specimen | $I_D$ | $I_G$ | $I_D / I_G$ |
|----------|-------|-------|-------------|
| FeD3     | 28657 | 19704 | 1.454       |
| CoB3     | 29577 | 19225 | 1.538       |
| NiC3     | 29799 | 20094 | 1.483       |

The crystallinity of CNTs, grown by variety of metal catalysts, has been investigated using Raman spectroscopy. The degree of crystallinity is determined through

calculation of the D band G band ratio. The results clearly indicate that the degree of crystallinity perfection is in the order FeD3 > NiC3 > CoB3, which is consistent with the TEM images and TGA results. From the results, it is believed that the crystallographic characteristics of catalyst particle play an important role in governing the crystallinity of CNTs.

## 4.5 Summary

During the course of this work, the outcomes have demonstrated the ability to prepare CNTs in powder form. Coiled and open-ended CNTs are formed in the presence of Fe, Co and Ni catalysts respectively.

Structural analysis has been carried out by using scanning electron microscope and X-ray diffractometry. The former has shown to be a powerful tool for analysing the morphology of the samples. The latter has the capability to analyse bulk samples for overall view of the structural analysis.

The SEM images of wet etched catalyst sample and the particle size results show that the longer the wet etching duration the smaller would be the particles size of the catalyst. A very consistent etching rate was obtained (see Figure 4.5). While the morphologies of all the non-purified CNTs samples are almost the same regardless of the catalysts used (see Figure 4.6 to 4.12). It is observed that the non-purified products seem to exhibit some polyhedral structure and irregular shaped particles around CNTs. It is believed that the former might be some disordered carbon, which is co-product of the process and the latter might be nanocatalysts used to grow CNTs (Ebbesen et al., 1993).

Here, the morphologies of purified CNTs have been carried out. The micrographs of the purified CNTs samples clearly illustrate the efficiency of the purification process by the sharp decrease of the impurities content (see Figure 4.13 to 4.18). CNTs grown on Fe exhibit a fairly straight structure compared to the curled ones grown on Ni and even some helical ones grown on Co. It is observed that the average diameter of CNTs follows the order of  $\text{FeD}_3 > \text{CoB}_3 > \text{CoC}_3 > \text{NiC}_3 > \text{CoD}_3 > \text{NiD}_3$ . However CNTs grown on Co seem to be exhibit narrower diameter range compared to other samples.  $\text{CoB}_3$  has shown to have the narrowest diameter range among all the samples.

The X-ray diffraction results also exhibit a significant reduction of impurities by comparing the non-purified CNTs sample with the purified one. The graphitic (002) diffraction peak with highest intensity peak was observed at Bragg angle  $26.5^\circ$ . It has shown its prominence in all the samples. Since the graphitic (002) diffraction are locally tangent to successive cylinders, distance between lattice fringe of CNTs can be determined by calculating the interlayer spacing of plane (002) diffraction peak (see Figure 4.20). The interlayer spacing values that obtained are in the range of  $3.37 \text{ \AA}$  to  $3.47 \text{ \AA}$  and slightly bigger than graphite, which is  $3.34 \text{ \AA}$ . This is due to the stacking of CNTs, which is in the form of turbostratic structure rather than ABABAB type (Saito *et al.*, 1993).

After the optical impression and X-ray diffraction were observed, three samples were chosen for further investigation on the crystallinity of the samples. FeD3, CoB3 and NiC3 were chosen for this purpose. The investigation was also to study the difference in term of crystallinity between different catalysts.

Examination on crystallinity was started by using transmission electron microscope (TEM). It is observed that all the samples exhibit multiwalled structure. The lattice fringes of the CNTs are evenly spaced with an almost equal number of fringes on either side of the central hollow core. The average interlayer spacing for all CNTs are found to in the range of  $0.32 \text{ nm}$  to  $0.34 \text{ nm}$ , which is very similar to the value found in XRD results.

Close examination of TEM images showing the walls of CNTs would allow one to determine the catalyst effect on the crystallinity of the grown CNTs. Figure 4.27 to 4.29 depict the images of the wall of CNTs grown on Fe, Co and Ni catalysts. The well-defined graphene layers of CNTs grown on Fe catalyst indicate a highly ordered crystalline structure. The defective structure in the form of short-range layers can be seen in CNTs grown on Ni catalyst indicating a lower degree of crystalline perfection compared to that of Fe catalyst. More defects can be observed in CNTs grown on Co catalyst. This structural observation of TEM images indicates that the highest degree of

crystalline perfection is shown by CNTs grown on Fe followed by that on Ni and Co catalyst.

The TEM images observation is focused on a tiny part of a particular nanotube amongst the many nanotubes in the sample. Thus, the determination of the degree of crystalline perfection based on TEM images does not reflect the crystallinity of overall CNTs grown on the catalyst. However, the results from thermal gravimetry analysis (TGA) and Raman spectroscopy would reflect the crystallinity of the bulk CNTs grown on the catalysts.

The temperature programmed oxidation technique is adopted in order to determine the relative amounts of defective and crystalline constituents in the CNTs grown on Fe, Co and Ni catalysts. CNTs with less crystalline structure will react preferentially with the oxidant and lose weight at a lower temperature compared to the more highly crystalline CNTs. Plots of the weight percentage against the oxidation temperature for CNTs grown on Fe, Co and Ni is shown in Figure 4.33. CNTs grown on Fe, Co and Ni catalyst start to gasify at approximately 550°C, 470°C and 540°C, respectively. TGA plots in Figure 4.33 indicate that the crystallinity of the CNTs grown on Ni catalyst is slightly better than CNTs grown on Fe, with the least crystalline structure shown by CNTs grown on Co. This result supported the observation made by TEM. Lee *et al.* (2002) had also reported similar findings on the crystallinity of CNTs grown on Fe, Ni and Co.

The crystallinity of CNTs, grown by variety of metal catalysts, has been investigated using Raman spectroscopy. The degree of crystallinity is determined through calculation of the D band G band ratio. The results clearly indicate that the degree of crystallinity perfection is in the order Fe > Ni > Co, which is consistent with the TEM images and TGA results. From the results, it is believed that the crystallographic characteristics of catalyst particle play an important role in governing the crystallinity of CNTs.

## **Chapter 5: CONCLUSIONS AND FUTURE WORKS**

### **5.1 Conclusions**

The research described in this thesis focussed on the synthesis and characterisation of catalytic grown carbon nanotubes (CNTs), which can be used as reinforcement components of composite and in nanoelectronics. The critical properties for such applications would be uniformity or narrow diameter range. The synthesised materials in this work may be a new development in producing narrow diameter range, since no one has reported such diameter range.

Generally, the catalytic synthesis method was adopted from most of the researchers report. The parameters like type of catalyst, gas flow rate, working temperature and type of gas were followed as reported from others researcher. However, some modifications have been done on catalysts preparation. In this work, a new technique of preparing nanosized catalysts was developed. This technique involves longer wet and dry etching duration. The wet etching time is varying from 30 minutes to 120 minutes, while dry etching time was prolonged to 5 hours. Even though this technique has prolonged the synthesis duration, however the results that obtained show a very promising outcome. It is believed to be due to the longer period and higher gas flow rate of ammonia pretreatment prior to the growth of nanotubes, resulting in very much smaller nanosized catalyst particles.

Chapter 4 of this thesis discussed the comparison on the type of catalyst used and the difference of CNTs morphologies grown from them. The surface structure of CNTs

were characterised using scanning electron microscope. The catalyst effect on the growth of nanotubes are observed on the diameter and shape of CNTs produced. It is shown that the morphology depends not only on the nature of the metal exposed, but also on the size of the catalyst. It is observed that the average diameter of CNTs for all the samples follow the order  $\text{FeD3} > \text{CoB3} > \text{CoC3} > \text{NiC3} > \text{CoD3} > \text{NiD3}$ .

CNTs grown on Co are found to have the narrowest diameter range compared to the ones on Fe and Ni. Lee *et al.*, 2002 had reported similar order in the size of CNTs grown. Among all the Co grown samples, CoB3 exhibits the narrowest diameter range of CNTs. CoB3 is the sample of purified CNTs grown on Co catalysts that has been subjected to wet etching for 60 minutes. Thus, CoB3 may be the most suitable sample to be used for composite reinforcement and nanoelectronics.

The X-ray diffraction (XRD) results illustrated significant reduction of impurities in purified samples. Despite purification treatment, impurities are found not to be completely eliminated. However, these remaining impurities are not visible in the SEM results. Thus, it is believed that the impurities like catalysts were encapsulated by CNTs itself due their hollow structure.

Transmission electron microscope (TEM) was used to probe the internal structure of nanotubes where the intricate structures of multiwalled nanotubes with evenly spaced graphene layers are revealed. The determination of crystallinity using TEM images is based on the observation of the intricate arrangement of the walls of nanotubes. The structural observation of TEM images indicates that the highest degree of crystalline perfection is shown by CNTs grown on Fe followed by that on Ni and Co catalyst.

However, the finding may not be accurate, as the images obtained may not represent the bulk crystallinity of CNTs. Thus, thermal gravimetry analysis (TGA) and Raman spectroscopy are used to confirm the results. The results obtained are consistent with TEM ones. This implies that the degree of crystalline perfection of CNT grown catalytically can be manipulated by selection of the catalyst.

In this works, it is concluded that the structure, diameter size, uniformity and crystallinity of CNTs can be determined by the particle size and selection of the catalyst. The outcome of producing CNT that has narrow diameter range and high uniformity would pave the way for more application research on CNT reinforced composite and nanoelectronics.

## 5.2 International Collaboration

Sample CoB3, the ones which exhibit narrowest diameter range CNTs was sent to Kyoto University for further investigation on the potential of the sample as reinforcement component for composites. This collaboration is a joint research between Nanotechnology Laboratory of Universiti Teknologi PETRONAS and Advanced Fibro-Science Division of Graduate School of Kyoto University. The research is headed by Professor Ishihara Hideaki, head department of Advanced Fibro-Science Division and funded by New Energy and Industrial Technology Development Organisation of Japan (NEDO).

Some preliminary tests have been conducted on the sample in order to understand the material before any fabrication is done. These tests have indicated that the material has a very good electromagnetic shielding effect. Thus, the sample was suggested to be use as a reinforcement component for electromagnetic shield composite.

However, more fundamental research will be carried out on sample CoB3, in order to understand the reasons that cause the sample to have good electromagnetic shielding. One of the applications which is currently working on is producing fabric by mixing sample CoB3 with others polymer. The produced fabric will be used by the textile industry to make garment, which has electromagnetic shielding effect required by certain industries.

Positive results of the test have asserted that the current work has achieved the objective to produce narrow diameter range CNT needed in advance composite research.

### 5.3 Recommendations of the Research

In this section, a brief introduction to some of the methods, which might be employed to investigate further the fundamental understanding about carbon nanotubes.

In situ characterisation in this context means conducting a characterisation test on a reaction chamber while growing the CNT. Thus, characterisation equipments like HRTEM, XRD, TGA, SEM, Raman spectroscopy and X-ray photoelectron spectroscopy will be attached onto the reaction chamber. Therefore, a custom-made reaction chamber with all the characterisation tools is needed. The chamber can have multiple rooms inside provided it has a robotic system, which would transport the particular sample to the destination room for characterisation.

Figure 5.3 illustrates an in situ HRTEM observation of the formation of CNT from methane decomposition over supported nanocrystals. All the images are obtained with a rate of 2 frames per second. This experiment was done by Helveg *et al.*, 2004 to study the formation or elongation process of the CNT. This may help to understand the growing process more.

Another example of in situ characterisation will be an in situ Raman spectroscopy on a growing sample by varying temperature. Figure 5.4 shows Raman spectra at different temperatures. It is observed that the evolution of the carbon structure with temperature. The crystallinity is increasing with temperature, resulting in a decreased  $I_D / I_G$  ratio. This study was done by Gogotsi *et al.*, 2003.

The two examples, have shown how powerful in situ characterisation in current research scenario. Thus, by having such in situ characterisation tools, most of the unexplainable problem in old days will be solved. Besides, more experiments on the growing process can be carried out. However, cost of building up such machine will be extremely huge.

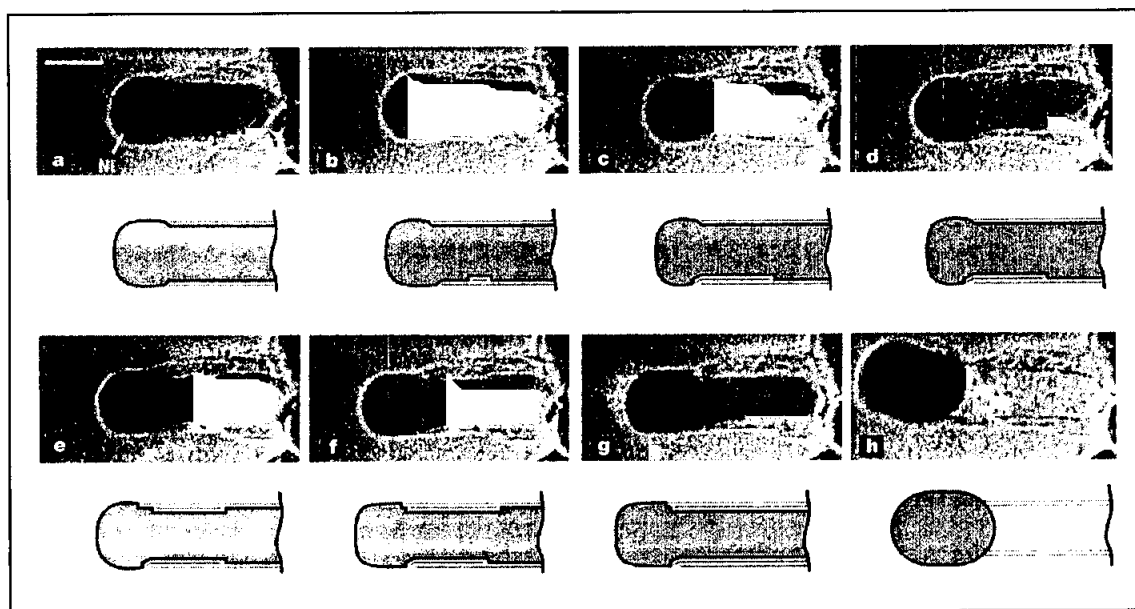


Figure 5.1: Images sequence of a growing CNT. (Reproduced from Helveg *et al.*, 2004).

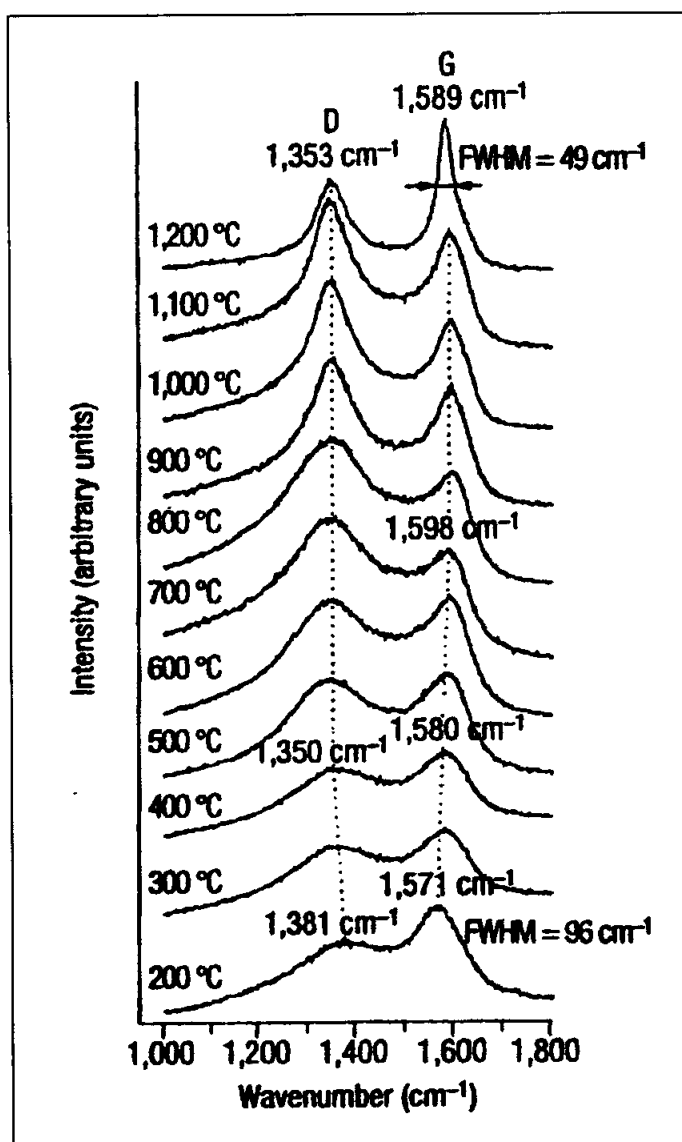


Figure 5.2: Raman spectra at different temperature. (Reproduced from Gogotsi *et al.*, 2003).

## REFERENCES

- Ajayan, P.M. (2000). Carbon Nanotube. In H.S. Nalwa. (Ed.), *Handbook of Nanostructured Materials and Nanotechnology: Vol. 5.* (pp. 375-406). San Diego: Academic Press.
- Ajayan, P.M., Stephan, O., Colliex, C. & Tranth, D. (1994). Aligned carbon nanotube arrays formed by cutting a polymer resin-nanotube composite. *Science*, *265*, 1212-1218.
- Amelinckx, S., Zhang, X.B., Bernerts, D., Zhang, X.F., Ivanov, V. & Nagy, J.B., (1994). A formation mechanism for catalytically grown helix shaped graphite nanotubes. *Science*, *265*, 635-639.
- Bacon, G.E., (1975). *Neutron Diffraction.* (3<sup>rd</sup> ed.). Oxford, U.K.: Oxford University Press.
- Bandow, S., Rao, A. M., Williams, K. A., Thess, A., Smalley, R. E., & Eklund, P. C. (1997). Purification of single-wall carbon nanotubes by microfiltration. *Journal of Physical Chemistry B*, *101*, 8839-8850.
- Bethune, D.S., Kiang, C.H., de Vries, M.S., Gorman, G., Savoy, R., Vasquez, J., *et al.* (1993). Cobalt-catalysed growth of carbon nanotubes with single-atomic-layer walls. *Nature*, *363*, 605-607.
- Borowiak-Palen, E., Pichler, T., Liu, X., Knupfer, M., Graff, A., Jost, O., *et al.* (2002). Reduced Diameter Distribution of Single-wall Carbon Nanotubes by Selective Oxidation. *Chemical Physics Letters*, *363*, 567-572.
- Cadek, M., Coleman, J.N., Ryan, K.P., Nicolosi, V., Bister, G., Fonseca, G. *et al.* (2004). Reinforcement of Polymer with Carbon Nanotubes: The Role of Nanotube Surface Area. *Nano Letters*, *4*, 353-356.

- Chen, D., Christensen, K.O., Ochoa-Fernández, E., Yu, Z., Tøtdal, B., Latorre, N. *et al.* (2005). Synthesis of Carbon Nanofibers: Effect of Ni crystal size during methane decomposition. *Journal of Catalysis*, 229, 82-96.
- Chiang, I. W., Brinson, B. E., Huang, A. Y., Willis, P. A., Bronikowski, M. J., Margrave, J. L., *et al.* (2001b). Purification and Characterisation of Single-Wall Carbon Nanotubes (SWNTs) obtained from the Gas-Phase Decomposition of CO (HiPco Process). *Journal of Physical Chemistry B*, 105, 8297-8301.
- Chiang, I. W., Brinson, B. E., Smalley, R. E., Margrave, J. L., & Hauge, R. H., (2001a). Purification and Characterisation of Single-Wall Carbon Nanotubes. *Journal of Physical Chemistry B*, 105, 1157-1161.
- Crandall, B.C. (1996). Molecular Engineering. In B.C. Crandall (Ed.), *Nanotechnology*. (pp. 1-2). Cambridge, MA: The MIT Press.
- Dekker, C. (1999, May). Carbon nanotubes as molecular quantum wires. *Physics Today*, 52, pp. 22-28.
- Dresselhaus, M. S., & Dresselhaus, G. (1996). *Science of Fullerenes and Carbon Nanotubes*. New York: Academic Press.
- Dresselhaus, M.S., Lin, Y.M., Rabin, O., Jorio, A., Souza Filho, A.G., Pimenta, M.A. *et al.* (2002). Nanowires and nanotubes. *Materials Science and Engineering C*, 1008, 1-12.
- Ebbesen, T. W. & Ajayan, P. M. (1992). Large-scale synthesis of carbon nanotubes. *Nature*, 358, 220-222.
- Ebbesen, T.W., Hiura, H., Fujita, J., Ochiai, Y., Matsui, S. & Tanigaki, K. (1993). Patterns in the bulk growth of carbon nanotubes, *Chemical Physics Letters*, 209, 83-90.

- Eklund, P.C., Pradhan, B.K., Kim, U.J., Xiong, Q., Fischer, J.E., Friedman, A.D. *et al.* (2002). Large-Scale Production of Single-Walled Carbon Nanotubes Using Ultrafast Pulses from a Free Electron Laser. *Nano Letters*, 2, 561-566.
- Falvo, M.R., Clary, G.J., Taylor II, R.M., Chi, V., Brooks, F.P. & Washburn, S. *et al.* (1997). Bending and buckling of carbon nanotubes under large strain. *Nature*, 389, 582-584.
- Gogotsi, Y., Nikitin, A., Ye, H.H., Zhou, W., Fischer, J.E., Yi, B. *et al.* (2003, September). Nanoporous carbide-derived carbon with tunable pore size. *Nature Materials*, 2, pp. 591-594.
- Guo, T., Nikolaev, P., Thess, A., Colbert, D.T. & Smalley, R.E. (1995). Catalytic growth of single-walled nanotubes by laser vaporization. *Chemical Physics Letters*, 243, 49-54.
- Harris, P.J.F. (1999). *Carbon Nanotubes and Related Structures: New Materials for the Twenty-first Century*. Cambridge, U.K.: Cambridge University Press.
- Helveg, S., López-Cartes, C., Sehested, J. Hansen, P.L., Clausen, B.S., Rostrup-Nielsen, J.R. *et al.* (2004). Atomic-scale imaging of carbon nanofibre growth. *Nature*, 427, 426-429.
- Hughes, M.P. (2003). *Nanoelectromechanics in engineering and biology*. Boca Raton, Florida: CRC Press.
- Iijima, S. & Ichihashi, T. (1993). Single-shell carbon nanotubes of 1-nm diameter. *Nature*, 363, 603-604.
- Iijima, S. (1991). Helical microtubules of graphitic carbon. *Nature*, 354, 56-58.

- Iijima, S., Brabec, C., Maiti, A. & Bernholc, J. (1996). Structural flexibility of carbon nanotubes. *Journal of Chemical Physics*, 104, 20892092.
- Iljin. (2001). Retrieved July 18, 2003, from <http://www.iljinnanotech.co.kr/en/home.html>.
- Ivanov, V., Fonseca, A., Nagy, J.B., Lucas, A., Lambin, P., Bernaerts, D., *et al.* (1995). Catalytic production and purification of nanotubules having fullerene-scale diameters. *Carbon*, 33, 1727-1738.
- Jung, S.H., Kim, M.R., Jeong, S.H., Kim, S.U., Lee, O.J., Lee, K.H. *et al.* (2003). High-yield Synthesis of Multi-walled Carbon Nanotubes by Arc Discharge in Liquid Nitrogen. *Applied Physics A*, 76 (2), 285-286.
- Kajiura, H., Tsutsui, S., Huang, H.J. & Murakami, Y. (2002). High-quality Single-walled Carbon Nanotubes from Arc Produced Soot. *Chemical Physics Letters*, 364, 586-592.
- Klug, H.P., Alexander, L.E. (1974). *X-Ray Diffraction Procedures for Polycrystalline and Amorphous Material*. (2<sup>nd</sup> ed.). New York: Wiley.
- Kong, J. Soh, H.T., Cassell, A.M., Quate, C.F. & Dai, H. (1998). Synthesis of Individual Single-walled Carbon Nanotubes on Patterned Silicon Wafers. *Nature*, 395, 878-881.
- Krishnan, A., Dujardin, E., Ebbesen, T.W., Yianilos, P.N. & Treacy, M.M.J. (1998). Young's Modulus of Single-Walled Nanotubes, *Physical Review B*, 58, 14013-14019.
- Kuzmany, H. (2001). Determination of SWCNT diameters from the Raman response of the radial breathing mode. *The European Physical Journal*, 22, 307-320.

- Kónya, Z. (2001). Catalytic production, purification, characterisation and application of single- and multiwall carbon nanotubes. In L.P. Biró. *et al.* (Eds.). *Carbon Filaments and Nanotubes: Common Origins, Differing Application*. (pp. 85- 109). Netherlands: Kluwer Academic Publishers.
- Lambin, P., Fonseca, A., Vigneron, J.P., Nagy, J.B. & Lucas, A.A. (1995). Structural and electronics properties of bent carbon nanotubes. *Chemical Physics Letters*, *245*, 85-89.
- Lee, C.J., Lee, T.J. & Lyu, S.C. (2001, December). Growth of Vertically Aligned Bamboo-Shaped Carbon Nanotubes. *Journal of the Korean Physical Society*, *39*, pp.59-62.
- Lee, C.J., Park, J. & Yu, J.A. (2002). Catalyst effect on carbon nanotubes synthesized by thermal chemical vapor deposition. *Chemical Physics Letters*, *360*, 250-255.
- Lourie, O., Cox, D.M. & Wagner, H.D. (1998). Buckling and Collapse of Embedded Carbon Nanotubes. *Physical Review Letter*, *81*, 1638-1641.
- Maser, W.K., Benito, A.M. & Martínez, M.T. (2002). Production of carbon nanotubes: the light approach. *Carbon*, *40*, 1685-1695.
- Moon, J.M., An, K.H., Lee, Y.H., Park, Y.S., Bae, D.J. & Park, G.S. (2001). High-yield purification process of singlewalled carbon nanotubes. *Journal of Physical Chemistry B*, *105*, 5677-5681.
- Otsuka, K., Kobayashi, S. & Takenaka, S. (2001). Hydrogen-Deuterium Exchange Studies on the Decomposition of Methane over Ni/SiO<sub>2</sub>. *Journal of Catalysis*, *200*, 4-9.
- Poole, C.P. Jr., & Owens, F.J. (2003). *Introduction to nanotechnology*. New Jersey: John Wiley & Sons.

- Pradhan, D. & Sharon, M. (2002). Carbon nanotubes, nanofilaments and nanobeads by thermal chemical vapour deposition process. *Materials Science and Engineering B*, 96, 24-28.
- Qian, D., Dickey, E.C., Andrews, R. & Rantell, T. (2000). Load transfer and deformation mechanisms in carbon nanotube-polystyrene composites. *Applied Physics Letters*, 76, 2868-2871.
- Rearce, R. & Patterson, W.R. (1981). *Catalytic and Chemical Processes*. New York: Leonard Hill.
- Ren, Z.F., Huang, Z.P., Wang, D.Z., Wen, J.G., Xu, J.W., Wang, J.H. *et al.* (1999). Growth of a Single Freestanding Multiwall Carbon Nanotube on each Nanonickel dot. *Applied Physics Letters*, 75, 1086-1082.
- Renishaw. (2001). Retrieved December 12, 2004, from <http://www.renishaw.com/client/product/UKEnglish/PGP-37.shtml>.
- Ruoff, R.S., Tersoff, J., Lorents, D.C., Subramoney, S. & Chan, B. (1993). Radial deformation of carbon nanotubes by Van der Waals forces. *Nature*, 364, 514-516.
- Saito, R. & Kataura, H. (2001). Optical Properties and Raman Spectroscopy of Carbon Nanotubes. In M.S. Dresselhaus, G. Dresselhaus & P. Avouris, (eds.). *Carbon Nanotubes - synthesis, structure, properties and applications*. (pp. 213-246). Berlin: Springer Verlag.
- Saito, R., Dresselhaus, G. & Dresselhaus, M.S. (1998). *Physical Properties of Carbon Nanotubes*. London: Imperial College Press.
- Saito, Y., Yoshikawa, T., Bandow, S., Tomita, M. and Hayashi, T., (1993). Interlayer spacings in carbon nanotubes, *Physical Review B*, 48, 1907-1909.

- Scott, C.D., Arepalli, S., Nikolaev, P. & Smalley, R.E. (2001). Growth Mechanisms for Single-wall Carbon Nanotubes in a Laser-ablation Process. *Applied Physics A*, 72, 573-580.
- Sinnot, S.B., Andrews, R., Qian, D., Rao, A.M., Mao, Z., Dickey, E.C. *et al.* (1999). *Chemical Physics Letters*, 315, 25-30.
- Smalley, R.E. (n.d.). *Image gallery of Richard Smalley group*. Retrieved October 25, 2003, from <http://www.cnst.rice.edu/pics.html>.
- Smith, W.F. (1996). *Principles of materials science and engineering*. (3<sup>rd</sup> ed.). New York: McGraw-Hill.
- Souza Filho, A.G., Jorio, A., Swan A.K., Ünlü, M.S., Goldberg, B.B. Saito, R. *et al.* (2002). Anomalous Two-peak G'-band Raman Effect in one Isolated Single-wall Carbon Nanotube. *Physics Review B*, 65, 085417.
- Spiewak, B.E., Cortright, R.D. & Dumesic, J.A. (1997). Thermochemical Characterization. In G. Ertl *et al.* (Eds.). *Handbook of Heterogeneous Catalysis: Volume 2*. (pp. 698-706). Weinheim: VCH Verlagsgesellschaft.
- Strong, K.L., Anderson, D.P., Khalid, L. & Kuhn, J.N. (2003). Purification process for single-wall carbon nanotubes. *Carbon*, 41, 1477-1488.
- Treacy, M., Ebbesen, T.W. & Gibson, J.M. (1996). Exceptionally high Young's modulus observed for individual carbon nanotubes. *Nature*, 381, 678-680.
- Tsang, S.C., Chen, Y.K., Harris, P.J.F. & Green, M.L.H. (1994). A simple chemical method of opening carbon nanotubes. *Nature*, 372, 159-162.
- Van Zant, P. (1997). *Microchip Fabrication* (3<sup>rd</sup> ed.). New York: McGraw-Hill.
- Warren, B.F. (1969). *X-Ray Diffraction*. Massachusetts: Addison-Wesley.

- Wat, I.M. (1997). *The principles and practice of electron microscopy*. (2<sup>nd</sup> ed.). Cambridge: Cambridge University Press.
- Wildöer, J.W.G., Venema, L.C., Rinzler, A.G., Smalley, R.E. & Dekker, C. (1998). Electronics structure of atomically resolved carbon nanotubes. *Nature*, 391, 59-62.
- Yao, Z. Postma, H.W.C. Balents, L. & Dekker, C. (1999). Carbon Nanotube Intramolecular Junctions. *Nature*, 402, 273-276.
- Yasuda, A., Kawase, N. & Mizutani, W. (2002). Nanowindow- Induced Molecular Sieving Effect in a Single-Wall Carbon Nanohorn. *Journal of Physical Chemistry B*, 106, 12668-12669.
- Yoshimura, M. & Calderon-Moreno, J.M. (2001). Hydrothermal Processing of High-Quality Multiwall Nanotubes from Amorphous Carbon. *Journal of American Chemical Society*, 123, 741-742.
- Yudasaka, M., Kikuchi, R., Matsui, T., Ohki, Y., Yoshimura, S., & Ota, E. (1995). Specific conditions for Ni catalyzed carbon nanotube growth by chemical vapor deposition. *Applied Physics Letters*, 67, 2477-2479.
- Yudasaka, M., Yamada, R., Sensui, N., Wilkins, T., Ichihashi, T. & Iijima, S. (1999). Mechanism of the Effect of NiCo, Ni and Co Catalysts on the Yield of Single-wall Carbon Nanotubes Formed by Pulsed Nd: YAG Laser Ablation. *Journal of Physical Chemistry B*, 103, 6224-6229.
- Zhang, X.B., Zhang, X.F., Amelinckx, S., Van Tendeloo, G. & Van Landuyt, J. (1994). The reciprocal space of carbon tubes: a detailed interpretation of electron diffraction effects. *Ultramicroscopy*, 54, 237-249.

**APPENDIX A: List of Chemicals**

1. Iron Powder 99.5% [Fe]  
MERCK KgaA, 64271 Darmstadt, Germany.
2. Cobalt Powder 99.0% [Co]  
MERCK KgaA, 64271 Darmstadt, Germany.
3. Nickel Powder 99.5% [Ni]  
MERCK KgaA, 64271 Darmstadt, Germany.
4. Ethanol [C<sub>2</sub>H<sub>6</sub>O]  
MERCK KgaA, 64271 Darmstadt, Germany.
5. Hydrofluoric Acid 49% [HF]  
R&M Marketing, Essex, U.K.
6. Hydrochloric Acid Fuming 37% [HCl]  
MERCK KgaA, 64271 Darmstadt, Germany.
7. Hydrogen Peroxide 30% [H<sub>2</sub>O<sub>2</sub>]  
MERCK KgaA, 64271 Darmstadt, Germany.
8. Purified Argon gas [Ar]  
Malaysian Oxygen Berhad (MOX)
9. Methane gas [CH<sub>4</sub>]  
Malaysian Oxygen Berhad (MOX)
10. Ammonia gas [NH<sub>3</sub>]  
Malaysian Oxygen Berhad (MOX)

## APPENDIX B: Size Determination from Micrograph

Carl Zeiss AxioVision 3.1, a surface analysis software was used to analyse micrograph of all the samples. This software, allow sample parameter such as particles size, diameter, and interlayer spacing to be determined accurately. The output of the software is as shown in Figure B-1. The following is a typical example of diameter determination:

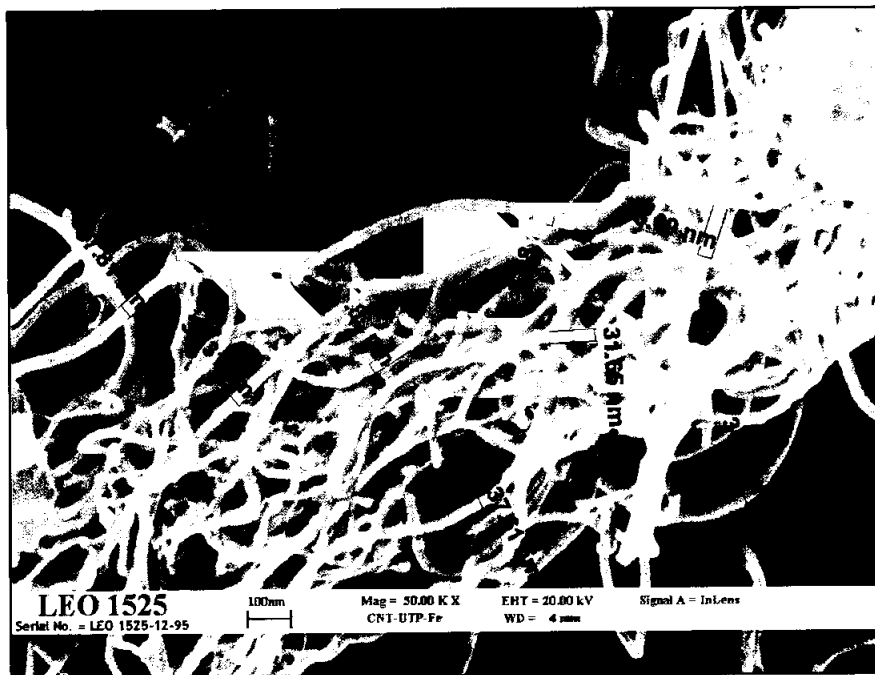


Figure B-1: Output of Carl Zeiss AxioVision 3.1 software.

From the results, mean,

$$\bar{x} = \left( \frac{30.94 + 37.81 + 35.31 + 30.85 + 37.48 + 31.65 + 37.61 + 38.09 + 36.7}{9} \right) nm$$

$$= 35.16 \text{ nm}$$

*Diameter Range = 30.94 to 37.81 nm*

Standard deviation of specimen FeD3,

$$\begin{aligned}
 s &= \sqrt{\frac{1}{n-1} \sum_{i=1}^n (x_i - \bar{x})^2} \\
 &= \sqrt{\frac{1}{9-1} ((-4.22) + 2.65 + 0.15 + (-4.31) + 2.32 + (-3.51) + 2.45 + 2.93 + 1.54)^2} \text{ nm} \\
 &= \sqrt{\frac{1}{8} (17.81 + 7.02 + 0.02 + 18.58 + 5.38 + 12.32 + 6.00 + 8.58 + 2.37)} \text{ nm} \\
 &= \sqrt{\frac{1}{8} (78.09)} \text{ nm} \\
 &= \sqrt{9.76} \text{ nm} \\
 &= 3.12 \text{ nm}
 \end{aligned}$$

Therefore, average external diameter of specimen FeD3, =  $(35.16 \pm 3.12) \text{ nm}$

## APPENDIX C: Interlayer Spacing Determination from X-Ray Diffraction

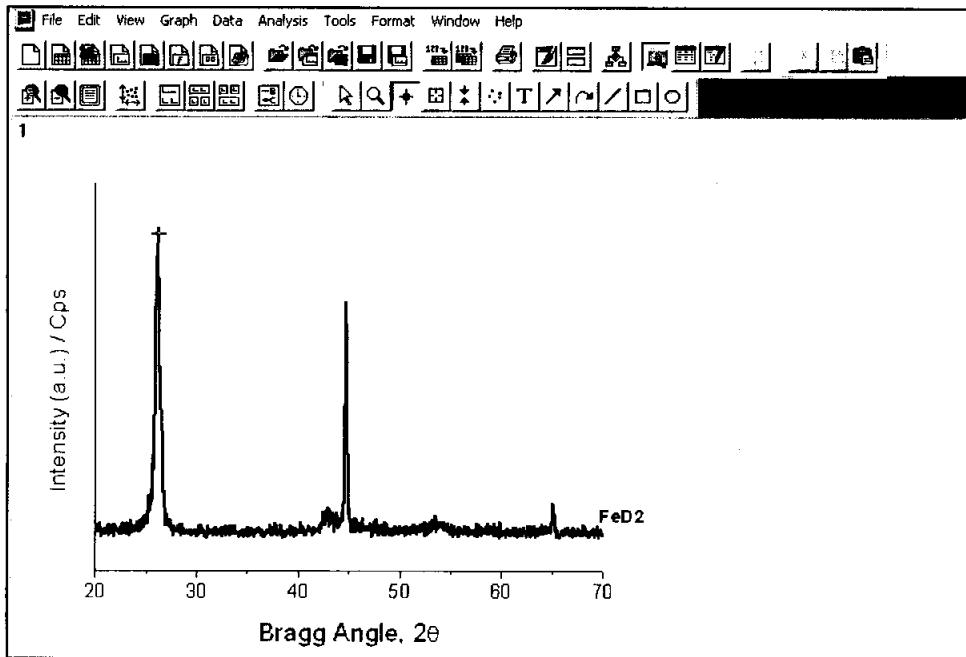


Figure C-1: Print screen from Microcal Origin software.

Microcal Origin software was used to analyse X-Ray diffraction pattern. The software was used to determinate the Bragg angle of (002) peak. Figure C-1 is an example of Bragg angle determination by using Microcal Origin.

From Figure C-1, Bragg angle,  $2\theta = 26.12^\circ$  and wavelength of  $\text{CuK}\alpha$ ,  $\lambda = 0.15418 \text{ nm}$ .

By using equation 3.1,  $\lambda = 2d \sin \theta$

Thus, interlayer spacing,

$$d = \frac{\lambda}{2 \sin \theta}$$

$$= \frac{0.15418 \text{ nm}}{2 \sin \left( \frac{26.12^\circ}{2} \right)}$$

$$= 0.3411 \text{ nm}$$

$$= 3.41 \text{ \AA}$$

## LIST OF PUBLICATION

### Conference Papers

- 1) Norani Muti Mohamed, Kadir Masrom, **Tan Yee Chech** and Saravanan Muniandy. (2003). Diameter Determination of Carbon Nanotubes (CNTs). In *Proceeding of National Symposium of Science and Technology: Strategic Research and Innovation Towards Economic Development*.
- 2) Norani Muti Mohamed, **Tan Yee Chech**, Saravanan Muniandy and Kadir Masrom. (2003). Surface Analysis of Catalytically Grown Carbon Nanotubes (CNTs). In *Proceeding of 12<sup>th</sup> Electron Microscopy Society Conference 2003*. (pp. 229-233).
- 3) Norani Muti Mohamed, **Tan Yee Chech** and Kadir Masrom. (2004). High Resolution Electron Microscopy of Catalytically Grown Carbon Nanotubes (CNTs). In *Proceeding of International Conference on X-Ray and Related Techniques in Research and Industry 2004*. (CD-ROM, Sept 2004).
- 4) **Tan Yee Chech**, Norani Muti Mohamed, and Kadir Masrom. (2004). Morphology Analysis of Catalytically Grown Carbon Nanotubes. In *Proceeding of 2<sup>ND</sup> Colloquium on Postgraduate Research National Postgraduate Colloquium on Materials, Minerals and Polymer 2004*. (pp. 186-190).
- 5) **Tan Yee Chech**, Norani Muti Mohamed, and Kadir Masrom. (2004). The Study of Catalyst Effect on the Quality of Carbon Nanotubes. In *Proceeding of The 3<sup>rd</sup> National Technical Postgraduate Symposium*. (pp. 153-157).
- 6) Norani Muti Mohamed, **Tan Yee Chech** and Kadir Masrom. (2005). Structural Characterisation of Catalytically Grown Carbon Nanotubes (CNTs). In *Proceeding of International Conference on Nanotechnology: Science and Application [NanoTech Insight '05], Luxor, Egypt*. (pp. 162-163).

- 7) Norani Muti Mohamed and **Tan Yee Cheh**. (2005). Crystallinity Investigation of Multiwalled Carbon Nanotubes (MWNTs) using Raman Spectroscopy. In *Proceeding of International Meeting on Frontiers of Physics 2005*.

### **Journal Papers**

- 1) Norani Muti Mohamed, **Tan Yee Cheh** and Kadir Masrom. (2004). High Resolution Electron Microscopy of Catalytically Grown Carbon Nanotubes (CNTs). To be published at *Journal of Industrial Technology*.
- 2) Norani Muti Mohamed, **Tan Yee Cheh** and Kadir Masrom. (2005). Structural Characterisation of Carbon Nanotubes (CNTs) Synthesised by Thermal Chemical Vapour Deposition. To be published at *Journal of Solid State Science and Technology*, Vol. 11, No. 2.
- 3) Norani Muti Mohamed, **Tan Yee Cheh** and Kadir Masrom. (2005). Narrow Diameter Carbon Nanotubes (CNTs) For Polymer Composite Reinforcement. Submitted for review in *Materials Science Forum*.

### **Award**

- 1) Bronze Medal – 16th International Invention Innovation Industrial Design and Technology Exhibition 2005 (ITEX'05)